Hochschule
Augsburg University of
Applied Sciences

Faculty of
Mechanical and
Process
Engineering

Lightweight Construction and
Composite Technology

Master Thesis

Evaluation and Development of a Continuous Longitudinal Joining Process for Carbon-Reinforced High-Performance Composites in Aircraft Primary Structure

Alexander Sänger, B.Eng.

Alexander Sänger, B.Eng.
Schornstraße 11
D-81669 München
+49 89 447 03 78
alexander.saenger1@hs-augsburg.de
Matricualtion Number: 95 27 04

First Examiner:	Prof. Dr.-Ing. André Baeten
Second Examiner:	Prof. Dr.-Ing. Ralf Goller
Supervisor:	Dr. Stefan Jarka
Topic received on:	22/05/2017
Date of submission:	13/11/2017

Hochschule für
angewandte Wissenschaften
University of Applied Sciences

An der Hochschule 1
D-86161 Augsburg
Telefon +49 821 55 86-0
Fax +49 821 55 86-3222
www.hs-augsburg.de
info@hs-ausgsburg.de

Spirit
of
Engineering

To
my parents
& Urli

Hochschule Augsburg
University of Applied Sciences Augsburg

Deutsches Zentrum für Luft- und Raumfahrt
German Aerospace Center

MASTER THESIS

Evaluation and Development of a Continuous Longitudinal Joining Process for Carbon-Reinforced High-Performance Composites in Aircraft Primary Structure

Alexander Sänger, B.Eng.

Discussed: 24/03/2017 / Received: 22/05/2017 / Submission: 13/11/2017

Abstract Although (carbon) composites seem to be arrived in aircraft structures, the full lightweight potential is not reached and state of the art processes are usually not fibre-fair. In addition, most frequently used are thermoset matrices which require energy demanding material cooling and curing, high added-value processing materials and labour-intensive process steps. This work presents the state of the art aircraft manufacturing with spotlights on the main challenges and potentials for thermoplastic resin systems. An overview and evaluation of fusion bonding approaches is given leading to ultrasonic welding as process of choice. Theoretical considerations on heating mechanisms lay the foundation for subsequent parametric study of statically ultrasonically welded CF/PEEK specimen. Observations and results are discussed and transferred to an continuous welding concept for robotic application. Therefore, this work does not only provide a technological overview and experimental data on – so far rather neglected – ultrasonic welding of CF/PEEK composites, but also suggestions and first steps towards the aircraft manufacturing of the future.

Keywords Ultrasonic Welding • Thermoplastic Composites • Heating Mechanisms • Continuous Joining • Robot Application • Aircraft Manufacturing

✉ Alexander Sänger
alexander.saenger1@hs-augsburg.de
Faculty of Mechanical Engineering
University of Applied Sciences
D-86161 Augsburg, Germany

Restriction Note

The presented master thesis contains confidential information. All remarks, data and results of the presented thesis must be treated as confidential and must not be available to third parties without written consent of Deutsches Zentrum für Luft- und Raumfahrt e.V. (DLR) and the author. Disclosure, publishing or duplication of the thesis in parts or in extracts – even in digital form – are not permitted without expressly authorisation. This thesis is liable to a prohibition of publishing, restriction in access and searching for persons who are not in charge of evaluating this thesis. Both parties, author and supervisors, agreed upon a conspiracy of silence.

Alexander Sänger, B.Eng.

Schornstraße 11
81669 München

Dr.-Ing. Stefan Jarka

Deutsches Zentrum für
Luft- und Raumfahrt e.V.
Am Technologiezentrum 4
86159 Augsburg

Prof. Dr.-Ing. André Baeten

Hochschule für angewandte
Wissenschaften Augsburg
An der Hochschule 1
86161 Augsburg

Table of Content

List of Figures

Note: All pictures, figures and graphics, as far as not indicated in captions, are taken or created by the author and the copyright belongs to him.

List of Tables

List of Abbreviation

AFP	Automated Fibre Placement
ALM	Additive Layered Manufacturing
APC	Aromatic Polymer Composite[1]
APC-2	PEEK matrix with AS4 carbon fibre reinforcement
ARW	Automated Resistance Welder
AS4	HexTow™continuous, high strength/strain, PAN based carbon fibre
ASTM	American Society for Testing Materials
BVID	Barely Visible Impact Damage
CF	Carbon Fibre
CFRP	Carbon Fibre Reinforced Plastics
CG	Centre of Gravity
CMC	Ceramic Matrix Composites
CRW	Continuous Resistance Welding
CTE	Coefficient of Thermal Expansion
DCB	Double Cantilever Beam
DIN	Deutsches Institut für Normung (German Institute for Standardisation)
DSG	Design Service Goal
EASA	European Aviation Safety Agency
EBM	Electron Beam Melting
ED	Energy Director
EN	European Normative
FAA	Federal Aviation Administration
FSM	Friction Stir Welding
HAZ	Heat-Affected Zone
HDT	Heat Deflection Test
IM	Intermediate Modulus
IM7	HexTow™continuous, high performance, intermediate modulus, PAN based carbon fibre
IR	Infrared
IRW	Infrared Welding

1. Mattia 2003

IW	Induction Welding
LBW	Laser Beam Welding
LSS	Lap Shear Strength
LTW	Laser Transmission Welding
MMC	Metal Matrix Composites
MWE	Minimum Working Example
NDI	Non-Destructive Inspection
NDT	Non-Destructive Testing
PA	Polyamide
PAN	Polyacrylonitrile
PAX	Passenger
PEI	Polyetherimide
PEEK	Polyetheretherketone
PTFE	Polyetetraflourethylene (aka *Teflon*®)
PU	Polyurethane
PVC	Polyvinylchloride
RC	Recurring Costs
RF	Radio Frequency
RW	Resistance Welding
SLM	Selective Laser Melting
SRW	Sequential Resistance Welding
TP	Thermoplastic
TPC	Thermoplastic Composite
TS	Thermoset
UD	Unidirectional
ul	Unit Length
US	Ultrasonic (here also: Ultrasonic Welding)

List of Symbols

in basis SI unit system

α	$\frac{\Omega}{K}$	Resistance-Temperature Coefficient
α_h	$-$	Hammering Coefficient
$a_{S,0}$	m	Sonotrode's Peak-to-Peak Amplitude
A	m^2	Area
c	$\frac{J}{kg \cdot K}$	Specific Heat / Thermal Capacity
D	$\sqrt{\frac{N \cdot kg}{m}}$	Damping Coefficient
η	$Pa \cdot s$	Dynamic Viscosity
η	$kg \cdot m$	Damping Coefficient
η_{cpl}	$-$	Coupling Efficiency
ε	$-$	Elongation
$\hat{\varepsilon}$	$-$	Amplitude Strain
E, E'	$\frac{N}{m^2}$, Pa	Young's Modulus (Elastic/Storage Modulus)
E''	$\frac{N}{m^2}$, Pa	Loss Modulus
E^*	$\frac{N}{m^2}$, Pa	Complex Elastic Modulus
f	Hz	Frequency
F_C	N	Contact Force
F_N	N	Normal Force
F_τ	N	Interfacial Friction
γ	$-$	Shear Strain
g	$\frac{m}{s^2}$	Gravitational Constant ($9.8065\ {}^{m}/_{s^2}$)
γ	Ω	Specific Electrical Resistance
G_{Ic}	$\frac{J}{mm^2}$	Interlaminar Fracture Toughness Mode I
$H(I)$	$\frac{A}{m}$	Current Dependent Magnetic Field
h_m	$\frac{J}{m^2}$	Specific Fusion Enthalpy
H_m	J	Fusion Enthalpy
I	A	Electrical Current
k_z	$\frac{W}{m^2 \cdot K}$	Thermal Resistance Coefficient

λ	$\frac{W}{m \cdot K}$	Thermal Conductivity
λ_{ij}	$\frac{W}{m \cdot K}$	Thermal Conductivity Tensor (2nd Order)
L, l	m	Length
μ	$\frac{H}{m}$	Magnetic Permeability
μ	$-$	Constant Sliding Coefficient
m	kg	Mass
M_A	Nm	Torque
∇	$-$	Gradient Operator
ν	$-$	Poisson's Ratio
ω	$\frac{rad}{s} = \sqrt{\frac{N}{m \cdot kg}}$	Angular Frequency
φ	$-$	Fibre Volume Content
p	$\frac{N}{m^2}$, Pa	Pressure
P	W	(Electrical) Power
$\dot{q}$	$\frac{W}{m^2}$	Heat Flow/Flux
$\dot{Q}_{fric}$	W	Friction Dissipated Power
$\dot{Q}_{in}$	W	Input Heat Power
$\dot{Q}_{mc}$	W	Intermolecular Dissipated Power
ρ	$\frac{\Omega}{m}$	Electrical Conductivity (Specific Electrical Resistance)
ρ	$\frac{kg}{m^3}$	Density
ρ_1, ρ_2	m	Curvature Radius
R	Ω	Electrical Resistance
R_a	m	Surface Roughness (Arithmetical Mean Deviation)
R_m	$\frac{N}{m^2}$, Pa	Ultimate Tension Strength
σ	$\frac{N}{m^2}$, Pa	Stress
σ_N	$\frac{N}{m^2}$, Pa	Normal Stress
σ_{yy}	$\frac{N}{m^2}$, Pa	Vertical Stress on Horizontal Interface
τ	$\frac{N}{m^2}$, Pa	Shear Stress
T	$°C/°K$	Temperature
T_d	$°C$	Decomposition Temperature
T_g	$°C/°K$	Glass Transition Temperature
T_m	$°C/°K$	Melting Temperature

T_s	$°C/°K$	Solidus Temperature (=T_m)
T_{SC}	$°C/°K$	Crystalline Melting Temperature
δu^*	m	Virtual Displacement
U	V	Electrical Voltage
v	$\frac{m}{s}$	Velocity
w	m	Width
W_d	J	Deformation Work

Indices

$\parallel$	In Fibre Direction
$\perp$	Perpendicular/Transverse Fibre Direction
f	Fibre
m	Matrix

Coordinate Systems

x, z	Global Robot Coordinate System
ξ, ζ	Local Coordinate System

1 Introduction

1.1 Market Review

In the last decades, aviation industry expedited a change climaxing in the recent years with the newest aircraft types of the market leaders AIRBUS and BOEING. The A350 and 787 Dreamliner, respectively, are the first aircraft in history manufactured predominantly of composite materials. Both are the outcome of trend which has been growing for about 50 years (Figure 1.1).

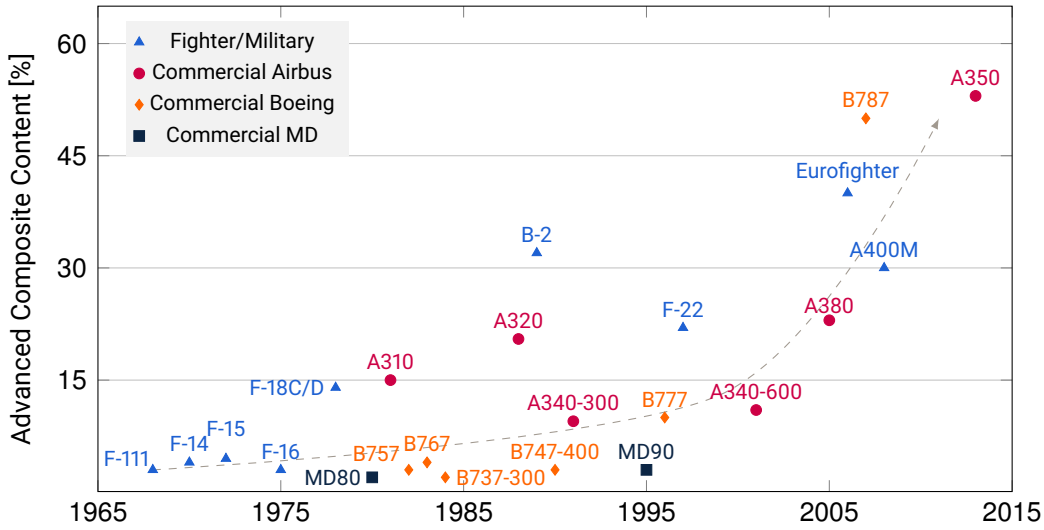

Figure 1.1 – Composite Content in Aviation Structures 1965-2015 (Data: Teßmer 2006, 5; Noor 2000, 32)

Initially discovered due to its lightweight and strength potentials, the utilisation of composite materials is these days driven by the pursuit of developing more efficient products concerning fuel consumption and air pollution, incorporating improvements in payload capacity and operating range. Such solutions are received with open arms by pressured airlines competing with low-cost carriers on the market.

Originally used only for secondary structures[1], composites have nowadays become the backbone of a modern aircraft forming essential fuselage and wing components. Although lightweight potentials are by far not exhausted due to certification requirements, aircraft performance has improved impressively with the development of various resin

1. non-load bearing structures that do not cause immediate danger upon failure

and fibre types. Starting with the invention of epoxy resins in the 1940s, followed by the invention of glass fibres in 1963 and carbon fibres in 1970, the corner stone for high strength applications was laid (Gerdeen et al. 2005, 5). Today, it is not possible to imagine aircraft manufacturing without carbon, glass or aramid fibres often times in combination with polymeric matrix.

1.2 Clean Sky Project

Apart from strongly risen number of passengers over the last years (UN DESA and Boeing 2014) and the predicted ongoing increase in air traffic and fleet size (Boeing 2016; DLR 2015, 4), there is a growing awareness of climate change, too, contrasting these trends. Focal points lie on the need to reduce greenhouse gases and further sources of environmental pollution without hampering efforts of a globalised market and society as this achievement is essentially based on developments and affordability of flights all over the globe. Furthermore it is not only about contributing to environmental sustainability but also to support European economy's competitiveness.

Picking up this trend, as part of the EU Horizon 2020 research and innovation programme by the European Union Funding for Research & Innovation, Clean Sky was founded as an initiative of the European Commission and the European aviation industry aimed at developing innovative, cutting-edge technology for future aircraft with reduced CO_2, gas emissions and noise levels. The new Clean Sky 2 Programme is scheduled from 2014 to 2020, in total, 527 institutions from 24 countries participate in this joint undertaking with a total budget of 4 € billion (Clean Sky JU 2016).

This work is located within the work stream conducted by AIRBUS and the GERMAN AERSPACE CENTER (DLR) targeted at developing a complete new approach of aircraft with thermoplastic primary structure and associated processes.

The DLR Institute of Structures and Design investigates in Augsburg and Stuttgart developments of thermoplastic high-performance structures focussing on holistic observation of a continuous process chain. This ranges from development of the construction and production technology to flexible automation solutions for production of carbon fibre reinforced thermoplastics.

Especially fusion bonding processes offer an opportunity for thermoplastic structural parts since they provide high-strength, areal and dense joints with a concurrent high potential for automation. So far, these joining methods have not been deployed in aircraft series production yet. In particular for the longitudinal seams of aircraft skins, special challenges arise.

1.3 Main Challenges

Although this trend of composites comes along with advantageous properties – especially low density and thus high specific strength –, there are disadvantages which must not be neglected. Aviation industry is facing new challenges with this promising material type.

Many manufacturing steps for composites are still completely manual, demand skilled workers and much high quality process materials which are wasted after curing. All in all, it is still a time, material and cost intensive manufacturing compared to conservative metal constructions.

Especially the joining approach is borrowed from well-known process in metal aircraft production, e.g. A320 family. Mostly deployed joining type even for composite structures is conventional riveting[2] which is not adequate for fibrous compounds.

As consequence, maintenance and repairability become complicated and costly – if even possible. Mostly deployed thermoset matrix systems which cannot be remolten after curing process divine another aspect of maintenance issue. Recycling comes into play here, too.

2. standard aluminium solid rivets were replaced by Hi-Lok™or Hi-Lite™fasteners for composite applications

1.4 Thesis' Structure

Composite materials have successfully arrived in aviation industry only at a first glance. In the next chapter, the state of the art in aircraft construction and composite technology is presented finally outlining potentials and requirements via the introduction of evaluation criteria. Chapter 3 gives a detailed overview of fusion joining processes setting spotlights on ultrasonic, resistance and induction welding. Subsequently, the evaluation of the latter three most promising process methods is carried out. Theoretical background about heating models, mechanism and parameters is deduced in chapter 6 relevant for the experimental set-up and parametric study in the following two chapters. The latter of both comprises a discussion of results. A transfer of these static results into a continuous welding concept development is executed in chapter 9. Finally, the conclusion provides a summary and outlook to next steps to be taken and leverage points for future developments.

2 State of the Art, Potentials and Criteria

2.1 Aircraft Structure

Main functions of the structure are to carry in-service loads, provide aerodynamic shape and attachment for other systems as well as protect payload (PAX/ cargo) from environment. Basically, the aircraft structure can be divided into primary and secondary structure. Secondary structure represents all non-load bearing structures (e.g. brackets, fairings, cowlings) rather for systems integration whereas the primary structure can be seen as skeleton of the aircraft which would endanger the aircraft upon failure. The latter is a semi-monocoque structure, i.e. a combination of a load bearing (stressed) thin sheet material skin with supporting stiffening (Figure 2.1a). These are usually (1) stringers or longerons[1], (2) circumferential frames, (3) skin and (4) clips (Figure 2.1b).

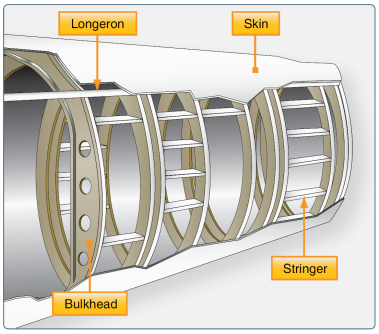

(a) Semimonocoque Aircraft Structure (FAA 2012, 1-9)

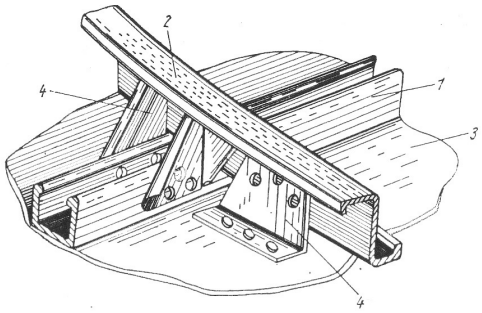

(b) Typical Aircraft Construction Joints (Schulshenko 2007, 220)

Figure 2.1 – Primary Aircraft Structure

The use of materials has shifted in the last decades, as already indicated above. Where over two-third of an aircraft was built out of aluminium and its alloys in the late 1980s (Figure 2.2a), the most recent aircraft developments consist predominantly of composites and only of one-fifth of aluminium and its alloys (Figure 2.2b). A trend to use more advanced lightweight metals and alloys like titanium, lithium and magnesium is remarkable, too.

1. “Longerons usually extend across several frame members and help the skin support primary bending loads. [...] These longitudinal members [Stringers] are typically more numerous and lighter in weight than the longerons.” (FAA 2012, 1-9)

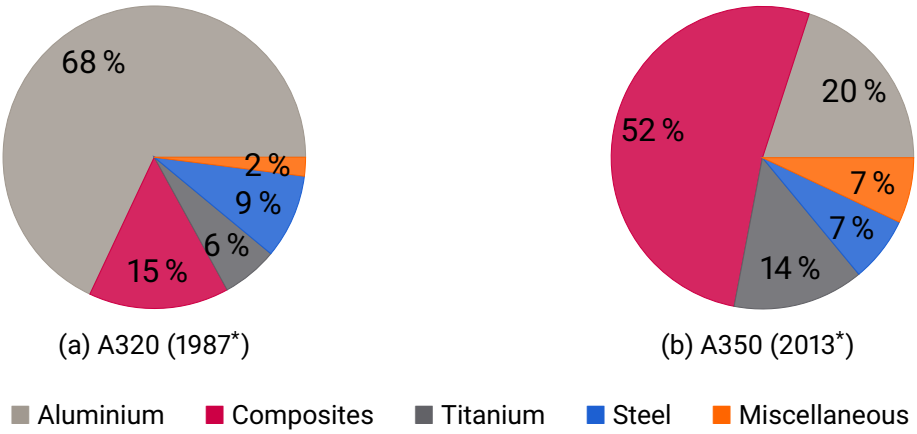

Figure 2.2 – Share of Structural Materials of Airbus Aircraft
(*Year of Maiden Flight; Data: Sturma 2016)

2.2 Composites Deployment

Composites are combinations of materials to combine favourable properties of at least two different material types. In general, it can always be distinguished between matrix and fibres (Neitzel et al. 2014, 31). Fibre's main task is to carry tension loads. With the use of carbon, glass or aramid fibres in aircraft manufacturing (Visakh and Lüftl 2016, 4-117), fibre's potentials are almost exhausted. Greater opportunity for improvements provide matrix systems. Main tasks of the matrix is fixation/positioning of fibres in the compound, connection/transmission of forces among fibres/laminate plies, carrying transversal/shear loads, supporting fibres under compression loads, acting as crack stopper (ductile matrix systems) and protecting fibres from environmental effects (Schürmann 2007, 83).

Despite some rare applications of other matrix types like metal[2] or ceramic[3], "[p]olymer-matrix fibrous composites, primarily because of their high specific strength and stiffness, have found increasing application in aircraft structures. The critical need for significant weight savings[4], design flexibility, and extended flight efficiency for advanced aircraft [...] has focused attention on composites [...]" (NRC 1996, 14)

Structural observations in polymeric systems like order condition (amorphous or semi-crystalline) or degree of cross-linking are decisive for mechanical properties and ther-

2. MMC: Metal Matrix Composites
3. CMC: Ceramic Matrix Composites
4. However, MMCs with lightweight metals like magnesium, are reasonable in the aircraft branch (Kaczmar et al. 2000)

mo-mechanical behaviour of plastics. Based on that, it can be distinguished between elastomers, thermosets (TS) and thermoplastics (TP).

What all have in common are acting binding forces namely primary and secondary valence forces. Where in thermosets chemical covalent bonds (which are not weakened until decomposition temperature) prevail, thermoplastic's properties are dominated by physical inter-molecular forces enabling a softening and melting behaviour hence higher temperature dependency. However, natural limitation of usage temperature lies for all plastics at about 300°C (Hopmann and Michaeli 2015, 14; Kaiser 2015, 67-71).

Figure 2.3 shows a schematic graph of the stiffness (Young's Modulus) over temperature for the three plastic classifications. It stands to reason that TS and TP resin systems are predominantly used due to their preferable thermo-mechanical behaviour over a much wider range of temperature. Elastomers are rather characterised by their high degree of elasticity leading to other fields of application, e.g. elastomer composites for aircraft's tire carcass (Mitchell and Landgraf 1996).

It should be noted that due to partly crystalline structure, a second plateau can be recognised between the glass transition point/area (T_g) and the crystalline melting point (T_{SC}), which usually sets the service temperature range of semi-crystalline thermoplastics. This difference is often emphasised by distinction of the terms *melting* for semi-crystalline and *(gradual) softening* for amorphous materials. For simplicity, both terms shall equally describe the process of melting in the following.

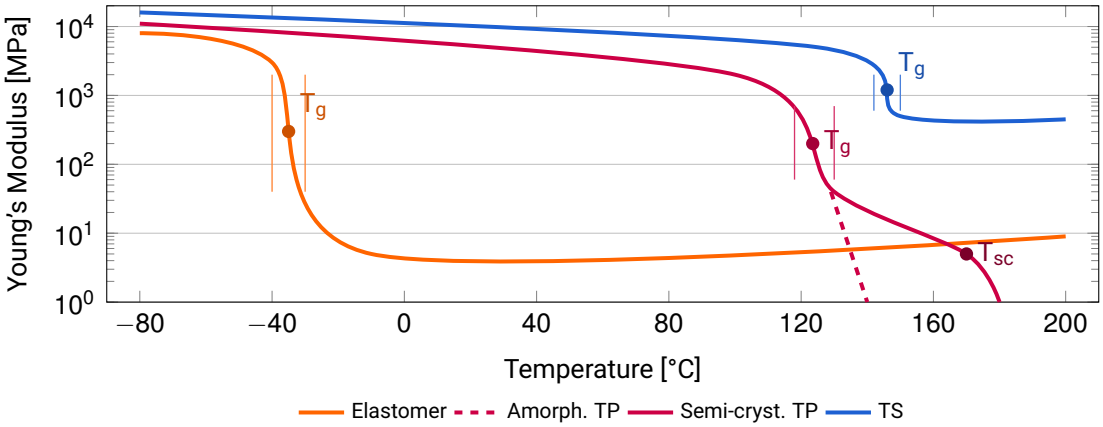

Figure 2.3 – Schematic Young's Modulus over Temperatures for the Different Plastic Classifications (Data: Domininghaus 2013, 6; Bargel and Schulze 2013, 450)

2.2.1 Thermosets (TS)

So far, thermosets are the most frequently used resin type in aviation composite applications. They show a better wetting of fibres due to low viscosity caused by missing cross-linking and low molecular weight before curing process starts. Curing process can be interrupted – actually slowed down – by cooling, too, which is intensively used for prepreg materials. Aforementioned, the net result of chemical curing is a clear solidification with increased strength, stiffness, creep resistance and glass transition/ melting temperatures as well as good thermal and chemical resistance – documented in much long-term experience. Though, TS are rather brittle and due to their non-meltable nature difficult to recycle (Strong 2008, 159-60; Schürmann 2007, 84). Eventually, melting points can be found over the decomposition temperature (T_d) hence the curing process cannot be reversed any more. In addition, curing is characterised by intensive manual preparation and long reaction times.

2.2.2 Thermoplatics (TP)

The increasing use of thermoplastic matrix systems is based on several advantages of this resin type. Although Strong (2008, 160) emphasises, the higher molecular weight (higher viscosity) makes processing of composites more difficult, on the other hand, it enhances most of physical and mechanical properties. Thermoplastic composites (TPC) profit from the absence of complex chemical reactions, slow cure kinetics hence shorter process times and no demanding cooled storage compared to TS. Among, TPCs show enhanced toughness, infinite shelf life, higher damage tolerance, fracture toughness and impact resistance as well as good fatigue resistance. Non-flammability, better environmental resistance against corrosion and solvents combined with very low level of moisture uptake hence less degradation under hot/wet conditions seem to outweigh the pros over the cons. Even of higher importance for following contemplations, TPCs provide reprocessability and repairability contributing to a more cost-effective fabrication – especially when regarding joining and recycling (Ahmed et al. 2006; Yousefpour et al. 2004; Costa et al. 2012). Nevertheless, disadvantages of high-performance thermoplastics can be named as requirements on high processing temperatures and pressure, high raw-material costs and repair procedures are not well-engineered since thermoplastics have not found its way into aerospace applications broadly (Vodicka 1996, 4).

New developments have given rise to an innovative group of high-performance thermoplastics pushing the limits towards unprecedented melting points. In particular, the

group of semi-crystalline thermoplastics exhibit a unique character with better heat resistance and higher strength properties of crystalline and more ductility of amorphous regions (Menges et al. 2014, 37) which give them higher relevance. Especially the family of polyetherketone (PEK_n) have arisen particular interest of aircraft manufacturers since they show superior properties concerning glass transition/melting temperatures and strength/stiffness, receptively (Table 2.1/Figure 2.4).

Table 2.1 – Mechanical Properties of Selected Semi-Crystalline TP and TS

		Semi-cr. TP		Thermosets		
		PEEK	PEK†	UP	VE	EP
ρ	g/cm³	1.3	1.3	1.22	1.14	1.2
E	GPa	3.5	4	4.8	4	3.4
σ	MPa	100	105	60	83	90
ε	%	5	5	2	6	5
T_g*	°C	140-145		125	130	140
T_s*	°C	343	365			
HDT*	°C	152	190	50†		80†

*T_g: glass transition temperature, T_s: solidus/melting temperature, HDT: Heat Deflection Test

Source: Schürmann 2007, 131-32; †Kaiser 2015, 448, 498

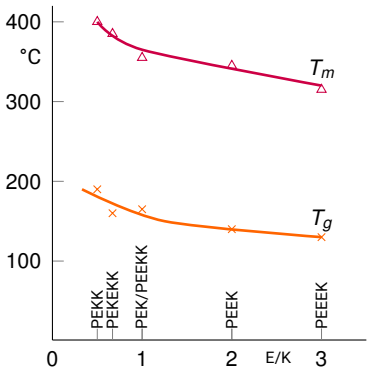

Figure 2.4 – Glass Transition/Melting Temperature of Different PEK_n Derivatives (Data: Domininghaus 2013, 1204)

"According to some industry experts, thermoplastic composites still have significant barriers to overcome before they are widely used in complex, contoured primary structures, particularly for aircraft produced in smaller volumes. These include cost, automated processing speed and quality, and lack of developed repair technologies." (Gardiner 2011) The price of PEEK is still an order of magnitude higher than average polymer systems (Tooley 2009, 199). Jen et al. (2008, 1142) report increasing applications of APC-2 composites (CF/PEEK composites; USDoD 1999, 4-302) in high performance aerospace structures due to superior mechanical properties. Such applications are the undercarriage door of C-130 Hercules aircraft by Lockheed consisting of graphite/PEEK thermoplastic composite, a composite fighter fuselage with a combination of various thermoplastic prepreg materials including AS4/PEEK (Vodicka 1996, 5) or the F-5F landing gear strut door and access panel, B-2 Bomber parts and Fokker-50 nose-wheel door (Beland 2012, 136-51).

With the enhanced properties and thus opening of the market towards thermoplastics, the composite world is changing drastically as many problems associated with the

classical thermoset matrix systems seem to be solvable now. The main drawbacks and challenges are presented in the following.

2.3 Main Drawbacks and Challenges

2.3.1 Fabrication

Composites are getting in a tight spot since material prices for aluminium and titanium – the most important lightweight metals in aircraft industry – have dropped steeply in the recent years (Tooley 2009, 199). Moreover, materials science develops continuously new lightweight metals and alloys which provide high strength and low densities, too. High standards in aerospace certification lead to even higher material costs by factor two to three (Rao et al. 2015).

"Lockheed Aeronautical Systems Company have used thermoplastics in the manufacture of an aircraft door structure [...] even though the raw material cost of the thermoplastic compared to aluminium was more than 20 times greater. Through automation the cost of assembly was drastically reduced and the final component was half the cost of the aluminium equivalent." (Vodicka 1996, 5)

Besides, fabrication processes of metal structures have become very efficient and automatised in the last decades where manufacturing composites still requires a lot of manual work and skilled labour.

For example, A350 side shells produced in the Augsburg plant are all made of prepreg/autoclave process. This production method promises the best and most accurate quality of high performance composites – paid with extensive expenses which can be identified as: (Irving and Soutis 2014, 59)

- energy demanding cooled storage of prepreg materials (limited lifetime)
- need for high added-value processing materials (thrown away afterwards)
- energy demanding curing in (argon/nitrogen) pressurised autoclave
- costly non-destructive inspection (NDI) methods to guarantee high quality
- labour-intensive process steps (stacking/lay-up/bagging/demoulding)

Shehab et al. (2013, 431) provide an estimation of production time and manufacturing cost for a single curved composite panel out of prepreg hand lay-up and autoclave curing process with ultrasonic NDT – use case is reasonably comparable with an aircraft shell. Just about two third of process time is directly related to the product (stacking,

curing, finishing, testing), but almost 30 % are used for preparation or other process steps. Regarding expenses, material costs still make up the largest part of overall manufacturing costs, followed by labour costs with almost one fifth – due to many manual steps and highly skilled workers. Automation and reduction of preparing steps would lead to a better fabrication efficiency.

In turn, Fokker (2013, 13) lists advancements in thermoplastic fabrication as "more freedom in defining form and in the number of production steps, [...] increase in speed and simplicity", as well as comparably easy realisation of integral structures instead of one-shot necessity.

Integral structures are also the aim of newest developments edging into the market: additive layer manufacturing (ALM). Although not ready for series production of primary aircraft structures, this trend could open a complete new way of engineering in the near future as it offers an even higher grade of tailoring and thus lightweight potential in aerospace applications definitely competing with composites. Analysing for specific load paths, material is produced only in position and direction needed using electron beam melting (EBM) or more common selective laser melting (SLM) processes, e.g. with titanium powder for high strength properties (Figure 2.5).

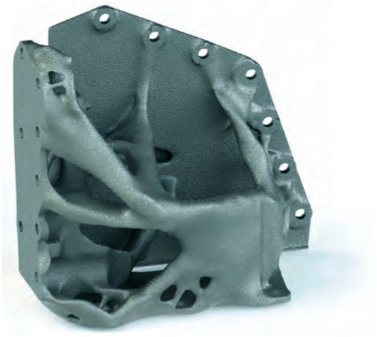

Figure 2.5 – MG Bracket Rear (Löwer 2017)

2.3.2 Joining

Classical metal construction in aviation branch is well known, huge experience and a lot of data has been gained throughout the last 50 years. Manufacturing methods and processes are rather easy as well as detectability and repairability during maintenance.

Based on that, aviation industry tried to implement composites very quickly by just "replacing material" rather than developing a suitable manufacturing method. The consequence is called "black metal design". Carbon-fibre reinforced plastics (CFRP) with their characteristic black colour joined together with classical metal joining methods like riveting or bolting.

Although the use of fasteners provides a robust process capable of high volume production and joining of dissimilar materials combined with the ability to reopen and a broad range of fastener types (Rotheiser 2004, 244), problems with mechanical fastening are also well-known and reported repeatedly in literature (Ageorges et al. 2001; Strong 1993; Schwartz 1994; Todd 1990; Qin et al. 2013):

- Local stress concentrations at notches, drillings and cut-outs which cannot be balanced due to lack of plasticity
- Risk of delaminations originating during drilling holes
- Different CTE[5] of fasteners and composite lead to thermal stresses
- Enhanced corrosion and sealing issue, either by different galvanic potentials of fastener and CFRP or by intruding fluids (drainage areas/fuel) between fasteners and composite
- Destruction of physical and electrical continuity in fibrous composites
- Expensive drilling tool demand and high labour skills required
- Long process times for drilling operation ($\approx$5000 holes per shell)
- High number of fasteners required lead to additional weight

Regarding the latter, Vodicka reports a Lockheed investigation of an aircraft door structure: "The aluminium door consisted of 67 parts and 465 fasteners while the thermoplastic equivalent used only 12 parts and 20 fasteners. [... T]he weight of the part ... was already 18 % lighter than the aluminium equivalent." (1996, 5) Integration and assembly costs for an aircraft structure are estimated as 19-42 % of the final aircraft cost (Wedgewood and Hardy 1996).

A more fibre-fair approach and already widely spread is adhesive bonding. This method creates joints over large areas with uniform stress distribution, dissimilar materials, good fatigue behaviour whilst providing weight savings and incorporated sealing (Rotheiser 2004, 194-95). Though, associated disadvantages are also renowned as intensive surface preparation, difficult process control in industrial environment, long curing cycles, required skilled labour and no compatibility amongst some plastic materials as well as with mass production benchmarks (Ahmed et al. 2006; Schwartz 1994).

Their utilisation is based on the fact that these two methods are the only possible for TS matrices. Moreover, fasteners offer a very reliable and predictable joining method (Ageorges and Ye 2012, 8). Therefore, main potential lies in the development of a fi-

5. Coefficient of Thermal Expansion

bre-fair, mass production compatible, reliable and predictable joining method desirably without foreign objects.

2.3.3 Maintenance

Neglecting defects caused during manufacturing, in service life, an aircraft is exposed to many different sources of damage. Therefore, certification authorities like EASA or FAA introduced the condition of "Airworthiness"[6] which is initially conferred. Continuing airworthiness needs to be achieved and sustained through a systematic approach of maintenance task and actions to minimise the risk of catastrophic failure caused by manufacturing defects, corrosion, fatigue and accidental damage.

Not only, metals are more insensitive compared to composites and less prone to impact damages due to elastic and plastic deformation. Moreover, composites are more difficult to examine, detect and repair. Where scratches, buckling or folds in metallic structure indicate clearly an area requiring repair (e.g. via doublers in unpressurised areas; Figure 2.6a), most defects in composites are hidden within the structure disguising true scale of damage. Damage during service is most abundantly caused by low velocity and rarely high velocity impacts. Matrix cracking and delamination invisible for naked eye is then referred to as "barely visible impact damage" (BVID). There are several repair approaches: 1) *patch repair* applying a patch overlapping and bonding to the surface of original laminate leading to a thicker structure and original strength. 2) *Taper sanded* or *scarf repair* are rather deployed to modern commercial aircraft. The detected damage area is sanded circular (Figure 2.6b) in order to expose a section of each ply until the damage is reached. By adding adhesive and overlapping plies (Figure 2.6c), thickness is nearly remained, but a straighter and stronger load path is created. This technique requires high skilled workers and due to its costlier method more time. Bolted repairs in composites structures are rather counter-productive and thus seldom, but possible and then quick, easy and heavier (R. A. Smith 2001; Zhang and Rong 2011, 1-7; FAA 2012, 7-28-45).

Thermoplastics and their ability to be remelted could ease maintenance tasks especially in terms of replacing damaged structure and reduce maintenance effort and time drastically.

6. Airworthiness is the aircraft's ability to fly in safe conditions within allowable limits

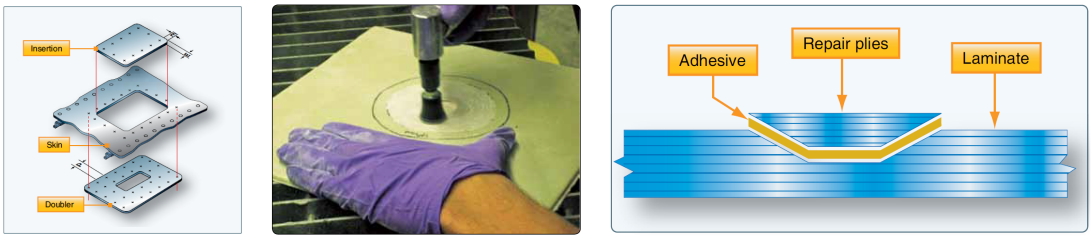

(a) Metallic Repair (b) Circular Sanding (c) Schematic Taper Repair

Figure 2.6 – Aircraft Repair Methods (FAA 2012, 4-97, 7-36, 7-39)

2.3.4 Recycling

Before major attention was drawn towards environment protection, composite waste was disposed on landfills. The European Union established the "Directive on Landfill of Waste" in order to reduce the amount of organic material landfilled hence the prohibition to landfill composites waste any more (EU 1999). Only one year later in 2000, the European Union introduced the "Directive on End-of Life Vehicle" (ELV) 2000/53/EC redeeming the consequences of motor vehicles at the end of their lifetime causing eight to nine tonnes waste per annum. The directive regulate by law a degree of recycling of 95 % of initial vehicle weight from 2015 on (EU 2000). The "*Process for Advanced Management of End of Life of Aircraft*" (PAMELA) project builds on the ELV directive for the aviation sector. "Although aircraft are made of materials that can be recycled or reused in a number of ways, prior to PAMELA there were no standardised procedures. PAMELA sought to fill this void, firstly by ensuring compliance with relevant waste regulation, and then, on a voluntary basis, by working towards achieving a target recycling rate of 85 %, comparable to the EU End-of-Life Vehicles Directive (2000/53/ EC), which does not currently apply to aircraft." (EC 2011) As consequence, new joining technologies shall enable a later recycling and not introduce materials that cannot be recycled any more. PAMELA reduced the non-recoverable material proportion out of a 61 tonnes aircraft down to 13 %.

So far, with the use of predominantly (non-meltable) thermoset matrix systems, recycling proved difficult. Mechanical processing (crushing) produces powdered or fibrous recycling products still as mixtures of original materials. Fibre reclamation uses aggressive thermal or chemical processes to separate fibres from matrix and is – due to their thermal and chemical stability – very suitable for carbon fibres. Besides, thermal processes are used in order to destruct the chemical cross-linking of thermosets. Most widely spread is *pyrolysis*, a thermal decomposition of organic molecules in inert atmo-

sphere. Also oxidation in fluidised bed, i.e. combustion in an oxygen-rich environment is field-tested. Chemical approaches use reactive media like catalytic solutions, benzyl alcohol or supercritical fluids. Finally, combustion with energy and material utilisation is still an – even if undesired – option, making use of the waste's calorific value when burning (Pimenta and Pinho 2011; Pickering 2006).

Thermoplastics could open a complete new field for recycling. By simply reheating, separation process can be eased drastically. Since no chemical reaction takes place, the original state can be almost fully restored. "In this fashion, material usage efficiencies approaching 100 % can be reached." (Rotheiser 2004, 71) Either grinding/shredding techniques for getting high-quality reinforcing material (press/injection moulding applications) or thermoforming processes for repurposing structures (Li and Englund 2017; Schinner et al. 1996).

2.4 Evaluation Criteria

Based on aforementioned drawbacks of state of the art technologies, evaluation criteria shall be set in order to better exploit potentials of composites in terms of mechanical performance, production efficiency and fibre-fairness design.

Furthermore, it is necessary to clarify the scope of relevance and priority of different process related characteristics even before reflections on available fusion bonding technologies are made to set spotlights on important facets.

Besides fundamental evaluation criteria in industrial environment such as concerning cycle time, costs, flexibility or heat affected zone (HAZ), more attention shall be drawn towards the driving criteria in this special case which are rated as primary evaluation criteria (Figure 2.9). These comprise in particular process capabilities and aircraft applicability with its respective derivatives and will be rated doubled in the following assessment system contrary to secondary criteria. A short legitimation of investigated criteria follows in the subsequent paragraphs.

2.4.1 Prerequisites

What should be pointed out is the fact that Chapter 3 gives an overview of available fusion bonding technologies in general. Not all of them do fulfil given prerequisites. Those will only round out the overview and present state of the art fusion technologies while being excluded a priori from later decision process.

These prerequisites comprise fibre-fairness (no fibre interruption/distortion), longitudinal areal lap joints (no butt joints), only use of a thermoplastic matrix system, maintaining (aerodynamic) shapes and surfaces while access is only possible from one side (adherend in tooling) and regards to large parts size.

2.4.2 Process Capability

Parameter. Seen as very crucial is the *cycle time*. It decisively influences the productivity hence guaranteeing a required production output (Sakamoto 2010). Exact quantification has not been stated yet, so relative proportion will tip the balance.

Two others regarded are *process pressure/forces* and *energy consumption*. Both are assigned to the sections *Automation* and *Environmental Aspects*, respectively.

Automation. Since degree of automation in composite parts manufacturing of aircraft industry is still relatively low compared to other branches namely automotive[7], future competitiveness in aircraft manufacturing will strongly depend upon the change from manual to automated processes. Already in 1993, US International Trade Commission claimed that the "[...] higher level of production automation at Airbus contributes to offsetting this [*author's note:* although similar commonality in aircraft derivatives but smaller production scales occurring] labor productivity disparity." (1993, 4-10) Chursin and Makarov (2015, 193-243) assign a direct mathematical relation of automation to competitiveness in their *Quantitative Evaluation of the Firm Competitiveness*.

Among the catchphrase "Automation", *closed loop capability* and *robotic capability* are of special interest.

For an automated system in high quality production, a balanced and stable control circle is necessary. This should not only maintain the process but detect and correct possible disturbances. For this purpose, distinctive process parameters must be recorded and processed. Also insensitivity to disturbances in general is important. There is a cross-link to *Reproducibility*, too.

Robots – due to their six axis construction – are prone to high process forces, especially in the far distance field. Reproducibility and repeatability suffer from harmful effects caused by such high forces and moments. Furthermore, size and thus price is dependent on weight and dimensions of the used end effector.

Process Chain Adoption. Process chain adoption represents the ability of a quick, simple and cheap implementation of new technologies in existing series production. Special regards shall be made onto *tooling*, *surface preparation* and *manufacturing schedule*.

State of the art production consists of negative metal toolings for automated fibre placement (AFP) of UD plies (Figure 2.7). Corrections or new acquisition of auxiliaries are expensive and time-consuming hindering a desired quick implementation. Same is valid for the manufacturing schedule. These procedures are highly developed and fundamental changes can imply long periods until series production is back in desired steady-state. Surface preparation partly picks up the automation target since most manual steps shall be minimised as far as possible in order to improve productivity.

7. BMW set new standards with an very high degree of automation in their i3 production reducing cycle times by factor 30 (Schulze 2013). Amongst others, adhesive bonding technique used in production is even fully automated (BMW Group 2017).

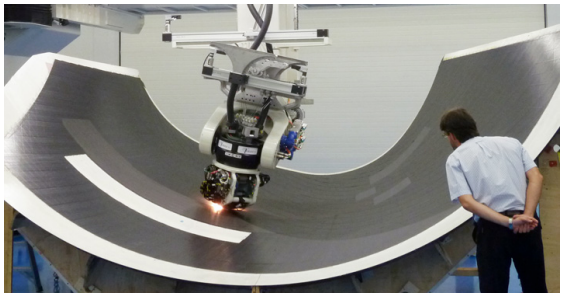

Figure 2.7 – Current Automated Fibre Placement Production Method (MTorres 2012)

2.4.3 Aircraft Applicability

Aircraft manufacturing sets special standards due to presence of certification authorities. But also in terms of product size and tolerances, aviation industry is confronted with other challenges than automotive or civil engineering.

Geometry. Geometry of parts exhibit probably the largest product dimensions[8] in engineering and therefore transfer from laboratory scale to large scale joining and continuity of joining process is very important. Since already Figure 2.1 implied, especially longitudinal stiffener elements (longerons/stringers) are in charge of supporting the skin and taking up primary bending loads over the whole length of the aircraft. A continuous joint is therefore essential to enable an ideal force flow without too high local stress concentrations which would lead to additional local reinforcements hence more material and weight – always a crucial parameter in aviation. Only local joining methods, e.g. spot welding, are eliminated self-evidently a priori by this prerequisite.

Lap joint design and accessibility is characterised by the scope of this work to form longitudinal lap joints peculiarly of different section parts (upper/lower/side shells) to assemble one barrel of aircraft section as well as longitudinal stringer joining over length of a section. Airbus (2006) promoted the so-called "*4 shells concept*" (Figure 2.8a) with associated advantage of weight savings due to solely lap joints needed, a lay-up and skin thickness optimisation and individually tailored panels to local load cases. They made another change in stringer design, too, according to new demands on joining technologies for CFRP structures. Since classical mechanical riveting was replaced by adhesive bonding, conservatively shaped stringers (Figure 2.8b) were replaced by new composite omega shaped stringers (Figure 2.8c) which provide a greater surface important for

8. A350-900 rear fuselage section (S16/18) side shell: length– 20 m, width– 6 m

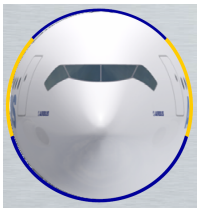

(a) 4 Shells Concept (Airbus 2006)

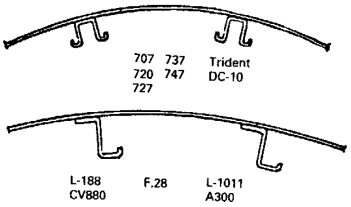

(b) Conservative Stringer Shapes (Niu and Niu 1999, 381)

(c) A350 Composite Omega Stringer (Luratec 2015)

Figure 2.8 – New Developments in A350 Structural Design

bonding lines and better inspectability. Both aforementioned changes are based on a lap joint design or areal joining interface.

Performance. Peformance is generally characterised by static and dynamic considerations. As static quantification, lap shear strength (LSS) if often referred to according to test procedure ASTM D1002[9]. German and European test standards are provided by DIN EN 1465[10], 2243[11] or 14869[12]. Villegas et al. (2013) regards fracture surface analysis as supplementing measurement to LSS determination, since Guess and Allred (1977) and Gleich et al. (2001) showed both the dependency of joint geometry on shear and peel stresses decisive for determined results.

Double cantilever beam (DCB) test is a standard test method to determine bond strengths. Regarded is energy per unit plate width required to create a unit crack growth as a result of peel forces perpendicular to crack plane. This values is referred to as G_{Ic}. Testing methods are described in ASTM D5528-13[13] or DIN EN 6033[14] The simplicity of experimental set-up, execution and evaluation with linear elastic fracture mechanics (Liu and Gent 1991, 1) has it made used frequently in testing composite components.

Besides static considerations, especially in aviation structures, cyclic stresses are of high importance. Therefore it is reasonable to execute a durability testing, too. Basis for comparability gives an S-N curve or WÖHLER *diagram* showing maximum stress am-

9. ASTM D1002: "Standard Test Method for Apparent Shear Strength of Single-Lap-Joint Adhesively Bonded Metal Specimens by Tension Loading (Metal-to-Metal)"
10. DIN EN 1465: "Determination of tensile lap-shear strength of bonded assemblies"
11. DIN EN 2243: "Non-metallic materials - Structural adhesives - Test method"
12. DIN EN 14869: "Determination of shear behaviour of structural bonds"
13. ASTM D5528-13: "Standard Test Method for Mode I Interlaminar Fracture Toughness of Unidirectional Fiber-Reinforced Polymer Matrix Composites"
14. EN 6033: "Carbon fibre reinforced plastics – Test method – Determination of interlaminar fracture toughness energy"

plitude over achieved number of cycles until failure. Below a certain limit of applied load – called *endurance limit* – no fatigue failure is expected. The procedure follows ASTM D1002, too.

As aforementioned, fracture surface analysis gives additional information about failure modes and thus possible weak points in the joint. Detection and propagation of failure types can be derived too with regard to certification and maintenance issues. Important criteria is the systematics or randomness of occurring failures in dependence of the failure mode.

Certification. Certification authorities – most noted representatives are in shape of EASA (Europe), FAA (North America) and CASA (Australia) – are responsible for control and execution of standards to guarantee aircraft's ability to fly in safe conditions – called airworthiness. By certifying the aircraft as well as its production, initial airworthiness is conferred. Since these certification authorities have gained its experience and ambition over decades of aviation and aviation accidents, certification framework has become very strict and distinctive aiming at making flying as safe as possible. On the other hand, in case of an accident, source of damage and failure should be identified in any case to establish appropriate countermeasures.

For this purpose, full traceability of executed manufacturing steps and used material batches must be enable. Process parameters, quality control and record of data go hand in hand. Derivatives of this philosophy are requirements on *reproducibility* and *online inspection* to maintain a degree of quality for initially checked production. If a process exhibits high scatter, random failure occurrence or failure proneness just as poor inspectability and less insight opportunities, certification is likely to be denied by certification authorities.

Since used materials must be certified, too, in order to eliminate unknown materials interactions, introduction of foreign materials is seen highly critical. Moreover, material compounds can show effects like galvanic corrosion, poor adhesion or introduced micro-cracks and notches causing stress concentrations which do most certainly influence short-term and long-term static and dynamic material properties with unpredictable consequences. Therefore, these cases must be avoided as possible.

2.4.4 Other Secondary Criteria

Investment. With every new technology and affiliated acquisition costs, question of investment and particularly of cost-benefit ratio comes along. *Cambridge Advanced Learner's Dictionary* defines *investment* as "the act of putting money, effort, time, etc. into something to make a profit or get an advantage, or the money, effort, time, etc. used to do this." (CUP 2008, 761)

It is difficult to quantify acquisition costs as they are depended on equipment, features, purchase quantity, conditions and offers. An indication shall be given relatively by equipment complexity and presence of recurring costs (RC).

Fibre-Fairness. One of the biggest disadvantages of conventional joining processes like bolting or riveting is the absence of fibre-fairness since load-carrying fibres are cut in order to drill rivet holes. Adhesive bonding follows the right approach which is picked up by fusion bonding techniques in general. This criteria should only confirm this point for regarded methods.

Heating Characteristics. Heating characteristics incorporate in this case basically two points of consideration: firstly, the heat affected zone (HAZ) which usually refers to area of heat induced. An important issue may be anisotropic behaviour of composites with high thermal conductivities in and low thermal conductivity perpendicular fibre direction. Desired is a distinct heating area with a concentration of input energy in the respective zone. Of equal importance is, secondly, the heating curve setting on the frame for maximum heating rates and thus cycle times. On the other hand, a too fast heating can either cause material damage or overshooting temperatures above desired melting range. In worst case, such an – even short – overheating can cause material decomposition and therefore weakening of the whole component. A balance between heating speed and safe temperature envelope must be found.

Maintenance. "Maintenance" is an important topic in aviation industry for two reasons: firstly, for continuing airworthiness and thus permission to use an aircraft in commercial service, a meticulous maintenance schedule is predefined in order to detect, repair and thus minimise the risk of catastrophic failure. Secondly, this goal turns out to be crucial since the design service goal (DSG) – desired life time an aircraft – usually ranges between 20 to 40 years. The importance of maintenance becomes obvious. In this con-

text, question of detachability hence replaceability of damaged parts/structure plays a major role as well as the portability of maintenance equipment.

Environmental Aspects. In the backdrop of Clean Sky and positioning of this work in the context of reduced CO_2/gas emissions and noise levels, the ambition to follow this mindset also during manufacturing is reasonable. The spotlight shall be turned to energy consumption of joining methods, responsible use of resources, presence of hazardous materials as well as recycling during manufacturing and after reaching the end of service life with a glance at legal framework presented in Section 2.3.4 on *Recycling*.

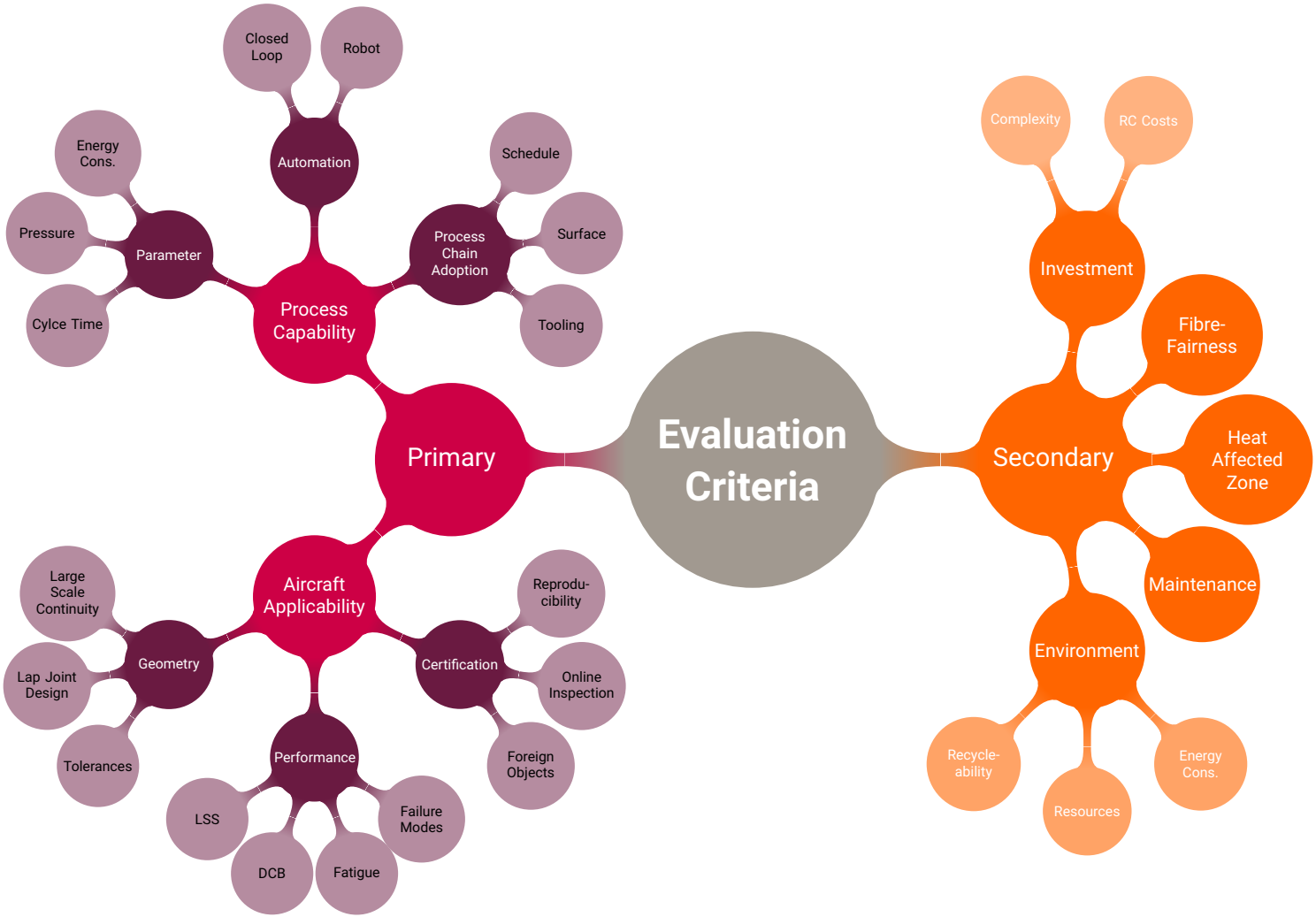

Figure 2.9 – Primary and Secondary Evaluation Criteria

3 Overview on Fusion Joining Processes

In literature, many different classifications and clusterings of joining technologies can be found (Neitzel et al. 2014, 469; Yousefpour et al. 2004, 305; Stokes 1989, 1312-13; Rudolf et al. 1999, 310). Commonly, they are divided into groups of mechanical fastening, adhesive and fusion bonding. The first two can be assigned to conventional state of the art technologies which shall be replaced.

Fusion bonding, also known as welding, describes according to DIN 1910-100 a process of joining two or more parts via creation of a material continuity under application of heat and/or force with/without a filler (DIN 1910-100 2005). The advantage lies in achieving bulk material strength in the welding joint and in its empirical values over decades. Assembly can be achieved by heating thermoplastic material at a temperature above melting point.

Generally, characteristics of heating classify fusion techniques. Detachability of the created joint can play a role, too. In the considered case, both conventional types (mechanical fastening/adhesive bonding) produce non-detachable, whereas fusion bonding provides also detachable joints. A modified overview and classification of Ageorges et al. (2001, 845) can be found in Figure 3.1, since he determined four classes of heat introduction: bulk, two stage, frictional and electromagnetic heating. Within this clusters several – sometimes highly developed – joining technologies are located.

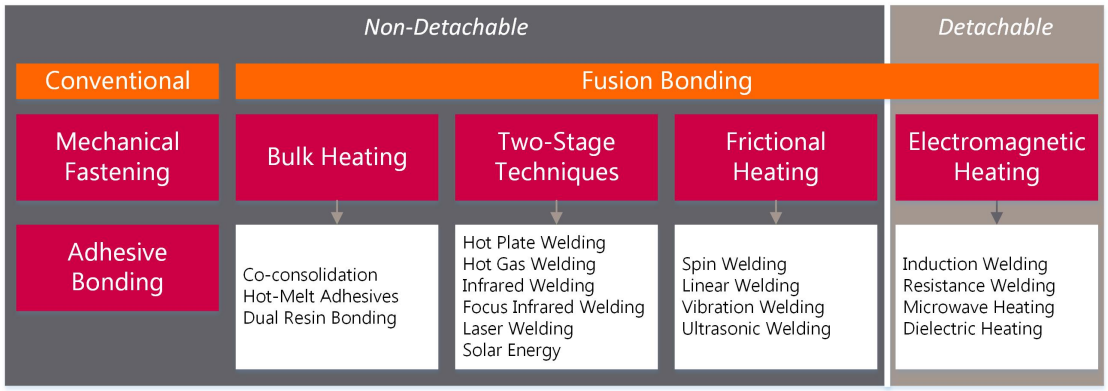

Figure 3.1 – Overview and Classification of Joining Techniques

Without prejudice, several studies state independently that the most promising approaches in fusion bonding technologies for composites are ultrasonic, resistance and induction welding (Ageorges et al. 2001; Yousefpour et al. 2004; Ahmed et al. 2006).

In accordance to that, these three types will be elucidated more detailed than the brief introductions of other techniques which shall only round out the listing. Final evaluation shall be done regarding this three types only, too.

3.1 Bulk Heating

Co-consolidation as a bulk heating typically resembles affiliated bulk processes like autoclaving, compression moulding or diaphragm forming. Basically, the entire part is heated up to solidus temperature; thus, strength properties achieved usually equal parent materials. Though, since pressure needs to be applied during the whole process to prevent deconsolidation, complex tooling is necessary. Advantages are absence of additional material hence no weight added and no surface preparation is needed (Ageorges and Ye 2012, 19; Zhang and Rong 2011, 6). Obviously, this process is rather insufficient for large and complex parts (Davies et al. 1991, 1035). Notwithstanding, it was already used for McDonnel Douglas helicopter primary flight structure consisting of CF-PEEK (Jouin et al. 1991), similar to the system envisaged in the regarded case.

For Hot-Melt Adhesives, a thermoplastic adhesive film is inserted at the bondline in molten state creating the bondline after solidification. This film acts as shim between two parts to be joined, too (Zhang and Rong 2011, 6). Don et al. (1990) showed the effect of amorphous interface layers to lower scatter for strength properties. Both, Davies et al. (1991) and Fish et al. (1992) investigated enhanced properties of APC-2 bondings with PEEK hot melt adhesive films.

Dual Resin Bonding, Amorphous Bonding, or Thermabond® processes consist of an amorphous thermoplastic interlayer film, co-moulded in a semi-crystalline thermoplastic laminate prior to bonding. Compatibility at a molecular level of both, amorphous and semi-crystalline matrix system, and thus good adhesion is essential for optimum properties. Already during laminating process, the interlayer films are positioned at the later areas to be bonded. Consolidation process creates a state where both materials are present in molten state which is necessary to form the bond between both polymers. After cooling, a thin layer of interlayer material remains on the surface. True joining is eventually achieved by heating the interlayer over its glass transition temperature, but below melting temperature of remaining composite structure (Smiley et al. 1991, 527; Ageorges and Ye 2012, 20; Zhang and Rong 2011, 6).

For Thermabond® processes, a PEI film is combined with an APC-2 laminate. This comes as ideal combination of materials since PEEK provides best mechanical properties among thermoplastics and PEI leaves a sufficient wide processing window preventing deterioration of structure with a over 100°C lower melting point, displayed in Figure 3.2.

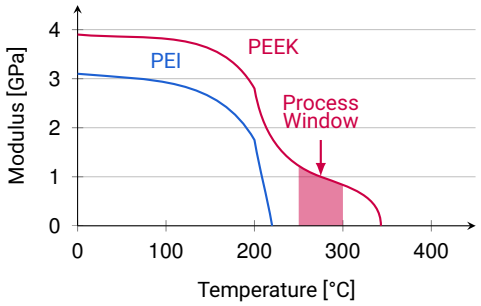

Figure 3.2 – Process Window of Thermabond® Process (Data: Smiley et al. 1991, 527)

Extensive studies were carried out on dual resin joining. Davies et al. (1991) found higher lap shear strengths for PEI films compared to PEI coated APC-2 laminates.

But Smiley et al. (1991) point out the crucial correlation of preparation prior to co--moulding and later achieved LSS. Very critical point for aircraft structures is the reported reduction in strength for low temperatures of about −54°C (Wu 1991). Besides, amorphous interlayer showed degradation when exposed to solvents such as hydraulic fluid unlike hot-wet conditions (Davies et al. 1991; Smiley et al. 1991). Ageorges and Ye (2001a) investigated resistance welding (Section 3.4.2) of thermoset-thermoplastic compounds of epoxy composites with PEI film.

3.2 Two-stage Techniques

In two-stage procedures, heat is introduced by an external heat source which must be removed before joining stage. Thus, size of joining parts is limited as a whole. Due to the heating technique – with highest temperatures below skin –, low thermal conductivity of composites lead to long cycle times (up to 30 minutes for large parts). Moreover, high pressures during heating and particularly joining ensure good consolidation, yet, can cause warpage/flow in hotter inner regions of the laminate. Another main disadvantage is the possibility of contaminations and inclusions (Ageorges et al. 2001).

One of the most popular approaches within this group is Hot Plate Welding due to its simple, robust and efficient process with strong welds. A crucial process parameter is the pressure parts to be joined are pressed against the hot tool since, if too little, no good heat conduction is achieved and if too high, melt may be pushed out of the bondline (precaution taken with mechanical stops). To prevent molten plastic from sticking to the tool, it is usually coated with PTFE. A classical hot plate welding process consists

of four phases: heating, tool removal, joining and consolidation (Figure 3.3a) Typical applications are in automotive and infrastructure sector, e.g. joining of large-diameter plastic pipes (PDL 2008, 9-13; Stokes 1989).

Hot Gas Welding and Extrusion Welding uses hot gas (instead open flame as for metals) for heating bond surfaces forming a groove for pushing in a filler rod, respectively – for extrusion welding – molten filler material is extruded into the joint. This process shows good automation possibility albeit mostly applied manually. Unless high flexibility in part geometry and complexity just as portability of equipment, it is a slow and difficult to control process hence not suitable for high-volume production (Yousefpour et al. 2004; Stokes 1989).

Infrared Welding (IRW) is rather new and a non-contact joining method within this subgroup using high-intensity quartz lamps emitting intense IR radiation to heat the bonding surfaces (Figure 3.3b). Advantages are high heating rates, reduced contamination risk hence higher reproducibility with low scatter strength properties (good for certification issues) as well as flexibility to join large flat or curved parts and good automation potential with online inspection. Disadvantages can be noted as strong dependence of the heating process on the colour of parts influencing absorption characteristics. This irregularities can lead to surface overheating or deconsolidation and warpage for deep heat penetration (Yousefpour et al. 2004; Costa et al. 2012).

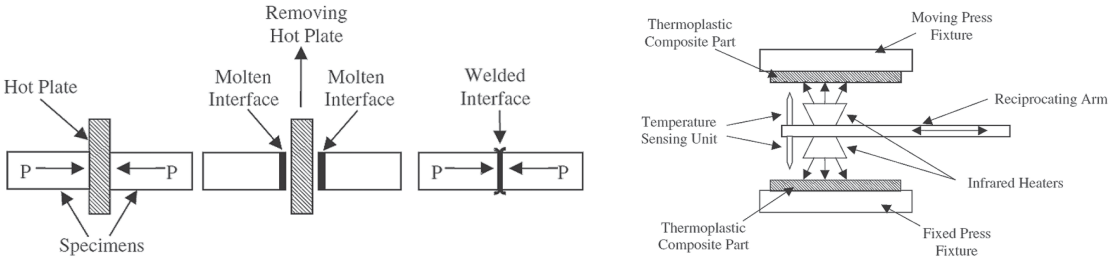

(a) Schematic Phases of Hot-Tool Welding

(b) Schematic Infrared Heating

Figure 3.3 – Two-Stage Techniques (Costa et al. 2012, 260-61)

Laser Beam Welding (LBW) or Laser Transmission Welding (LTW) in context of thermoplastic composites is also a rather new and not deeply investigated non-contact technology but promising in terms of suitability especially for thin to medium thick parts in aerospace applications. “Moreover, size, geometrical requirements, and specifications of aeronautical parts can be more easily fulfilled by applying LTW technique rather than alternative technologies.” (Labeas et al. 2010, 114) Notwithstanding, one of the joining parts (top materials) needs to be transparent in order to guarantee absorption of laser

energy by the bottom material and simultaneous heating of both parts via conduction. Fibre reinforced composites are therefore eliminated for this technique. Unless "transparent" set-up, only butt joints are within possible applications of LBW. For this process, the laser beam decomposes polymeric material while a thin molten layer remains which is used to form the bondline after solidification under pressure. Either way, it exhibits low cycle times, clean process leading to weight and cost reduction while achieving acceptable strength. Drawbacks are transparency prerequisites for lap joints and laser intensity as crucial process parameter which is decisive for a successful heating rather than polymer decomposition. Most abundantly utilised in polymer welding, a laser-assisted thermoplastic composite tape/tow winding process has been developed in composites field (Yousefpour et al. 2004; Costa et al. 2012; Labeas et al. 2010).

3.3 Frictional Heating

According to the *Handbook of Plastics Joining,* frictional welding is "a welding method for thermoplastics in which friction provides the heat necessary to melt the parts a the joint interface." (PDL 2008, 525) Therefore, frictional movement classifies different heating principles.

3.3.1 Various Processes

Spin Welding was already introduced in the 1930s and is still one of the most common friction welding techniques. Circular shaped parts – whereof one is fixed and one is rotating about its axis with a defined angular velocity – are pushed together under a specific axial pressure. At the interface, rubbing due to relative movement induces frictional heat that eventually melts the polymer. After retarding, solidification forms upon cooling the bondline. The whole process can be described in four phases: 1) initial heating, 2) un-steady melting and flow, 3) steady state flow and 4) solidification. Main processes parameters are, partly aforementioned, angular velocity, welding pressure, forging pressure and welding time. For an optimum welding pressure and angular velocity, an optimum can be recognised, whereas for longer welding times a better strength can be achieved. Advantageous is the simplicity, little to no surface preparation, high weld quality with good reproducibility and a good automation of drill presses or lathes. Main disadvantages are restrictions to circular shaped parts; otherwise a angular alignment must be applied or orbital welding is getting introduced. Thereby an oscillatory motion forces each point on a small-radius circular curve. Best applicable parts are thermo-

plastic composite tubes welded together or to flat panels (Ageorges and Ye 2012, 21; Yousefpour et al. 2004; Stokes 1989).

Unlike the latter method, Linear Vibration Welding creates heat via an oscillatory movement on a linear path, but the principle of spin welding remains the same. Two parts pressed together and with a relative motion to each other in an appropriate frequency induce heat by Coulomb friction and shear stresses. Due to higher rigidity of fibre reinforced composites, higher frictional energy leads to shorter heating times. Further influence on strength has the fibre orientation, welding pressure, weld type and most important penetration depth. Moreover, this process is applicable to various thermoplastic types of small-to-medium size (flat-seamed) without intensive surface preparation. Drawbacks are inability to weld non-flat-seamed parts, low modulus thermoplastics and particularly for composites joining, fibre distortion and displacement is very likely (PDL 2008, 15-27; Stokes 1989).

Friction Stir Welding (FSW) is rather for particle-filled or short-fibre reinforced plastic since a metallic head-pin intrudes with a rotating motion in the butt weld between two closely positioned parts. The shoulder of the tool eventually sets on the surface of both parts and the heat induced softens the thermoplastic. While the tool moves along the bondline, both parts are welded together. Notwithstanding, greatest disadvantages are fibre breakage due to the penetrating tool and the restriction to butt welds (Yousefpour et al. 2004).

3.3.2 Ultrasonic Welding

Application of ultrasonic vibrations in aviation manufacturing goes far back in history: since over a hundred years, ultrasonic waves have been used as non-destructive defect detection method and are still state of the art to inspect composite aircraft parts these days (Rose et al. 2012).

The principle of Ultrasonic Welding (US) lies in oscillatory vibrations at high frequencies about 15 to 70 kHz (Costa et al. 2012) and low amplitudes of 15 to 60 µm (Stokes 1989) which act perpendicular to the faces to be joined (main process). Surface and intermolecular friction induces heat utilised to soften the thermoplastic system. Volkov et al. (1997a; 1997b) showed the influence of surface micro irregularities on later welding quality. This effect can be used when man-made asperities are introduced – called energy directors (ED) or susceptors (Ageorges et al. 2001). Once these susceptors are molten, they soften the interface with a subsequent diffusion/entanglement of polymer chains forming the bondline. However, a second process produces shear joints made

without any artificial susceptors since a major portion of vibration energy is converted directly to frictional (shear forces) (Figure 3.4a; Yousefpour et al. 2004).

Equipment essentially consists always of seven components: stand, generator/power supply, converter, booster, horn/sonotrode, fixture and controls (Rotheiser 2004, 515). A schematic set-up is shown in Figure 3.4b. The power supply provides high frequency electrical energy exciting a piezoelectric or magneto-restrictive material as part of the actuator. This hosts the converter (converting electrical energy in vibrations), booster and horn whereof the latter two increase amplitude of originally very small converter oscillations finally to 13 – 64 µm for amorphous and up to 130 µm for semi-crystalline materials and connect actuator to the top surface of the substrate.

"The objective is to focus the heat at the bondline and keep the remainder of the part interior and the heat-affected zone, or HAZ (the area next to the bond) from deconsolidating. Since this method only heats the parts in the area being bonded, pressure only needs to be maintained directly under the sonotrode and any associated HAZs. Pressure between 500 and 1400 kPa (70 and 200 psi) must be maintained until the part has cooled to below the T_g of the matrix resin." (McCarville and Schaefer 2001, 1499)

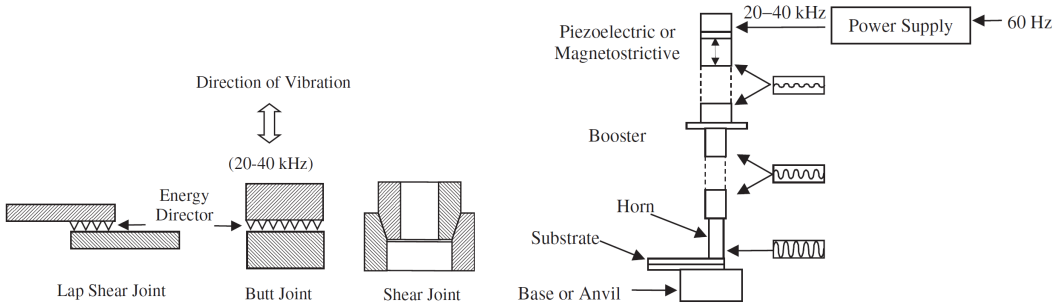

(a) Joint Variants (b) Schematic Welding Devices

Figure 3.4 – Ultrasonic Welding Fundamentals (Yousefpour et al. 2004, 316)

Benatar and Gutowski (1989) cluster ultrasonic welding into five steps: 1) mechanics and vibrations of the parts, 2) viscoelastic heating of the thermoplastic, 3) heat transfer, 4) flow and wetting and 5) intermolecular diffusion.

Benatar and Gutowski (1989) further pointed out the importance of detecting dynamic mechanical impedance as relation to molten polymeric material flow for online monitoring of weld quality. For flow improvement and gap filling, typically, a thin layer of neat resin film is inserted (Campbell 2003, 393). Villegas (2015) introduced in-situ monitoring of ultrasonic welding through power-displacement curves recorded by microprocessor--controlled machines itself.

Process parameter are reported as welding pressure, welding amplitude, welding time and welding frequency. Benatar and Cheng (1989) and Strong et al. (1990) investigated them with concluding weld strength (quality) improves with higher pressure (better energy transfer), longer welding time and increased amplitudes (energy dissipation increase), whereby an optimum can be observed over that a degradation of property values sets in again. Suresh et al. (2007) report a similar behaviour for interface temperature and ultimate tensile strength of ABS specimen showing an optimum at a certain temperature, too, for both, amorphous and semi-crystalline. In addition, they regard viscoelastic heating as most crucial depending on applied frequency, square of the amplitude and loss modulus of material . The heat generation concentrates around asperities in the surface (Wolcott 1989).

Volkov and Kholopov (1998a; 1998b) found induced misorientation and distrotion of fibres due to applied welding pressure and proposed a reduced (not removed to maintain physical/acoustical contact) pressure at thermoplastic's melting point and a re-increase after vibration phase to guarantee a good consolidation. Fischer et al. (2015) investigated detrimental overheating and penetration of the horn into the laminate as well as disruption of fibres depending on process parameter .

Suresh et al. (2007) pointed also out the good welding quality of amorphous as well as semi-crystalline thermoplastics in the near field, but rather poor quality for semi-crystalline thermoplastics in the far field. This phenomenon does not occur for composites due to reinforced stiffness (Grimm 1990).

Moreover, semi-crystalline thermoplastics need more energy since they absorb more energy and additional energy is required to break crystalline structured areas and thus, they are more difficult to control as the process window for temperatures is narrower as depicted in Figure 3.5 (Rotheiser 2004, 484-87).

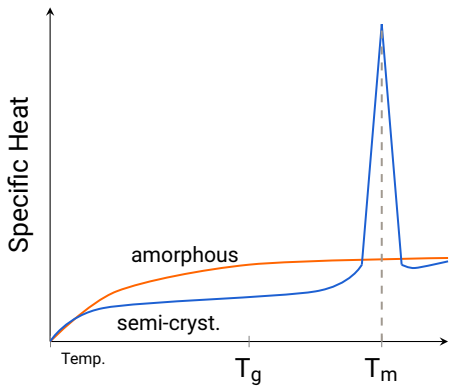

Figure 3.5 – Specific Heat over Temperature for Thermoplastic Types (Data: Rotheiser 2004, 485)

The influence of energy directors was and still is subject of intensive studies since they are source of heat and therefore crucial for a successful process. Where ED modelling is achieved quite easily in plastics manufacturing, composites face serious prob-

lems since fibres must not be distorted. Furthermore, an additional process step would be necessary. Triangular protrusions are most commonly used – although other shapes were investigated (Benatar and Gutowski 1989) and tie layers with modified and preferential melting properties were proposed by Tateishi et al. (1989) and Zach et al. (1989) instead of any energy susceptors. Most recently, investigations go in the direction of flat energy directors in form of films (Senders 2016; Villegas and Palardy 2017; Palardy and Villegas 2017; Villegas et al. 2014). These flat EDs turn out as competitive alternatives to standard triangular shapes. Although the latter possess superior properties compared to semi-circular or rectangular shapes (Suresh et al. 2007), differences in weld strength, dissipated power or heating time compared to flat EDs are rather marginal (Villegas et al. 2014).

Stokes (1989) introduces the issue of joint positioning and design in ultrasonic welding since parts geometry is decisive for vibration behaviour and thus transmission of energy to the joint influencing heating and melting.

Strong et al. (1990) determined four failure modes for ultrasonic welded lap shear joints (in order of increasing strength): 1) weld interfacial failure in resin-rich areas, 2) combined interlaminar and interfacial failure, 3) interlaminar failure above and below energy susceptor layer and 4) coupon failure due to fibre damage (no weld failure).

Rotheiser (2004, 481-82) lists advantages amongst others:

- No additional materials hence inherently lower in cost and less expensive to disassemble for recycling
- Ease of assembly– requires only alignment of two parts in fixture thus it is well suited to automated assembly
- Permanence– permanent joint without creep, cold flow or stress relaxation effects, or other environmental limitations
- Contour freedom– no limitations in contour geometry like f.i. spin welding
- Hermetic seals possible
- Energy efficiency– highly energy efficient process including no excess heat which must be removed from workplace
- Clean Atmosphere– Unlike adhesive and solvent joining systems no environmental requirements
- Immediate handling– no curing times delaying process chain hence good for automated assembly line applications
- High production rates– due to very short cycle times 20 to 60 parts per minute are possible

Very short cycle times hence very small heat-affected zones (Todd 1990). Krüger et al. (2004) showed also the opportunity of joining combined composite-metal compounds ($AlMg_3$) with ultrasonic welding process achieving satisfactory tensile/shear properties. Nonetheless, HAZ can be slightly increased with a greater sonotrode diameter to lower applied welding pressure avoiding disruption of fibres (Volkov and Kholopov 1998a, 1998b).

In maintenance and repair, ultrasonic processes are well-known. Damaged areas are drilled out and filled with a plug of thermoplastic resin. Only for small areas, reduction in strength due to cutting of load carrying fibres is acceptable (Vodicka 1996, 14). Concerning possible maintenance applications, ultrasonic welding equipment has been characterised as "[...] too heavy for practical in-field work." (Lewis 1990)

Schwartz (1994) sees the main barrier for ultrasonic welding applications to continuous-fibre reinforced materials at the insertion of energy susceptor on sheet components with associated possibility of fibre disruption under high oscillation motion. Another issue is heat conduction by carbon fibres away from the bonding interface consequently increasing cycle time (C. Eveno and Gillespie 1989). Size and power of welding machines limits the size of a one-shot bonding area (Benatar and Gutowski 1986). Largest ultrasonic welders cover areas of about 0.23 m × 0.3 m (Rotheiser 2004, 482). Otherwise, a multiple horn application must be deployed (Taylor and Jones 1990).

Frantz (1997) emphasised the limitation of ultrasonic welding to large and complex shaped parts whereas McCarville and Schaefer (2001, 1500) rate scaling of an ultrasonic welding process to large and/or complex shaped parts with reference to Davies et al. (1991) at least as critical. Heimerdinger (1995) reported unsuitability of ultrasonic welding for repairing large parts as bonds produced showed only poor strength, only partial bonding or burnt material."The ultrasonic energy is highly directional and multiple passes of the beam are required to cover a large area." (Vodicka 1996, 14)

Generally, ultrasonic welding is only applicable to (nearly) flat joining surfaces large enough to move over with the sonotrode. Further disadvantages are tight surface tolerances and prerequisites on prior manufacturing processes which can achieve them or even enable insertion of energy directors. In addition, electrical components near to a part under repair, e.g. during maintenance, can be damaged due to vibrations. Workers must be protected from the shrill, high-pitched whistlelike sound created by the horn. Basically, the simplest equipment versions are not very expensive, but with additional accessory to improve weld quality and ensure stable process, price can increase rapidly

(Rotheiser 2004, 482-83). Moreover, with such a method, only non-detachable joints can be manufactured akin to its type of metal joining.

"This process is somewhat similar to spot welding[...]" (Campbell 2003, 394), for which Yousefpour et al. (2004) sees great potential especially in the aerospace branch. Nevertheless, in context of this work, a continuous joining method is sought for. Investigations in direction of continuous ultrasonic composites welding can be found intensively upcoming in the last decades (Villegas and Bersee 2009). Joining of woven and non-woven as well as large parts, sheets and plates have been reported with continuous, scan or sequential ultrasonic welding processes, respectively (Grewell et al. 2003; A. Benatar et al. 1997; Benatar and Gutowski 1986; Lu et al. 1991).

As depicted in Figure 3.6, either the adherends are positioned on a rotary drum or the horn moves over stationary clamped parts; alternatively, a moveable table positions parts under the fixed horn. The former is normally featured with a constant feed, gap and a round edged sonotrode preventing snagging and better pressure distribution. During scanning ultrasonic welding, sonotrode traverses or scans the pars at a lower velocity hence longer ultrasonic vibration times due to thicker parts joined with this variant (Gallego-Juárez and Graff 2014, 302-03).

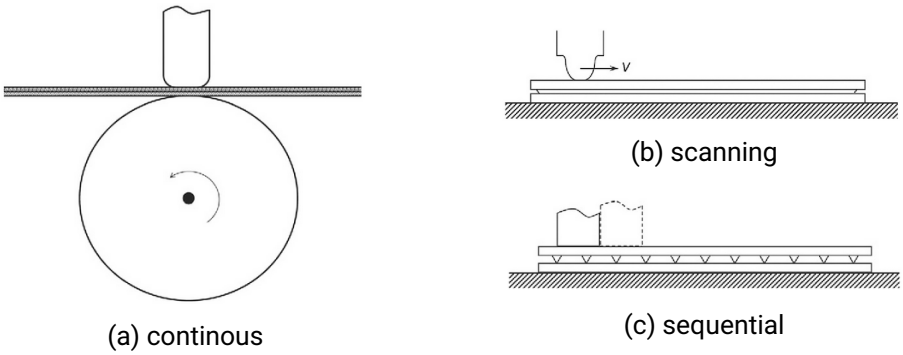

(a) continous (b) scanning (c) sequential

Figure 3.6 – Variants of Ultrasonic Welding (Gallego-Juárez and Graff 2014, 302-03)

Most of these methods are used to join flexible thermoplastic films, woven and non-woven fabrics and coated materials (BRANSON 2011). Particularly for neat thermoplastics, it is the most promising method achieving high quality and reliable weld seams (Khmelev et al. 2010).

Those principles can be modified to ultrasonic seam (roll) welding (Figure 3.7) where circular disk sonotrodes on transducers are moved translationally for generating vibrations suitable for long length sheet joining particularly of dissimilar materials. An alike process is ultrasonic torsion (ring) welding which is however rather for spot welding of circular joint shapes (Ahmed 2005, 252-53).

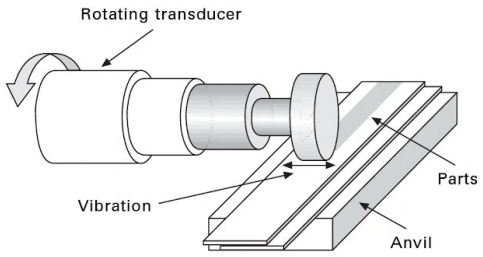

Figure 3.7 – Ultrasonic Seam Welder (Ahmed 2005, 253)

Typical applications are within various branches, e.g. electrical, computer, automotive, energy, medical and packaging and aerospace engineering is keen on exploiting this technology for lightweight applications (Yousefpour et al. 2004; Costa et al. 2012). Particularly optimum process parameters and control in a stable manner is the goal of several studies (Siddiq and Ghassemieh 2008; Krüger et al. 2004).

As already implied before, promising studies have been carried out to expedite the continuous approach of ultrasonic welding for composites, too. Already in 2007, EADS conducted experiments finally leading to a patent in a “Ultrasonic Assembly Method” (Soccard 2011) providing a continuous process. Levy et al. report that “[u]ltrasonic continuous welding of thermoplastic composite plates is a very promising process of particular interest for the assembly of aeronautics large parts. [...] First results reveal a good mechanical quality of the welding. In particular the advance of the sonotrode enable air removal along the director and avoids the trapping of bubbles. [...] This opens possibilities for this process to be used at an industrial level to assemble large parts keeping an excellent weld quality.” (2014) Fokker Aerostructures realised the A380 fixed leading edge with ultrasonic spot welding and Boikon expanded this approach to a ultrasonic UD tape laying head establishing a new fixed wing leading edge concept (Figure 3.8). “With ultrasonic fibre placement, the challenge was to succeed in tacking a tape onto an underlying thick stack of plies at high speed, without slowing down the process and thus making it ineffective.” (Offringa 2010)

Back from manufacturing to joining, the Faculty of Aerospace Engineering of Delft University of Technology developed under the F1 Eco-Design programme spot and sequentially ultrasonically welded aircraft primary structure parts consisting of CF/PEEK and thus proved the feasibility of this joining method for large-scale applications (Palardy et al. 2015). As one outcome, Senders (2016) developed and proved in his master thesis the feasibility of such a technology. In an annexed article, Senders et al. introduced a

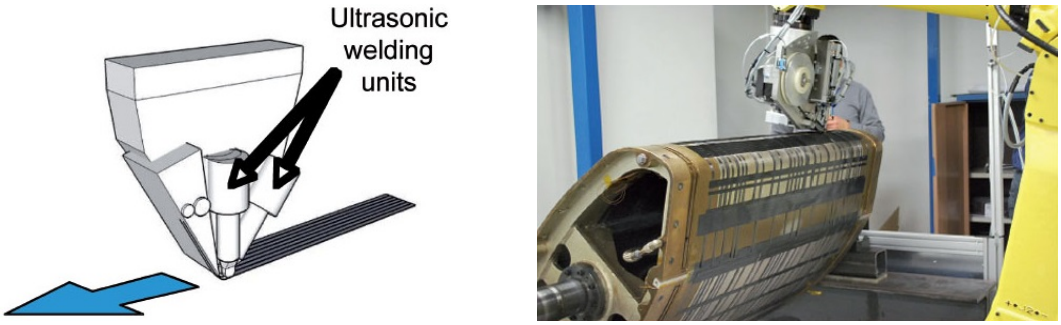

(a) Schematic (b) Development Robotic Cell

Figure 3.8 – Ultrasonic Fibre Placement Head and its Application (Offringa 2010)

"Zeroflow" approach inheriting "[..] a welding procedure in which no squeeze flow of the energy director is required to achieve sufficient weld strength, [and which] is enabled by the use of very thin (0.08 mm) flat energy directors. The zero-flow approach allows continuous welding of stiff thermoplastic composite plates since it does not require local deformation of the adherends as the sonotrode moves along the weld line. The results presented in this paper for a basic zero-flow continuous ultrasonic welding process prove its feasibility and indicate its potential to deliver high-strength welded seams at very high speed." (2016)

The ultrasonic welding methods was favoured for joining the 30-300 Westland helicopter tailplane (horizontal stabiliser and fin) unlike resistance and induction technologies (Cole 1992).

3.4 Electro-Magnetic Heating

As the name indicates, heating is induced via electro-magnetic fields, waves or effects. The appearance of heat further depends on the kind of physical principle used out of the huge field of electro-magnetic effects. For industrial process, four methods are most common: microwave and dielectric heating as well as induction and resistance welding.

3.4.1 Various Processes

Both, Microwave and Dielectric Heating are underprivileged a priori when it comes to "... multi-layer composites, which are excellent shield in the microwave range, microwave welding is poorly suitable especially when composites are reinforced by carbon fibers."(Boyard 2016, 236) As a consequence, bulk heating sets in within the top

layers (Volpe 1980); same holds true for dielectric heating (Benatar and Gutowski 1988). Nonetheless, by adding suitable absorbent materials in the interface, Varadan and Varadan (1991) achieved good welding qualities and applications for glass or aramid reinforced composites are possible anyway (Vodicka 1996), but out of scope in this work.

Microwave welding came up with development of magnetron in the 1940s (Costa et al. 2012). Generally, a range of 3 x 10^8 to 3 x 10^{10} Hz is referred to as microwave radiation. Within this wavelength range, most of thermoplastic systems do not show any significant heating when exposed to radiation. In turn, microwave energy is absorbed by microwave sensitive implants causing heating which leads through conduction to a melting of adjacent polymeric material (Wise 2001). The physical principle of microwave heating is a combination of several loss mechanisms, amongst others dipolar, Maxwell-Wagner and Ohmic loss effects which are often summarised in an effective loss factor (Metaxas and Meredith 1983). The four process steps are 1) heat generation, 2) heat conduction and melting, 3) flow and diffusion and 4) cooling. For this, main process parameters influencing the amount of heat generated can be characterised as heating time, power level, welding pressure and percentage of conductive polymer (PDL 2008, 80). Advantages are freedom for designers since parts are usually not excited by radiation, possibility for complex three-dimensional joints in very short welding times of less than a minute, fast and clean behaviour, automation in a continuous process, especially for butt welds (Wise 2001; Yousefpour et al. 2004) and consequently high processing speed and energy efficiency (Ku 2003). A wide range of implant materials is available, ranging from metals, carbon to polymers – all are consumable (Costa et al. 2012). Although these implants act as very local heat sources, quite a uniform heating is achieved; high energy coupling efficiency causes volumetrically heating (Yarlagadda and Chai 1998; Ku 2003).

However, the size of joints is limited with proportion of absorbent material. Figure 3.9 shows a schematic continuous butt welding process with microwave heating. A disassembly can be considered with a similar process of reheating but inverse "pressure" to pull the parts apart (Yousefpour et al. 2004).

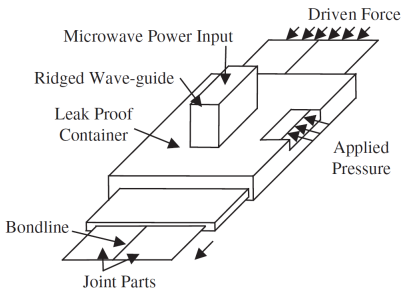

Figure 3.9 – Schematic Continuous Microwave Joining Set-Up (Siores and Rego 1994)

Where materials with low or medium dielectric loss factor require no electromagnetic absorbent material for microwave joining, joint elements with high dielectric loss factors are rather predestined for dielectric heating. The principle is the same as for microwave radiation, albeit the polymer is directly heated at much lower frequencies.

Dielectric or Radio Frequency Welding (RF) uses 13 to 100 MHz radiation (PDL 2008, 75). Key process parameter for good weld qualities is undoubtedly the dielectric loss factor which is decisive for heat amount induced during irradiation. Thus, PVC, PU or PA are favourable joining materials for this process. Further influences have the dielectric power source, thickness, area and properties of welded parts as well as welding time and pressure. Just as for microwave heating, the dielectric effect is enhanced for reduced part or increased weldline thickness (Yousefpour et al. 2004). Process advantages are simple and compact set-up which does not introduce other bonding materials minimising risk of inclusions (PDL 2008, 78). However, for composites, main drawback is the likelihood of bulk heating hence de-consolidation which requires counter-measurements like expensive tooling. Corrective can be achieved by adding thin layers of higher dielectric loss material than the surrounding composite. As result, the thin layer melts before deconsolidation of the entire composite part.

As depicted in Figure 3.10, contacting electrodes directly transmit the alternating field onto the joining elements, which are usually automated bonding film and thin sheets bonding processes (Stokes 1989). Another application is thermoset or adhesive curing, too (Yousefpour et al. 2004).

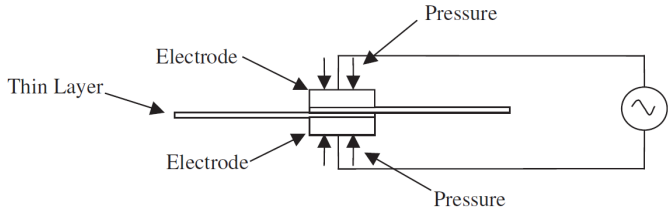

Figure 3.10 – Schematic Dielectric Joining Set-Up (Yousefpour et al. 2004)

3.4.2 Resistance Welding

Resistance Welding (RW) – often also referred to as Resistive Implant Welding or Electrical-Resistance Fusion (Ageorges et al. 2001) – uses the principle of a current-carrying conductor (heating element) inserted in a sandwich configuration producing heat directly at the bonding interface due to resistive effects (Figure 3.11).

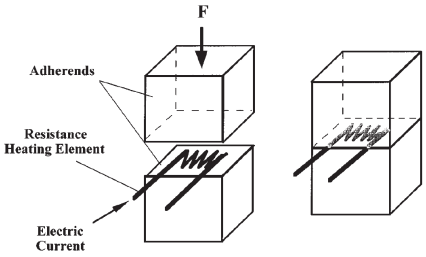

Figure 3.11 – Working Principle of Resistance Welding (Hou et al. 1999b)

Once the current is applied and heat losses from the joint are exceeded, supplied heat energy conducts to adjacent thermoplastic structure which eventually reaches its melting point. The longer the energy supply persists, the deeper is the heat penetration. In order to avoid unnecessary distortion of fibres, heat-affected zone is tried to be minimised to the bonding layer. After satisfying heating, the current is took away and cooling sets in under application of pressure to guarantee a good consolidation with sufficient intimate contact and molecular diffusion. The heating element remains in the bondline and can be used for reheating at a later point in time, e.g. for replacements during maintenance. Instead of added implant material, electrical conductive carbon fibres open the possibility to be used as "internal" heating element (Stavrov and Bersee 2005; Hou et al. 1999b; Yousefpour et al. 2004).

This process features a rather simple set-up with non-expensive and easily portable equipment (Yousefpour 2006). Most of the parts are standard parts like implant mesh plies, pressure application tools, electrical power supply, clamping and measurement devices (Figure 3.12). Welding pressure should have a uniform manner and can be applied diversely, e.g by pneumatic cylinders or calibrated spring clamps. Electrical power supply can either provide direct or alternating current (Stavrov and Bersee 2005).

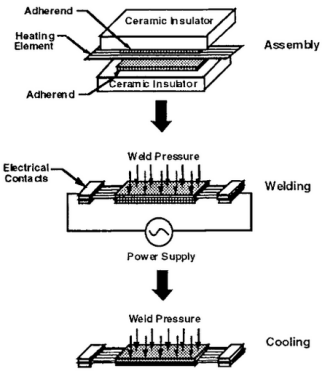

Figure 3.12 – Resistance Welding Set-up and Process Steps (PDL 2008, 83)

RW can be divided into three simple process steps: 1) assembly of the stack-up, 2) welding (heating) and 3) cooling. According to that, three stages can be observed:

1) ramp up, 2) peak current and 3) ramp down stage with an overall process time of typically one minute (PDL 2008, 83-84).

Various process parameters can be identified, starting with the energy (current) applied. According to Ohm's and Joules Law, energy dissipated can be derived as in (Eq. 3.1) from the material dependent resistivity used for the conductor.

$$E = U \cdot I \cdot t = R \cdot I^2 \cdot t \qquad \text{with} \qquad R = \rho \cdot \frac{L}{A} \quad \text{or} \quad R = \gamma \cdot \frac{L}{w} \tag{Eq. 3.1}$$

with electrical current I, time-dependent resistance R, (material) specific resistance ρ anc conductor's length L and cross-sectional area A. M. Hou and Friedrich (1992) introduced the specific resistance γ as proportionality factor of length L and constantly assumed width w of the conductor. Since a huge temperature range is expected, the change of electrical resistance over temperature must not be neglected. The correction follows the linearised Taylor series

$$R(T) = R_0 \cdot [1 + \alpha_{T_0} \cdot (T - T_0)] \tag{Eq. 3.2}$$

with the resistance-temperature coefficient α_{T_0} valid for a starting temperature T_0. For typical conductor materials (e.g. copper, aluminium), $\alpha_{T_0} > 0$ holds true hence an increase of resistance and heat energy for higher temperatures. Investigations on this phenomenon were carried out showing an increase of stainless steel resistance of about 25 % and a decrease of carbon fibre heating element resistance (with rather insulating behaviour) between 6.3 and 16 %, both at 340°C (Stavrov et al. 2003; Ageorges et al. 2000a).

Proleptically, material with its resistivity and temperature behaviour in combination with the current applied forms the first process parameter.

Furthermore, there are several possible configurations for welding execution: 1) constant input voltage during entire welding (but variable power level due to changing electrical resistance over temperature), 2) constant power during entire welding process hence temperature peaks which a difficult to predict, 3) constant temperature which is maintained via thermal sensors to monitor, control and adjust power, 4) ramped voltage with a gradually increase, constant heating rate for a more uniform temperature distribution and less heat losses in surrounding medium hence lower input energy, or 5) impulsive resistance welding with energy supplied in form of intense pulses (followed by a 1 to 3 seconds interruption) leading to less heat losses hence less energy consumption. Although others consistently show more evenly temperature distributions, the constant

power approach is more practicable and thus more abundantly used (Yousefpour et al. 2005; Arias and Ziegmann 1996; Ageorges and Ye 2001b; Stavrov and Bersee 2005). Monitoring and controlling of electrical resistance/input power as well as associated heating and cooling rates are decisive for later weld quality and thus mechanical properties of the joint (Yousefpour et al. 2004).

As addition to (Eq. 3.1), the welding power/energy per unit area $[\frac{W}{m^2}, \frac{kJ}{m^2}]$ can be computed according to

$$P = \frac{R \cdot I^2}{L \cdot w} \qquad \text{and} \qquad E = P \cdot t = \frac{R \cdot I^2}{L \cdot w} \cdot t \tag{Eq. 3.3}$$

Interestingly, Hou et al. (1999) proved a difference in processes with high power levels and short welding time to a process vice versa. Tests revealed for increasing power levels an decrease in lap shear strength as well as a dramatic reduction of LSS for lower welding energies.

On the one hand, a good thermal insulation and carefully dimensioned input energy (Costa et al. 2012) can increase weld quality, but on the other hand, the power supply can also be a limiting factor for power level hence weld time and size (Stavrov and Bersee 2005). Thus, the insulation issue is closely intertwined and turned out to be crucial since satisfying weld results are not achievable without it (Xiao et al. 1992; Jakobsen et al. 1989; Stavrov and Bersee 2003). Either tooling is heated in a way the bondline does not reach melting temperature or the other way around, bulk heating sets in with a consequent deconsolidation. Various different insulation material like ceramics, wood, silicon rubber or fibrous matter were investigated for this reason – also with additional coating foils (e.g. PTFE) to prevent sticking and improve surface quality. The selection of material must be carefully done since the implant remains in the bond and compatibility with joint materials is required for long durability. In literature, only stainless steel and carbon fibres (CF) co-moulded in several resin layers are reported as heating element materials whereof carbon fibre show very good compatibility with the prevailing structure as it is produced from the same source. Metal mesh are advantageous in terms of better performance, consistency and strength of formed joint as well as less sensitivity to process disturbances. However, issues like added weight, corrosion and different CTE arise (Stavrov and Bersee 2005).

Another critical issue is the electrical connection essential for sufficient current flow. Different approaches are reported, amongst others 1) direct clamping, either on prepreg or bare fibres, 2) bare fibres coated with silver-epoxy filler or 3) dipping prepreg in a liquid metal bath or 4) low melting point alloy pressed on bare fibres (Costa et al. 2012;

Stavrov and Bersee 2005). Nevertheless, Ageorges et al. (2000a) concluded in the light of cost and time for prepartion, method of choice is direct clamping on bare fibres hence clamping pressure gets into focus. They further found a direct relation between clamping pressure and resistance value which shows a minimum plateau for pressures between 4 and 20 MPa for CF heating elements. Similar to that, stainless steel provides an optimum process window around 2 MPa (Stavrov et al. 2003).

For welding pressures, either a constant load or constant displacement approach are common (Yousefpour et al. 2004). Where constant pressure provides full pressure control but hardly predictable variations in final thickness, constant displacements achieve defined geometry but fluctuating pressure during welding process (Stavrov and Bersee 2005). For aerospace applications, especially concerning lap joints at the outer skin with great importance of aerodynamical surface, maintaining the shape is of primarily importance and thus constant displacement control seems more appropriate.

Don et al. (1990) report four failure modes of resistance welded specimens (in order of increasing strength): 1) interfacial failure (separating laminate from heating element), 2) cohesive failure (through heating element), 3) tearing of heating element (jump of failure path through heating element) and 4) tearing of the laminate (mainly within HAZ).

Advantages of resistance welding lie in the fast and simple process which does not require complex tooling or intensive surface preparation. As aforementioned, in terms of maintenance and repair, rather easy and portable equipment contributes additionally (Yousefpour 2006). Furthermore, heat is mainly generated at the interface layer, there is no restriction to flat surfaces to be joined, joins found to be insufficient (flaws/defects) as well as damaged parts can easily be reheated and replaced/repaired or even completely disassembled and recycled. Out of scope but possible is the application as curing support for thermosets or adhesive bonding as well as to join hybrid/dissimilar materials (PDL 2008, 86; Hou et al. 1999b).

Process drawbacks are potentially occurring effects, just as preferential heating which has various forms of appearing with the same result of incomplete welding hence weak joints. Either due to poor contact, broken heating element or reduced heat transfer at the end of the heating element to air and thus steep thermal gradients. The latter is called edge effect describing a rapid melting process in that area and consequently contact of heating element and fibre leading to an immediate current leakage. Melt flow propagation does its bit as it “benefits” from edge effects and propagates from the out- to the inside (E. Eveno and Gillespie 1988). The longer presence of melt at the outsides rises the risk for current leakage. Moreover, matrix at the critical outer positions might

reach thermal degradation temperature even before the centre is melted. Therefore, edge effects contribute twice. Countermeasures were discussed in literature, e.g. active cooling, insulation or clamping closely at the part to overcome the biggest difficulty in resistance welding of carbon fibre reinforced composites. Another option is to completely electrically insulate the heating element via glass fibre, Thermabond® or coating layers (Stavrov and Bersee 2003, 2005).

Although most experimental data was achieved with coupon test, main field of applications – particularly in context of this work – will lie in large scale joining. Simple extension of heating elements was found out to fail as there is no possibility of utilising up to infinite length heating elements due to Ohm's law (Swartz and Swartz 1989). Greatest potential was discovered for long, narrow, sequentially welded lines/areas (Fernie et al. 1991; Maguire 1989). Sequential resistance welding (SRW) – stepping the entire process – was introduced achieving double lap joints up to 1.2 m length and thus proving feasibility for large-scale resistance welding application, although further improvement is necessary – especially part alignment, cost and cycle time (Taylor and Davenport 1991). This should also overcome the problematic nature of power/pressure requirements, which would have to be scaled up the same way as the specimens – which is about two orders of a magnitude (McKnight et al. 1997). Lambing et al. 1991 (1991; 1993) proposed a pressure controlled automated resistance welder (ARW) with active nitrogen cooling which simultaneously prevents oxidation of the heating element.

Other difficulty for large areas is a uniform temperature distribution which was identified by Ageorges et al. (2000a). They proposed a criterion equation to compute maximum length of a weld line preventing thermal degradation of matrix as aforementioned. This reads

$$L_{max} = 2\left(\frac{T_{max} - T_{min}}{\frac{\Delta T_1}{L}}\right) \qquad \text{(Eq. 3.4)}$$

with T_{max} as degradation and T_{min} as melt temperature, ΔT_1 as temperature difference between centre point and penetration area and L the half length of tested specimen.

The latter lead also to another problem: a continuous resistance welding is hardly possible or at least very difficult and thus not surprisingly not very common. Not only that heating elements have an inherited limitation in length as showed above, series-connected heating elements to achieve a quasi-continuous process requires complex equipment prone to disturbances, introduces many more process parameters and is much more difficult to simulate. After Yousefpour and Octeau published a patent on that topic in 2009, the NRCC claimed three years later "[t]he focus of current research is

on developing resistance welding, a new technology for joining large parts in a continuous/progressive manner."(2012) However, not much scientific work and studies have been caried out since then. Even research on skin/stringer joints were conducted out with cut-out specimen instead of full-scale tests (Dubé et al. 2007).

One remarkable exception is presented by Shi et al. (2015) whereof the PhD thesis of Shi comprises a chapter about "Process modelling of continuous resistance welding" (2014). The chain of progress got from original resistance welding process to sequential resistance welding and finally to continuous resistance welding (CRW). Although CRW simplifies advanced SRW further, both exhibit an increased complexity for the target to join large areas with reasonable power and pressure efforts (Shi et al. 2015). CRW established by Shi (2014) combines single-piece heating elements with a number of copper blocks positioned one after another parallel to the welding direction – one above and one underneath both adherends for single lap joints – maintaining a clamping distance of 1 mm. Two copper wheels close the circuits one after another to start and interrupt heating in the respective elements while applying clamping force/pressure of 55 N (0.30 MPa). Wheels motion along the welding line creates a continuous process (Figure 3.13).

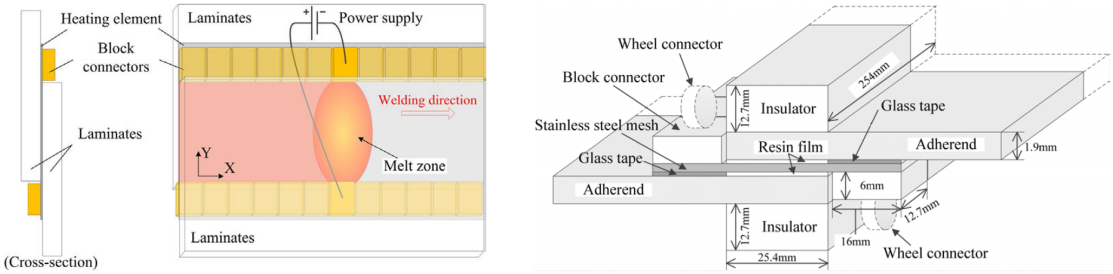

(a) Schematic Welding Progress (b) Cross Section and Components

Figure 3.13 – Continuous Resistance Welding (Shi 2014)

Contact resistance, heat transfer efficiency, welding voltage and welding speed were found as influencing parameters on temperature distribution – particularly the latter two –, which was observed quite uniform along, but very unequal transverse the bonding line with a significant edge effect. The size of the blocks affects the selection of welding parameters (Shi et al. 2015).

Nevertheless, resistance welding technique is typically applied in automotive sector, for plastic pipes, containers and medical devices (Ageorges et al. 2001). "It is believed that the combination of sequential resistance welding and impulsive resistance welding

as one welding system can provide a high-quality weld for large aerospace structures and replace traditional techniques such as adhesive bonding and mechanical fastening. However, this has yet to be demonstrated." (Yousefpour et al. 2004) Costa et al. (2012) see resistance welding also as "[...] a very promising joining technique for aerospace application", but in the light of a continuous joining this method needs to catch up with other approaches.

3.4.3 Induction Welding

Faraday firstly discovered electromagnetic induction while James Clerk Maxwell found four differential equations describing these effects (Bayerl et al. 2014) and thus building the backbone of a controlled induction process. Electrically conductive materials exhibit induced recirculating eddy currents when exposed to an high-frequency alternating current hence magnetic field. In turn, resistive effects of induced currents create eventually the heat required to melt the matrix and form under pressure the bondline. The exact source of heat in composites is controversial: reported is fibre heating (Joule loss) and junction heating (either dielectric hysteresis or contact resistance heating) with different opinions concerning the major mechanism. In magnetic materials, additional hysteresis losses can occur (Ahmed et al. 2006; Shridhar Yarlagadda et al. 2002). With this heating method, transferable heat is increased drastically, e.g. by over three orders of a magnitude compared to conduction (Benkowsky 1990).

Equipment consists of five basic components: 1) Induction generator (converting to high-frequency output frequency ranging from 3-8 MHz, in general from 2-40 MHz), 2) heat exchanger to carry away heat and cool, 3) work coil (providing magnetic field), 4) pressure device and 5) fixture to hold joining adherends and ensure a good consolidation (Rotheiser 2004, 337-38). Process characteristics are a heating stage reaching maximum temperature, a slow but subsequent cooling due to heat convection to surrounding air sets in before joining pressure is applied, e.g. by an externally cooled roller, and final consolidation until cooling to ambient temperature can be observed (Rudolf et al. 2000).

As aforementioned, necessary prerequisite for this method is the presence of electrically conductive joining adherends. Since carbon fibres are electrically conductive, they can be used as internal energy susceptors (Ageorges and Ye 2012, 29). Yet, anisotropy and the need for closed loops appear as some difficulties. Unidirectional even carbon fibre reinforced composites cannot get welded, plain weave materials shows better heating behaviour and eventually $\pm$45°UD plies achieved superior properties concern-

ing heating just as multi-directional CF plies. What all have in common due to susceptorless[1] set-up is a heating of the entire part which in turn requires adequate tooling to prevent adherends from deconsolidation and fibre disturbance (Rudolf et al. 2000; Vervlied and Heward 1991). For two reasons, susceptors inserted in the bondline can be favourable: firstly, to induce preferential heating at the interface and, secondly, for non-conductive and/or low permeability polymers. These can be deployed in form of tapes of thermoplastic with filler particles, f.i. iron, stainless steel, ceramic, ferrite or graphite (Schwartz 1994). Another approach was introduced by Leatherman (1977) using a metal mesh providing preferential heating but also connection between two incompatible thermoplastics. Further studied is the so-called EMAWELD® bonding comprising a thermoplastic paste with metal particles (S. Yarlagadda et al. 1998; Costa et al. 2012) or nickel-coated graphite/J-polymer prepreg layers (Benatar and Gutowski 1986). However, Hou et al. (1999) point out modified attitudes due to metal particles which can lead to weaker mechanical properties since these particles act as micro-cracks and notches.

In literature, several process parameters are named for induction welding: Ahmed et al. (2006) list current frequency, input power, welding pressure and time. According to that, frequency is crucial since it is not only responsible for induced eddy currents but also influences penetration depth. Thus, a higher frequency causes higher power but lower penetration – this phenomenon is called "*skin effect*" (Bayerl et al. 2014). Contrary to dielectric heating, frequencies are in any case higher to avoid that plastics are affected and exhibit direct heating (Stokes 1989).

Power defines the amount of energy applied for heating. It can be determined from an in- or output point of view:

$$P = \frac{u_{ind}^2}{R_f} = \frac{(2\pi f \mu H(I) A)^2}{R} \qquad E = P_w \cdot t = m_w \cdot c \cdot \Delta T \qquad \text{(Eq. 3.5)}$$

with the current dependent magnetic field $H(I)$, cross-section of affected zone A, permeability μ and electrical resistance R_f of the joining adherends, respectively, the mass of workpiece m_w, its specific heat and corresponding temperature increase ΔT (Rudolf et al. 2000; Ahmed et al. 2006). The higher the pressure, the better the consolidation hence bond strength until it reaches a maximum. The residence time behaves in the same way, three stages can be distinguished whereof one exhibits the maximum for

1. Bayerl et al. (2014) remark that the term "*susceptorless*" introduced by Ahmed et al. (2006) refers to no additional foreign materials added for heating purpose; however, susceptors need to be present anyway to enable an inductive heating, in this case these are already incorporated in electrical conducting carbon fibres

weld strength (Rudolf et al. 2000; Zach et al. 1989).

Bayerl et al. bring susceptor influences into play as well as extended observations from above that "[t]he main influences of the induction setup originate from the coil geometry, the applied electrical power and the coil current. In addition, the frequency and the coupling distance play an important role." (2014) The reduction of the latter can cause higher temperature increases hence non-uniform heat distribution. Same effect has an current increase. The common thread for all this phenomena is the coil geometry since it is decisive for basic magnetomotive force hence induction and heat. This parameter has been therefore subject to several studies investigating the correlation between coil geometry and heating pattern (Lin et al. 1991; Rudolf et al. 2000; Benatar and Gutowski 1986). Nonetheless, standard coil shapes have been reported and deployed regularly (Figure 3.14a) and "[...] the modification and improvement of coil geometry and machine parameter adaption are essential for an increased applicability of induction heating in the composites industry." (Bayerl et al. 2014) Despite some constants like copper material or integrated water cooling, new developments are reported in that field: Rotheiser (2004) presents a hairpin coil for joining large flat sheets (Figure 3.14b), frequency variation approach was introduced (Puyal et al. 2007) and additive manufacturing techniques could open the field to complete new coil designs (Bayerl et al. 2014).

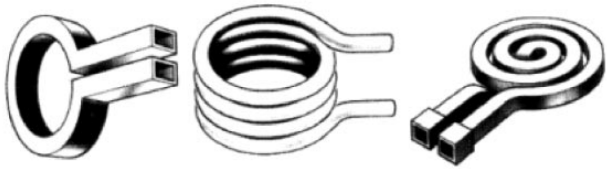

(a) Single-Turn, Multi-Turn and Pancake Coil (Sanders 1987)

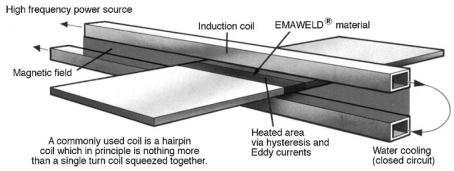

(b) Hairpin Coil (Rotheiser 2004, 341)

Figure 3.14 – Various Coil Designs

Apart from coil geometry, Rudolf et al. (2000) provide an intensive research study on exact influences of different parameters.

Other effects reported are proximity, ring and edge effects. All describe stimulation of the magnetic field, e.g. interference with close conducting elements (Rapoport and Pleshivtseva 2006, 3-5). Another possibility to focus magnetic fields is the utilisation of magnetic flux concentrators which increase coil efficiency and limit the area affected by the magnetic field more strictly (Haimbaugh 2001, 46-49) .

Despite carbon fibres are processed in composites, susceptor particles can be still added for better control of the heating stage. By this means, Worrall and Wise (2014)

introduce a novel approach for focused induction heating at a defined interface layer. They use a stack-up of unidirectional plies separated by insulating glass fibre plies except near the interface layer, where 0° and 90° UD plies are placed in direct contact to allow induction heating there. Therefore, range of application can be expanded to parts where risk of thermal degradation was estimated too high so far.

Rotheiser (2004, 335-36) assigned the following advantages to induction welding:

- High production rates– weld times of 1 to 10 seconds
- Joint strength can reach very high levels
- Permanence (even hermetic seals) as well as reopenable joints possible
- Flexibility to similar or non-similar materials
- Freedom in adding filler materials
- Shape freedom– complex contours or even hidden joints are possible; at least the coil must be able to pass the bond line
- Clean atmosphere– no ventilation/solvent removal required
- Process freedom– thermoplastic parts of all manufacturing processes can be inductively joined
- Large part capability and continuous processes are deployed
- Non-destructive testing of produced joints is easily achieved
- Loose tolerances due to flowing melt material
- Very precise process control

Especially the latter opens the field for a high potential of automation and closed-loop applications (Rodgers and Mallon 1993). Several utilisations of automated systems and robots in combination with induction joining processes were reported (Moser et al. 2008; Wijngaarden 2005; Bayerl et al. 2014; Rudolf et al. 1999, 2000).

Ahmed et al. (2006) emphasised the advantage of this non-contact welding process and the opportunity to clearly define heat affected zones. Yousefpour et al. (2004) point out the fast and clean technique and the ability to reopen the joint in case of inaccurate welds, internal repair or part replacements. Particularly flexibility and versatility is a major point: induction welding can provide structural, pressure-tight joints for small or large parts, three-dimensional and complex bond line contours and geometries, either as spot or continuous welding technique resulting in high quality stress-free welds. Performance can be increased by adding resin/filler material and enhance preferential heating and allow loose tolerances and various manufacturing methods. Not only welding times are short, associated costs for machine/worker stay therefore low, too, as

well as reject rate and energy consumption (PDL 2008, 72). Border and Salas (1989) report high lap shear strength for APC-2 composite and Rodgers and Mallon (1993) assign good repair attitudes to inductive joining with achieved 50 to 80 % compressive strength in impact damaged parts under vacuum bag configuration. Lewis (1990) accented portability and applicability in field repair.

Literature often adduces main drawbacks as inserted susceptor material with its high (recurring) costs and possible (negative) influence on joint properties (Rotheiser 2004, 336; PDL 2008, 72; Yousefpour et al. 2004; Stokes 1989). For carbon fibre composites and no envisaged enhancement or preferential heating behaviour with auxiliary filler material, no additional insert materials are required. In such a case, a first major issue arises: if necessary filler materials are deployed, foreign particles are introduced in the joint region. This is seen highly critical by certification authorities since possible initial points for cracks or stress concentrations are introduced.

Another point is the bulk heating nature causing significant volumetric heating unless precautions are take, e.g. with novel focused heating approach by Worrall and Wise (2014). Especially concerning aerodynamic surfaces but also global tolerances, geometry changes are not desired. Even points above matrix decomposition temperature can be reached near the induction coil, while inner plies merely reach melting temperature due to the weaker magnetic field (Matsen and Hodges 1998). Avoiding overheating Duhovic et al. (2015) introduced an air cooling with compressed air through the induction coil to keep the surface (exposed to strongest magnetic field) under decomposition temperature.

Thirdly, experiments conducted by Airbus Helicopters using an induction welding process were reported quite insufficient since the metal mesh deployed as lighting protection caused preferential heating on outer surface of the aircraft skin (2016). To overcome this problem, deployment of lightning protection must be postponed after induction joining step challenging well-established scheduling and planning of lay-up and manufacturing of the aircraft skin.

Induction's versatile nature is present in other applications apart from TPC welding: thermoset curing, selective heating, triggering effects in polymers and inductive mould heating are among common utilisations (Bayerl et al. 2014). The latter leads to the fourth major issue: tools used for tape laying of UD plies are usually made out of metal. Prevalently, the iron-nickel alloy "Invar" is preferred due to its very low CTE similar to carbon fibre composites and concurrently comparably high thermal conductivity λimportant for fast and efficient curing processes.

Table 3.1 shows properties for electrical and thermal conductivity (ρ / λ), respectively, and coefficients of thermal expansion for Invar36 and Fused Castable 120 Silica reported in literature. Both have a similar CTE, but resistivity is much higher for the alike insulating behaviour of ceramics and thus no induction sets in. Moreover, thermal conductivity of Invar36 is one order of magnitude higher compared to regarded ceramic material.

Table 3.1 – Comparative Invar36 and Ceramic Properties

		Invar36*	Ceramic†
λ	W/m·K	11	0.62
ρ	10^{-8} Ω m	0.823	↑↑
CTE	10^{-6}/K	< 2	0.8

*Source: *Martienssen and Warlimont 2006, 783; †Fused Castable 120 Silica: Hussey and Wilson 2012, 135*

Although most far away from the induction coil, the metal tooling is directly exposed to redeemed magnetic field and still acts at least as massive heat sink causing much higher energy consumption (Matsen and Hodges 1998) and the still present risk of too intensive heating of the tooling which could in turn melt/damage the outside of the part. An overcome for this problem is either a cooled tooling or induction-unsusceptible tooling materials such as ceramics (Matsen and McCarville 1998), both immensely increasing costs and complexity. Most of the experiments or in-field applications are conducted with clamped/fixed but levitating parts where the mould heating is absent. In their experimental set-up, Pappadà et al. 2015 (2015) welded the lower adherend onto a composite base plate maintaining an induction situation where all materials are equally excited but the distance from the coil decides how strong the induction heating appears. Mitschang et al. (2002) emphasised the use of a “non-conductive” base plate.

Grumman Aircraft Laborаties assessed induction heating as highly suitable in aircraft construction and repair – particularly the F-111A horizontal stabiliser leading edge out of carbon fibre reinforced thermoplastics – possessing comparable or enhanced properties than structural parts processed with autoclave co-consolidation (Mahon et al. 1991; Kagan and Nichols 2005). Costa et al. (2012) confirmed suitability of induction heating while achieving acceptable joint strength.

Rotheiser (2004, 336-37) identifies further disadvantages in the need for coil accessibility hence shape limitations, possible high costs for acquisition and development of achieving optimal process configuration as well as simultaneous heating of adjacent metal inserts. Other cons are related to metallic filler materials like additional insertion operations, stress concentrations and decomposition at the metal-polymer interface which are not present in case of susceptorless induction welding.

4 Evaluation

The following evaluation of *ultrasonic, resistance* and *induction welding* assesses the respective process attitudes mentioned above according to stated evaluation criteria at the beginning of this work. The content refers to the same literature as aforementioned as far as not named explicitly.

For a quantitative assessment, points are assigned to the three regarded processes (displayed in squared brackets at the end of each criteria elucidation in the order: ultrasonic, resistance and induction welding). Starting with three points for the technique with the best properties going down to two and one point for the following methods. Similar results are regarded as equal points. Primary criteria are factored doubled unlike secondary criteria. If one criteria is not sufficiently fulfilled by a process, zero points are assigned. **[US–RW–IW]**

4.1 Process Capability

4.1.1 Parameter

The following elucidation of process parameters is based on the work of Villegas et al. (2013) who regarded CF/PPS composites. Table 4.1 gives a comparison of PPS and PEEK material properties suggesting a reasonable transferability of PPS results to PEEK although authors emphasised the dependency of results on the substrates (type, thickness, quality, weave) and thus difficult generalisations out of them. The intention is nevertheless to reveal at least the magnitudes dealt with in such processes.

Table 4.1 – Mechanical and Thermal Properties of PPS and PEEK

	Structure	ρ [g/cm^3]	E [GPa]	R_m [MPa]	ε [%]	T_g* [°C]	T_s* [°C]	HDT* [°C]
PEEK	semi-cr.	1.3†	3.1 - 3.8	92 - 103	11 - 50	140 - 145	343	152
PPS	semi-cr.	1.62‡	3.9 - 4.3	65 - 82	3 - 20	85 - 90	275 - 290	115 - 260

*T_g: glass transition temperature, T_s: solidus/melting temperature, HDT: Heat Deflection Test

Source: Schürmann 2007, 131-32; †Kaiser 2015, 498; ‡Dominginhaus 2013, 392

There are results for CF-PEEK composites using the considered joining methods, but these were either not available for the author of this work (Beevers 1991) or only inves-

tigating one or two joining methods separately. Since material and process parameters play a key role in achieving good welding quality, a comparative summary of different papers is therefore doubtful. The investigated optimum process parameter by Villegas et al. (2013) are presented in Table 4.2.

Table 4.2 – Process Parameters for Ultrasonic, Induction and Resistance Welding

Method	Cycle Time [s]	Welding Pressure [MPa]	Power [W]	Energy Consumption [kJ]
Ultrasonic	4.43	3	1980	0.7
Resistance	90	0.1	90	1.8
Induction	85	0.8	420	23

Source: Villegas et al. 2013

Regarding cycle time, ultrasonic welding exhibits a by factor 20 shorter process period compared to resistance and induction welding, respectively. Not only the heating phase (0.43 s) is by far the fastest compared to the others, moreover, heating primarily occurs direct at the bonding interface comparable to resistance welding (no bulk heating as for induction heating). Yet, during cooling stage, high thermally conductive metallic sonotrode enhances energy dissipations. Though, Villegas et al. (2013) point out multiplication of cycle times for continuous ultrasonic or induction welding approaches as actuators must be moved along the bondline. Notwithstanding, resistance welding gets into same trouble since potential joint length considered are far beyond electrical or power limitations. Another point to be considered is the dependency of heating time on the weave as investigated by Rudolf et al. (2000) and according to that, UD plies – assigned to later application – exhibit longer heating times by almost one order of magnitude compared to plain weave fabrics. [3–1–2]

Welding pressure and energy consumption will be discussed in sections "*Automation*" and "*Environmental Aspects*", respectively.

4.1.2 Automation

Closed Loop Capability. All three methods show good automation potential since all exhibit distinctive process parameters recorded for process observation, control and modification, respectively. Resistance and induction welding uses power records unlike ultrasonic welding with additionally displacement data and part's mechanical impedance

to determine joint quality. Induction welding offers a certain distance margin since it is a non-contact methods whereas ultrasonic's sonotrode needs a certain contact pressure for achieving high quality weld. For more complex shaped parts with rough tolerances, utilisation of distance sensor are conceivable. Main drawback against this background is contacting of heating element in resistance welding which requires high precision positioning. [2–1–3]

Robotic Capability. Basically, all systems are realisable with robots. Endeffector size and weight range within technical limits of standard robots as well as process forces. DLR demonstrated on the JEC World 2017 exhibition a fully automated robot cell joining thermoplastic composites with resistance welding (DLR 2017b). Automated induction welding robots have been reported by Moser et al. (2008), Wijngaarden (2005) and Bayerl et al. (2014). Automated ultrasonic applications are reported by Gardiner (2011), Offringa (2010) and AM (2013).

One important factor will be welding pressures since robots are not capable of high process forces. Results presented in Table 4.2 show marked differences: resistance welding needed low pressures due to direct interface melting and low desired squeeze out followed by induction welding. For both, pressure applied is merely for consolidation and preventing delamination. In contrast, pressure in ultrasonic welding serves both, sufficient contact for good energy transmission as well as flow and fuse of molten energy directors with the adherends (Avraham Benatar et al. 1989) and thus directly related to the process' heating. Villegas et al. (2013) determined optimum heating and consolidation pressures for CF/PPS composites as 2.2 and 3.0 MPa, respectively. Computing process forces for a use case according to HERTZIAN pressure and sonotrode area yields about 1000 N. Compared to realised robotic friction stir welding machines with high payload industrial robots and pressures up to 10 kN (Völlner 2009, 36; Zaeh and Voellner 2010), doubts can be redeemed but should still kept in mind. Also concepts with force control devices have been developed (C. B. Smith 2000). [1–2–3]

4.1.3 Process Chain Adoption.

Tooling. For ultrasonic and resistance welding, standard metal toolings can still be used unlike inductive technique. "The dies should not be susceptible to inductive heating so mat heating is localized in die retort. We prefer a ceramic that has a low coefficient of thermal expansion, good thermal shock resistance, and relatively high compression

strength, such as a castable fused silica ceramic." (Matsen et al. 1996) Several patents introduce ceramics as tooling material for inductive heating processes (Matsen and McCarville 1998; Matsen et al. 1996; Matsen 1997, 1995; Matsen and Hodges 1998) increasing complexity and costs. Since predominantly metal forms have been utilised so far, complete new toolings need to be produced making a simple, fast and cheap implementation in series production impossible. [3–3–1]

Surface Preparation. Accurate cleaning of joining surfaces is enough for ultrasonic and induction welding. Nature of of "dissimilar" joining when incorporating a metal mesh in a composite matrix rises the need for good adhesion between both materials. This zone is already regarded as the most critical for failure initiation particularly fatigue which is more severe in aerospace applications (Dubé et al. 2008a, 2008b, 2009). The importance and severity of surface preparation for good metal-matrix adhesion in resistance welding is emphasised repeatedly in literature (Hou et al. 1999a; Delgado Labrandero 2009, 22; Freist 2013, 32-33) and therefore requires a costlier additional manufacturing step. [3–1–3]

Manufacturing. Ultrasonic and resistance welding do not require re-scheduling of manufacturing process steps whereas lightning-strike protection in the top layers of the skin lay-up turned out to be a severe issue when regarding inductive welding. Airbus Helicopters (2016) conducted such experiments coming to the conclusion of preferential heating rather on the outside of the skin and not at the interface. In addition, maintaining outer aerodynamic shape becomes just as critical as achieving joining temperature at the bonding interface. Consequently, lightning-strike protection deployment must be outsourced during skin lay-up face and raised at a later stage of production. Again, a simple, fast and cheap implementation in series production is hardly possible. [3–3–1]

4.2 Aircraft Applicability

4.2.1 Geometry

Large Scale Continuity. Ultrasonic and induction welding are capable of large geometries via a moving sonotrode or coil, respectively, and such applications have already been reported, f.i. with subsequent consolidation rollers and sensor implementation in complete endeffectors. Resistance welding is limited in welding length due to factors

like Ohm's law and leakage current tendency. Continuous approaches have been reported very rarely and show more complex experimental set-ups compared to the other two techniques. SRW and ARW are known in this context whereof the first one produced joints with a maximum length of 1.2 m (Taylor and Davenport 1991; Lambing et al. 1993) which is comparably short to aircraft dimensions. [3–1–3]

Lap Joint Design/Accessibility. Envisaged are lap joint designs of which all three bonding techniques are able to produce. The point of accessibility is regarded as the additional space needed despite the actual bonding surface: the sonotrode is just as big as the desired joint width is and thus no extra space is needed. Largest ultrasonic welders are reported as about 0.23 m × 0.3 m (Rotheiser 2004, 482) which should be sufficiently big to achieve one-shot welding in width direction. What must be kept in mind is the correlation of parts curvature and size of the sonotrode: greater curvatures require shorter sonotrodes whereas little curvature enables longer sonotrodes – at least a planar contact surface for optimum transmission of ultrasonic vibrations must be guaranteed. Depending on edge effects due to eddy currents induction, needed space is the joint width or slightly broader, too. More crucial is the coil design, number of turns and supply pipes for water cooling which can extent the required space significantly – also in length. Although the heating element is entirely covered by adherends, contacting requires extra space at least on one side. In case of the regarded continuous approach with copper blocks as connecting element, additional space needed is significant and required accessibility from two sides is hardly manageable with the existing tooling concept. Utilisations of consolidation rollers for achieving welding pressure can be seen as similar for all approaches. [3–1–2]

Tolerance Management. According to Rotheiser, induction welding is well suited for closing gaps and voids of irregular surfaces allowing loose tolerances of pre-manufactured parts, yet, high surface qualities of final parts "... are particularly difficult to achieve with processes that have only one controlled surface [...] These are also methods in which the type of tolerance needed for such joints is held only with difficulty." (2004, 336, 346) Therefore, bulk heating leads to uncertainties in final shape especially on upper and side surfaces – although a consolidation pressure is applied. Comparably local heating of resistance and ultrasonic welding causes usually only little volumetric heating near the interface hence maintaining easily basic part's shape. Considering compensation of loose tolerances, although regarded critically from a process point of

view, ultrasonic welding performs best as the inserted resin film as energy director provides additional matrix material to fill porosities. [3–3–1]

4.2.2 Performance

Lap Shear Strength. The static capability is often quantified by the lap shear strength (LSS). Villegas et al. (2013) investigated LSS for identical CF-PPS composites with ultrasonic, resistive and inductive welded specimens as indicated in Figure 4.1. Although desired matrix system shall be PEEK, this work is of interest since it directly compares same substrates with different joining methods. Thus, ultrasonic and induction welding achieved similar strength values about 27.3 MPa whereas resistance welding dropped down to 23.3 MPa with considerable higher scatter than the other two methods (see also *Certification*).

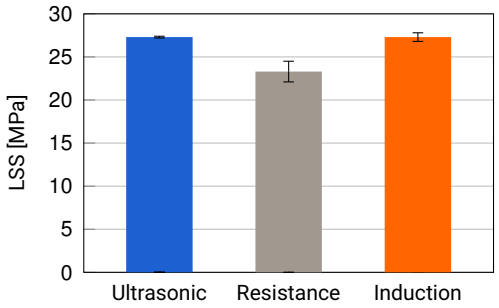

Figure 4.1 – Comparative LSS of Ultrasonic, Resistive and Inductive Welded CF/PPS Specimen (Data: Villegas et al. 2013)

Dubé (2007, 21), Ageorges and Ye (2012, 10-11) and Yousefpour et al. (2004) collected LSS values for APC-2 (CF/PEEK) composites and different joining methods. Computed average values are presented in Figure 4.2 resembling the general trend from above presented results for CF-PPS composites. In both cases, ultrasonic and inductive welded specimens possess superior properties compared to resistance welding.

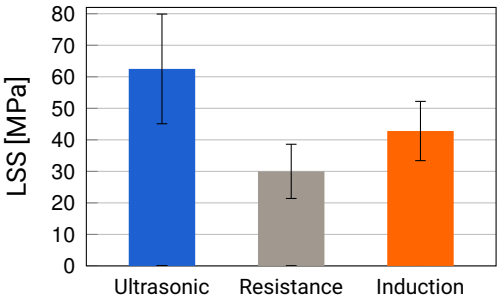

Figure 4.2 – Averaged LSS values for APC-2 (CF/PEEK) Specimen

Scatter is noticeable higher than for the comparative study of CF/PPS which can be accounted for different materials and set-ups in various studies, averaged values are computed out of. This is another argument for the reasonability of attaching values to the study of Villegas et al. (2013).

Undoubtedly, resistance welding behaves inferior again resulting from poorly welded areas on the outer edges due to edge effects – accounting for about 10-15 % reduction in joint area hence LSS (Ageorges et al. 2000b). This fits quite well with obtained average values. With respect to computed standard deviation, LSS for ultrasonic and induction welding can be seen as equal again, albeit with slight advantages for the ultrasonic approach. All in all, the conclusion of consistently higher static strength values for ultrasonic and inductive welding can be drawn with a distant resistant method. [3–1–3]

DCB. Values of interlaminar fracture toughnesses (G_{Ic}) are presented in Table 4.3. Despite intensive research, no comparative study of all three joining types could be found. Therefore, presented results must be treated carefully since differences in material and configurations might falsify comparability. No value for inductive welded CF/TP specimen has been found either. Since no conclusion can thus be drawn, no points will be awarded.

However, Harras et al. (1996) achieved highest G_{Ic} values with optimum ultrasonic welding parameters up to 3.2 KJ/m^2. Also Jakobsen et al. (1989) achieved slightly higher fracture toughness than reference CF/epoxy system investigated by Markatos et al. (2013). Already from this rough consideration (Table 4.3), it is obvious that there is no significant reduction of mechanical properties; quite the contrary.

Table 4.3 – Interlaminar Fracture Toughness G_{Ic} for Different Joining/Material Configurations

Laminate	Joining Method	G_{Ic} [kJ/m^2]
CF/Epoxy (Baseline)	Autoclave Co-consolidation	1.21*
CF/PEEK	Resistance W.	1.9†
CF/PEEK	Ultrasonic W.	3.2‡

*Sources: *Markatos et al. 2013; †Jakobsen et al. 1989; ‡Harras et al. 1996*

Fatigue. Again, the first regarded study (Villegas et al. 2013) provides a starting point and magnitude (Figure 4.3). All three welding techniques lead to more or less similar fatigue behaviours. Ultrasonic exhibits a slightly deeper decrease in % LSS compared to the other two. Eventually, an endurance limit was determined at about 40 % LSS and run out samples (10^6 cycles) where tested statically with no significant fatigue damage found.

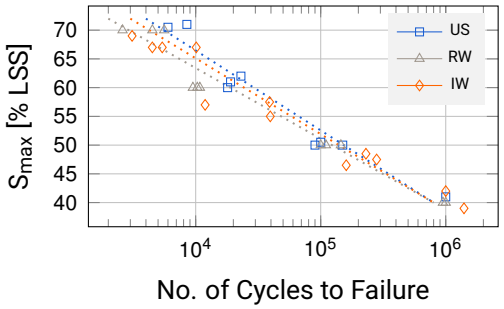

Figure 4.3 – S-N Curves of Differently Welded CF/PPS Specimen (Data: Villegas et al. 2013)

Similar behaviours where obtained for CF/PEEK specimens with endurance limits between and 35 and 40 % (Yousefpour and Hojjati 2007). The similarities of S-N curves in general for different welding technologies is proven by Withworth (1998) Villegas et al. (2010). Therefore all welding types possess a comparable fatigue behaviour with only marginal differences. [3–3–3]

Failure Modes. Before final coupon failure occurs with highest strength (independent of welding quality), other failure modes appear (Figure 4.4). Interlaminar failure represents a failure within the laminate, the heating element or both. Lower strength is observed for interfacial failures between adherends and heating elements depicting an imperfect bonding (Stavrov and Bersee 2005).

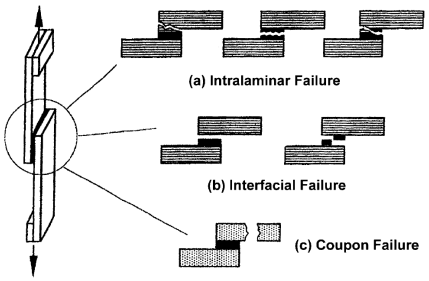

Figure 4.4 – Failure Modes in Lap Shear Tests (Meng Hou and Friedrich 1992)

These failure modes are applicable and reported for all three welding methods (Strong et al. 1990; Don et al. 1990). O'Shaughnessey et al. (2016) showed occurrence of only interlaminar failure modes for all three types of welding techniques when recommended process parameters are applied. If interfacial failure – due to poor adhesion between metal mesh and matrix – can be excluded with sufficient pre-treatment, all process provide favourable results.

4.2.3 Certification

Reproducibility/Scatter. Number of parameters as variables and its fluctuation plays an important role for reproducibility. Ultrasonic welding inherits variables in frequency, amplitude, energy director shape and height/thickness, welding pressure/force and vibration/consolidation time (Troughton 2008, 31; Villegas and Palardy 2017). Induction welding incorporates frequency, generator power, distance between coil and laminate, induction coil geometry, number of coil turns, coil position and flux concentrator, laminate structure and material, welding pressure/force and time, cooling rate which is represented by flux of compressed air for surface cooling and flux of water through the coil (prevent overheating of coil and laminate by convection) and consolidation rollers (cooling time to solidification) as well as deployment of additional susceptor particles (Rudolf et al. 2000; Ahmed et al. 2006; Troughton 2008, 120). Resistance welding shows parameters in input power (current/voltage), resistance (length/diameter/material), clamp-

ing/welding pressure (Stavrov and Bersee 2005). Despite not explicitly mentioned, just as for adhesive bonding, surface preparation is crucial to achieve good metal-matrix adhesion. In the same manner, its rather unpredictable behaviour dramatically influences the joint's mechanical properties just as occurrence and position of poorly welded areas (Ageorges et al. 2000b). In the comparative study of the three methods (albeit for CF/PPS composites) by Villegas et al. (2013), a similar conclusion to previous elucidations can be drawn regarding lap shear strength as shown above: not only LSS of resistance welding parts is considerable lower compared to the other two, but scatter shows a much higher value. In the test series, ultrasonic process with its less parameters was operated near the optimum with very low scatter. Slightly higher but still low scatter was obtained with induction welding and its more numerous but good controllable variables (Figure 4.1). When regarding continuous joining, the feed velocity is an additional variable for all. [3–1–2]

Online Inspection. Most recent developments in resistance welding at DLR Augsburg (2017a) go in the direction of monitoring power respectively voltage/current data to get an insight of weld quality and its improvement. Lambing et al. (1991), Holmes et al. (1991) and Tackitt and Gillespie (1996) introduced a non-contact monitoring of the softening process via ultrasonic probes. Similar approaches with power (current/voltage) are reported for induction welding (Ahmed et al. 2006) expanded by pyrometers directly mounted near the induction coil (Bayerl et al. 2014; Moser et al. 2008) or making recourse of the impedance behaviour of the entire system (Puyal et al. 2007). "Most ultrasonic welding machines nowadays feature fully programmable, microprocessor control to program and monitor all welding parameters. Some machines monitor to adjust the entire process every millisecond." (Troughton 2008, 32) Beyond that, dynamic mechanical impedance gives indication of molten polymer flow (Benatar and Gutowski 1989). Villegas (2015) introduced an in-situ monitoring method assessing power and displacement data recorded by the microprocessor-controlled welder for quality inspection. Insofar, the advantage of ultrasonic machines is the already implemented microprocessor system whereas custom-made extensions need to be utilised for the others. However, all three show enough possibilities for a sufficient online inspection. [3–2–2]

Foreign Object Issue. Only induction joining works theoretically without any additional filler materials regarding carbon fibre composites. If a complete susceptorless induction welding is possible in the current case needs further investigation. If not, metal-

lic particles/meshes are needed in the bondline to induce preferential heating. These are seen as possible initials for micro notches and cracks and thus undesired from certification authority's perspective – holding true for resistance welding as well with its heating element. Dubé et al. (2009) investigated fatigue behaviour of resistance welded carbon composites and found delaminations always located at the weld interface. Despite observed good adhesion between TiO_2 coated metal meshs and the polymer, coating tended to separate from the metal mesh base material. For stainless steel meshs, even poor adhesion was found just as striations suggesting crack propagation in through-thickness-direction and peel stresses causing debonding of the heating element at the edges (2008). Arising issues are galvanic corrosion, different mechanical properties as well as induced stresses due to different CTEs. Unlike ultrasonic welding requiring energy directors of additional matrix material, no "foreign" material is introduced. Only in case of too thick matrix films, resin rich regions can reduce mechanical properties. Yet, this can be overcome by optimisation. Similar to previous elucidations, additional weight penalty must not be neglected for higher density filler materials.

[3–1–2]

4.3 Secondary Criteria

4.3.1 Investment

Acquisition/Equipment Complexity. Ultrasonic welder only need an electrical power supply for generating high-frequency voltage analogical to resistance welding. However, contacting for RW is more difficult and crucial for welding quality. Since both methods generate heat predominantly at the interface and desirably no bulk heating sets in, the consolidation unit only needs to apply a welding pressure and no additional cooling is necessary. Induction welding not only requires electrical power but also water cooling[1] and ideally compressed air for surface cooling to prevent adherend surface overheating (Duhovic et al. 2015), since bulk heating of the part set in, consolidation rollers need to be water-cooled for rapid solidification and maintaining the desired basic shape of the components. Thus, this procedure has by far the most complex equipment requirement.

[3–2–1]

1. necessary due to strong heating of copper; so-called *cold inductors* with low electrical conductivity like iron exhibit less heating but higher electrical resistance hence power losses

Recurring Costs. Despite expenses for electrical power (see "*Parameter*"), additional resources are needed consistently. Ultrasonic technique requires energy directors, e.g. in form of a thin PEEK film, resistance welding requires heating elements and in case of preferential heating with susceptors, e.g. metallic particles are necessary for inductive welding. For the latter, the availability of compressed air and cooling water brings additional costs. [2–2–1]

4.3.2 Fibre-Fairness

All three processes create no fibre interruptions in contrast to mechanical fastening methods (basis for potential improvements). Ultrasonic welded parts can exhibit imprints of the sonotrode due to the applied pressure (Fischer et al. 2015). However, this phenomenon is rather an issue for spot welding and not for a continuous process with moving sonotrode along joint line. In such a case, potential change in thickness would occur over the whole length and local effects can be excluded. On the other hand for resistance and induction welding, possible filler materials could introduces interference effects due to dissimilar materials between carbon fibre and metal meshs/particles.

4.3.3 Heating Characteristics

Heat Affected Zone (HAZ). The heat affective zone for all three methods can be easily characterised either by size of the sonotrode, heating element or coil. However, there are distinctive differences in finiteness. The sonotrode directly applies vibrations which are converted into heat. Through the sharp limitation of the sonotrode geometry and the deployment of ED material, the heat affected can be limited to a distinctive area.

Unlike resistance and induction welding show either poorly welded areas (see "*Performance*") or additionally inductively influenced areas by diffusion of the magnetic field. The latter can be corrected but not eliminated by magnetic flux concentrators. Nonetheless, such an equipment increases weight and costs of the endeffector. [3–2–2]

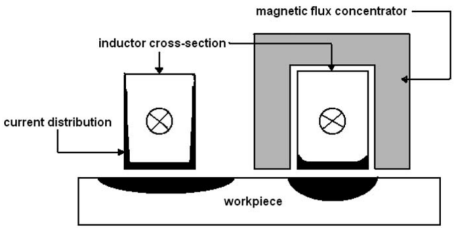

Figure 4.5 – Magnetic Flux Concentrator (Ahmed et al. 2006)

Heating Curve. Levy et al. (2014) simulated heating behaviour during ultrasonic welding of PEEK composites with triangular energy directors showing a clear initialisation and concentration of heating at the EDs, even in case of assumed equal stiffnesses of composites and neat resin EDs. Furthermore, a quadratic influence of the vibration amplitude on the heating rate was proven. The data revealed holding force as instrument to adjust the maximum temperature in the EDs – especially since temperature is approximated asymptotical without overshooting (Figure 4.6a) – and lower temperatures for flatter ED angles. This leads to the assumption that a flat ED shows an even lower and thus less dangerous heating behaviour in terms of thermal degradation by overshooting (Figure 4.6b). Khmelev et al. (2007) confirms the inability of a welding process under too high static pressure leading to an even more enhanced damping of the oscillatory system hence decrease in vibration amplitude respectively input energy necessary for the melting process.

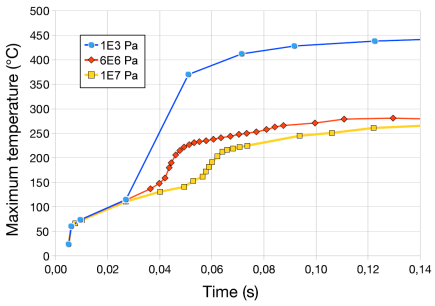

(a) Maximum ED Temperature over Time for Different Welding Forces

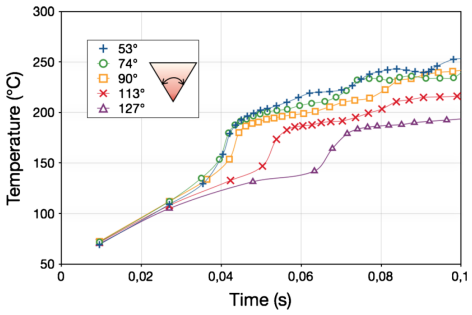

(b) Maximum ED Tip Temperature over Time for Different Angles of EDs

Figure 4.6 – ED Temperature Development during Ultrasonic Welding for Different Configutations (Levy et al. 2014b)

Basically, the mechanism can be seen as self-stabilising: EDs act as heat initiators

disappearing when exposed to ultrasonic vibrations and subsequent melting which in turn causes a diminished heat generation and a quasi-constant temperature at melting point level for a certain period of time until heat conduction/consolidation sets in.

Though, particularly semi-crystalline materials show a sharp melting point due to additional energy for breaking up crystalline structure (see Section 3.3.2). Vice versa, solidification appears very abruptly due to sudden recrystallization of molecules. Moreover, their orderly molecular structure absorbs vibrational energy unlike amorphous plastics with lower attenuation (Dukane 2011, 10).

Rudolf et al. (2000) investigated the induction heating and determined the four stages of heating (Figure 4.7) whereby the constraints for temperature points are given by:

$T_m < \theta_1 < T_d \qquad \theta_4 < T_{cry}$

$T_m < \theta_2$

Since there is no asymptotical convergence rather than a peak – in context with the high heating rates due to the by far larger amount of transferred heat –, achieving the appropriate process envelope with the requirement on low cycle times is more difficult.

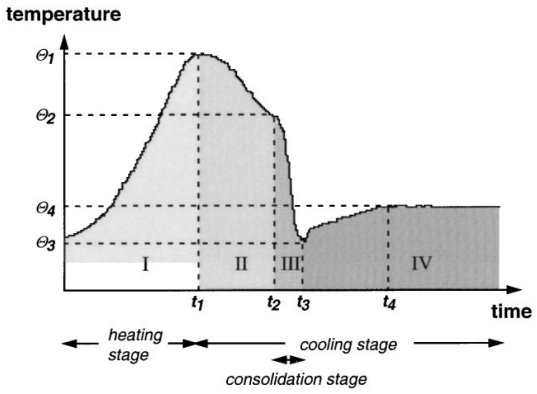

Figure 4.7 – Typical Temperature-Time-Curve of the Continuous Induction Welding (Rudolf et al. 2000)

Quite a similar behaviour can be observed for resistance welding. In their investigation on continuous resistance welding, Shi et al. (2015) modelled and simulated the heat generation exhibiting a similarity in high heating rate, peaking temperature and subsequent consolidation (Figure 4.8) – evoking same difficulties of overshooting and overheating and the higher sensitivity to disturbances. In this case, the peak is even more distinct due to the sudden switch off of the electrical power source.

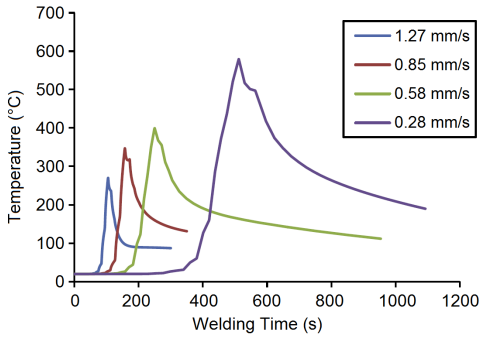

Figure 4.8 – Temperature Development over Time for Different Welding Speeds (Shi et al. 2015)

Finally, the conclusion can be drawn that ultrasonic heating behaviour provides the

most desirable attitude with its asymptotical convergence rather than steep increase and peaking temperatures for induction or resistance welding involving danger of local overheating and decomposition hence weakened joint strength. [3–1–1]

4.3.4 Maintenance

Portability plays a role as well as the ability to reopen and replace damaged parts/structure. Concerning both, ultrasonic welding has to wait in line. Once energy directors are consumed during initial joining, no later heating with ultrasonic vibration is possible. In addition, Lewis characterised equipment "[...] too heavy for practical in-field work" (Lewis 1990), in contrast to the other two methods regarded as easily portable (Yousefpour 2006; Lewis 1990). Furthermore, possibility of joint reopening joint is given – albeit only with bulk heating of the complete part for (susceptorless) inductive welding. Resistance welding therefore exhibits more practicable detachability properties using the still existing heating element. [1–3–2]

4.3.5 Environmental Aspects

Energy Consumption. Electrical power records presented in Table 4.2 exhibit big differences. Although it must be noted that power required for resistance welding is directly dependent on the resistance of the heating element and therewith on the length, cross section and material, (Eq. Eq. 3.1), and can vary therefore, the power needed for ultrasonic welding is still higher by factor 5 and 20 compared to induction and resistance welding, respectively. However, when determining the total energy consumed by the process, the very low cycle time of ultrasonic benefits in a magnitude that it possess clearly the lowest value of all three techniques, followed by resistance and the distant induction approach. [3–2–1]

Resources. As already mentioned in the section "*Investment*", equipment complexity for induction heating is mainly due to the necessity of air and water cooling. Therefore, the use of resources (electrical power, water, compressed air) is more crucial for the inductive approach than for the other two.

Recycleability. Regarding the recycleability, no hazardous materials are introduced during joining processes. It can be basically broken down into carbon fibres, thermoplastic

resins and metallic meshes (stainless steel) – all enable the achievment of a closed loop recycling system.

4.4 Resumée and Final Remarks

The evaluation matrix yield the ultrasonic welding as method of choice followed by induction and resistance welding which thereby confirms the overall impression of the assessment.

Resistance welding showed a promising approach for static welding of thermoplastic composites, is however hardly compatible with a continuous process. Issues in upscaling (size of heating element/power requirements), continuity and access concerning this work limit this process to an unfavourable degree as well as the generally steep heating behaviour with distinct temperature peaks and a process sensitivity to disturbances leading to difficult control. Research is generally progressing, though in the field of continuous applications it seems to have stalled.

Induction and ultrasonic welding both exhibit advantages in heating time, upscaling, continuity, energy consumption, areal joining and access all benefiting the aim of this research.

Disadvantages of ultrasonic welding appear as need for presence of an energy director, consequently no ability to reopen after initial joining and higher process forces are present. However, those can be handled.

Drawbacks of induction welding turn out to be much more severe. The perk of a non-contact process in turn does not provide a defined geometry. Heating with envisaged unidirectional plies is reported as difficult and ineffective (weak forming of eddy current circuits) bringing up the need for metallic insert materials (paste, particles) for preferential heating. Foreign object issues are seen more than critical by certification authorities. Moreover, the prior applied lightning protection consisting of a metal mesh on the outside of the thermoplastic shells causes preferential heating there, too, as well as the metallic tooling. Production schedule and process auxiliaries/tooling would evoke a costly re-design and delays series production implementation. In addition, the steep heating behaviour and need for air/water cooling are further complexing the equipment.

The tendency towards ultrasonic welding is enhanced by the current very intensive research and high number of publications on this topic in the last few years – and on joining of thermoplastic structures for aviation applications in particular. In contrast,

research on induction welding is rather outmoded and large progress in this field has not been identifiable.

Eventually, it stands to reason to persevere the ultrasonic welding approach as it combines desirable benefits with acceptable and solvable disadvantage whilst offering best performance in the numerical assessment.

Table 4.4 – Evaluation Summary

		US	RW	IW
Process Capability		**19**	**16**	**16**
Parameters				
	Cycle Time	3	1	2
	Pressure	1	3	2
	Energy Consumption	3	2	1
Automation				
	Closed Loop Capability	2	1	3
	Robotic Capability	1	2	3
Process Chain Adoption				
	Tooling	3	3	1
	Surface Preparation	3	1	3
	Manufacturing	3	3	1
Aircraft Applicability		**24**	**13**	**18**
Geometry				
	Large Scale Continuity	3	1	3
	Lap Joint Design/Accessibility	3	1	2
	Tolerance Management	3	3	1
Performance				
	Lap Shear Strength	3	1	3
	DCB	-	-	-
	Fatigue Behaviour	3	3	3
	Failure Modes/Detectability	-	-	-
Certification				
	Reproducibility/Scatter	3	1	2
	Online Inspection	3	2	2
	Foreign Objects Issue	3	1	2
Secondary		**9**	**9**	**6**
Investment				
	Equipment Complexity	3	2	1
	RC costs	2	2	1
Fibre Fairness		-	-	-
Heat Affected Zone		3	2	2
Maintenance		1	3	2
Environmental Aspects				
Total		**97**	**67**	**74**

5 Pre-Testing Campaign

5.1 First Series

First pre-testing was performed at DLR Augsburg with a mobile test stand for ultrasonic welding (Figure 5.1a) introduced by Dorsch (2013).

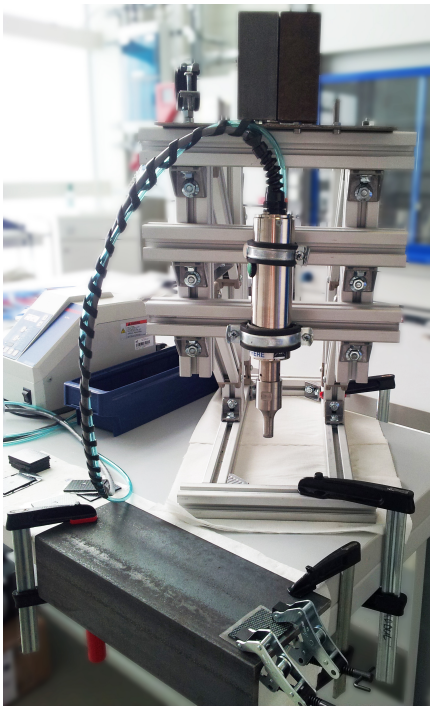

(a) Mobile Test Stand

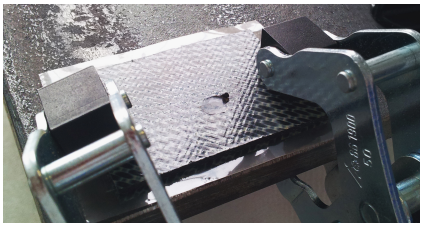

(b) Specimen/Clamping Set-Up

(c) Spot-Welded Specimens: soot-blackened 50 µm, 1000 J

Figure 5.1 – First Pre-Testing Campaign Set-Up

Test specimen of about 60 x 40 mm were clamped with two vices onto a steel plate; in-between a PEEK film with 25 µm/50 µm thickness (Figure 5.1b). BRANSON 40 kHz generator of type LPe 40:0.50:4T with a circular bellied sonotrode (⌀ 3/8") was centred and positioned onto upper adherend surface. Additional weights on the construction created a contact force $F_C \approx$150 N (Dorsch 2013). Input energies were varied between 500 and 1000 J per specimen. A welded joint could be achieved for all of them (Figure 5.1c) withstanding shear loads applied by hand. Although no further investigations of strength and/or formation of joints was conducted, feasibility of ultrasonic welding of CF/PEEK composites – even with 40 kHz system – was proven for static tests.

5.2 Second Series

A second pre-testing campaign was arranged at the ultrasonic welding machine manufacturer BRANSON at their laboratories in Dietzenbach, Germany.

Two CF/PEEK plates with a 25 µm / 50 µm PEEK film in-between were used for static welding tests with a 20 kHz system of type 2000X with same circular bellied sonotrode (⌀ 3/8"). Initial welding tests for loose adherends at various weld times (0.2-0.3 s) and forces (200-1000 N) revealed no weldability, only slight to strong melting in the contact region between top surface and sonotrode. In a second stage, similar to the first campaign tests, set-up was changed with a tight fixturing of probes near the sonotrode position. Indeed, in this configuration a distinct fusion bonding was observed at the interface area of adherends with subsequent nearly no imprint/melting on top surfaces.

Consulting BRANSON, welding of CF/PEEK plates with flat EDs is still seen critical. Although they experienced good welding joints with PEEK material in the past – all such joints were manufactured using three-dimensional ED shapes, e.g. triangular. Estimated heights of desired shaped EDs for this application are 0.5-0.8 mm.

Supporting this theory, CF/PEEK was already spot-welded even for aircraft applications (Palardy and Villegas 2016), however, all publications stating no difference between shaped and flat EDs were predominantly conducted with composites of semi-crystalline CF/PPS (Senders 2016, Villegas and Palardy 2017, Palardy and Villegas 2017, Villegas et al. 2014) This leads to the assumption of a strong material dependence and the tendency of less good applicability of flat energy directors to CF/PEEK composites. Detailed contemplation on that issue can be found in chapter 6 (“*Heating Models, Mechanisms and Parameters”*).

5.3 Third Series

A third pre-testing campaign at DLR Augsburg investigated the feasibility of ultrasonically welded lap joints with CF/PEEK material. Set-up was identically with the first pre-testing series (F_C = 150 N); only adherends were positioned in overlap configuration with clamping at averted edges (Figure 5.2). Input energy was held constant at 1000 J. Film thicknesses were varied with 25 µm, 50 µm and 100 µm (2x50 µm loosely inserted). All three exhibited a welded joint (Figure 5.3) withstanding shear loads applied by hand again. Configuration with 25 µm film showed the most distinct imprint of the sonotrode on the top surface (Figure 5.3a) whereas there could not be found such on the other two variants (Figure 5.3b) implying the highest top surface temperatures hence weakening

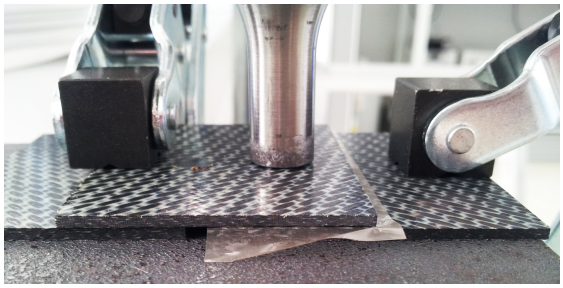

Figure 5.2 – Third Pre-Test Overlap Configuration

(a) Spot-Welded Overlap Specimen: transparent 25 µm, 1000 J. Distinct imprint marked

(b) Spot-Welded Overlap Specimens: soot-blackened doubled 50 µm, 1000 J

(c) Spot-Welded Overlap Specimen (Backside): soot-blackened 50 µm, 1000 J. Molten matrix material marked

Figure 5.3 – Spot-Welded Overlap Specimen

of matrix stiffness there. For 50 µm film tess, molten matrix on the lower adherend hidden edge was observed (Figure 5.3c) indicating a far advanced melt front at the interface. Once more, no further investigations of strength and/or formation of joints was conducted despite the feasibility of static ultrasonic welding in overlap configuration of CF/PEEK composites was proven.

6 Heating Models, Mechanisms and Parameters

After proving basic feasibility, in order to understand the fusion bonding process and how it can be manipulated towards an optimum weld strength and quality, relevant influence quantities must be determined. Therefore, the following sections focus on theory and modelling of ultrasonic welding revealing mathematical equations and variables representing process parameters. As a consequence, presented theory shall be confirmed and quantified with experimental testing in following chapters.

A fusion bonding process requires molten matrix material resulting from heating. In ultrasonic welding, heating occurs when sonotrode's mechanical deformation work is transferred into interfacial and intermolecular friction (Villegas 2015), whereof interfacial friction induces initial melting at the energy directors and disappears when adhesion sets in (Levy et al. 2014a). The amount of heat transferred must therefore meet the magnitude of the required melting energy expressed as enthalpy of fusion.

6.1 Enthalpy of Fusion

The enthalpy of fusion denotes the amount of energy required to transfer material from solid to liquid state with an isobar process by overcoming intramolecular forces. Starting from the specific enthalpy, energy needed for melting a certain amount of polymer follows

$$h_m = \frac{H_m}{m} = \frac{H_m}{\rho \cdot V} = \frac{H}{\rho \cdot A_C \cdot dz} \quad \Rightarrow \quad H_m = h_m \cdot \rho \cdot A_C \cdot dz \qquad \text{(Eq. 6.1)}$$

with the specific enthalpy of fusion h_m, density ρ, contact area A_C and incremental height dz of temporarily molten polymer. Specific enthalpy, density and incremental height (based on the heat conductivity of the material) are substance-specific properties hence contact area as only remaining adjustable parameter to control the required amount of energy for matrix melting in direct proportionality.

6.2 Deformation Work

The generator's electrical input energy supplies the converter which in turn creates a vibration via a piezoelectric or magneto-restrictive actuator. This vibration excites the sonotrode pressed against the adherend top surface by a contact force F_C. The so-

notrode's amplitude $a_{S,0}$ is thereby a factorisation of the original converter amplitude multiplied by booster and horn gain factors.

Important to note is that ultrasonic machine manufacturers usually refer to the amplitude as peak-to-peak travel distance and not as commonly defined the height of upper or lower sine wave.

The following derivation is based on the approach by Dorsch (2013) to determine the deformation work W_d starting from of the basic work definition

$$W_d = \int F dx \tag{Eq. 6.2}$$

with the force F that acts along the path of the incremental distance dx. Assuming the contact pressure of the sonotrode on the top surface F_C as pre-load condition and the sonotrodes motion oscillating around this origin, the actual contact force is time dependent and reads

$$F_{C,a}(t) = F_C + F_\Delta \cdot \sin(\omega t) \tag{Eq. 6.3}$$

whereof F_Δ is the alternating time-dependent part of actual contact pressure. In addition, the actual motion of sonotrode can be described as

$$x_{S,a}(t) = \frac{a_{S,0}}{2} \cdot \sin(\omega t) \qquad \frac{2x_{S,a}(t)}{a_{S,0}} = \sin(\omega t) \tag{Eq. 6.4}$$

with sonotrode's peak-to-peak amplitude $a_{S,0}$. Inserted in (Eq. 6.3) yields

$$F_{C,a}(t) = F_C + F_\Delta \cdot \frac{2x_{S,a}(t)}{a_{S,0}}. \tag{Eq. 6.5}$$

Integration of (Eq. 6.5) reads

$$W_d = \int_{-\frac{a_{S,0}}{2}}^{\frac{a_{S,0}}{2}} \left(F_C + F_\Delta \cdot \frac{2x_{S,a}(t)}{a_{S,0}} \right) dx = \left[F_C \cdot x + F_\Delta \cdot \frac{x_{S,a}^2(t)}{a_{S,0}} \right]_{-\frac{a_{S,0}}{2}}^{\frac{a_{S,0}}{2}} \tag{Eq. 6.6}$$

with integration limits of half the peak-to-peak amplitude in each direction. By this, the latter term eliminates itself during insertion of limits, only remaining the first term expressed as

$$W_d = F_C \cdot \left[\frac{a_{S,0}}{2} - \left(-\frac{a_{S,0}}{2} \right) \right] = F_C \cdot a_{S,0} \tag{Eq. 6.7}$$

This energy is put into the adherends during first half of the oscillation (positive sign)

leading to the expression for the power P_d by deformation as

$$P_d = \frac{dW_d}{dt} = \frac{W_d}{\frac{T}{2}} = 2F_C \cdot a_{S,0} \cdot \frac{1}{T} = 2F_C \cdot a_{S,0} \cdot f \qquad \text{(Eq. 6.8)}$$

with the linear dependence on applied (converter) frequency f. Since there are coupling losses between sonotrode and adherend surface, the efficiency factor η_{cpl} shall be introduced leading to the transferred power

$$\dot{Q}_{in} = 2F_C \cdot a_{S,0} \cdot f \cdot \eta_{cpl} \qquad \text{(Eq. 6.9)}$$

Higher degree of deformation work can be achieved either with increased weld/-contact forces F_C, amplitudes $a_{S,0}$ or generator frequencies f as well as with an improved sonotrode-sample coupling.

Dukane (2011, 75) quantifies transition efficiency for sonotrode/part and part/fixture as 50-95 % each, depending on tool fitting. Furthermore, these interfaces are critical since they cannot be predicted and compensated as well as disturbances in the converter/ booster/ sonotrode unit.

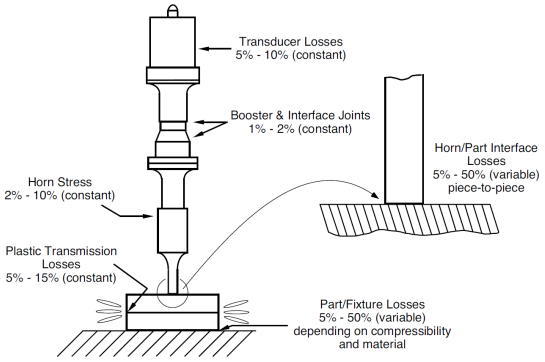

Figure 6.1 – Energy Losses in Ultrasonic Welding Process (Dukane 2011, 74)

According to that, coupling efficiency from the sonotrode downwards can be calculated by (n denotes the variability from one welding to another)

$$\eta_{cpl} = \eta_{sonotr-part}(n) \cdot \eta_{interface} \cdot \eta_{part-tooling}(n) \qquad \text{(Eq. 6.10)}$$

6.3 Interfacial Friction

Since interfacial friction heat is crucial for initial melting, modelling can refer to dry friction between two solids according to Coulomb's Law as

$$\vec{F_\tau} = -\mu \cdot F_N \cdot \frac{\vec{v}}{|\vec{v}|} \qquad \text{(Eq. 6.11)}$$

with constant sliding friction coefficient μ throughout the motion (unless state of melting is reached), normal reaction force F_N and relative velocity v. With respect to the

applied area A, (Eq. 6.11) can be re-written as

$$\vec{\tau} = -\mu \cdot \sigma_N \cdot \frac{\vec{v}}{|\vec{v}|} \qquad \text{(Eq. 6.12)}$$

whereof the normal stress consists of a constant and a oscillating term recalling (Eq. 6.3). Based on this, Levy et al. (2014) developed a model for friction dissipated power on flat energy directors as

$$\dot{Q}_{fric}(x) = \alpha_h^2 \frac{\omega}{\pi} \mu \left| \sigma_{yy}^*(x) \delta u^*(x) \right| \qquad \text{(Eq. 6.13)}$$

with the hammering coefficient α_h considering contact losses between sonotrode and adherend surface, oscillation frequency ω, friction coefficient μ, vertical stress on the horizontal interface σ_{yy}^* and horizontal displacement $\delta u^*(x)$.

The latter can be qualitatively compared to the amplitude and considering other process parameters, (Eq. 6.14) can be reduced to

$$\dot{Q}_{fric}(x) \sim f \cdot \mu \cdot \frac{F_N}{A} \cdot a_{S,0} \qquad \text{(Eq. 6.14)}$$

exhibiting linear dependencies of frictional heat generation on the vibration/generator frequency f, friction coefficient μ, welding/contact force F_C and amplitude $a_{S,0}$ as well as an indirect proportionality to the applied area A. Jiang et al. (2008) proved the indirect proportionality of the friction coefficient μ and surface roughness R_a of which the latter is an adjustable process parameter. It stands to reason that shaped energy directors increase drastically the surface roughness and increase friction heat generated.

6.4 Intermolecular Friction

Second stage of heating is predominated by intermolecular friction. Thus, a visco-elastic model of the polymer shall be established. Unlike elastic behaviour (here σ), modified shear stress-strain behaviour (here τ) for a viscous fluid is a time-dependent approach following

$$\sigma = E \cdot \varepsilon \qquad \tau = \eta \frac{d\gamma}{dt} = \eta \dot{\gamma} \qquad \text{(Eq. 6.15)}$$

When exposed to sinusoidal oscillations, strain follows stress with a phase angle difference δ hence time dependency according to

$$\varepsilon(t) = \varepsilon_0 \cdot \sin(\omega t) = \varepsilon_0 \cdot e^{i(\omega t)} \tag{Eq. 6.16}$$

$$\sigma(t) = \eta \dot{\varepsilon} = \eta \cdot \frac{d}{dt}(\varepsilon_0 \cdot \sin(\omega t)) = \eta \cdot \varepsilon_0 \cdot \omega \cdot \cos(\omega t) \tag{Eq. 6.17}$$

$$\sigma(t) = \eta \cdot \varepsilon_0 \cdot \omega \cdot \sin(\omega t + \delta) = \sigma_0 \cdot e^{i(\omega t + \delta)} \tag{Eq. 6.18}$$

Since viscous loss occurs, the elastic modulus is expressed complex as

$$E^* = \frac{\sigma^*}{\varepsilon^*} = \frac{\sigma_0 \cdot e^{i(\omega t+\delta)}}{\varepsilon_0 \cdot e^{i(\omega t)}} = \frac{\sigma_0}{\varepsilon_0} \cdot (\cos\delta + i\sin\delta) \tag{Eq. 6.19}$$

whereof $E' = \Re\, E^*$ represents the storage and $E'' = \Im\, E^*$ the loss modulus. The ratio defines the loss tangent δ

$$\tan\delta = \frac{E''}{E'} = \frac{\sin\delta}{\cos\delta} = \tan\delta \tag{Eq. 6.20}$$

Energy dissipated per cycle can be determined following the definition of the elastic modulus

$$W = \oint \sigma d\varepsilon = \oint \sigma \dot{\varepsilon} dt \tag{Eq. 6.21}$$

The complex stress-strain relationship reads

$$\sigma(t) = E' \cdot \varepsilon_0 \cdot \sin(\omega t) + E'' \cdot \varepsilon_0 \cdot \cos(\omega t) \tag{Eq. 6.22}$$

Inserting this in (Eq. 6.21) with integration limits of one period yields

$$\begin{aligned} W_{mc} &= \int_0^{\frac{2\pi}{\omega}} \left[E' \varepsilon_0 \sin(\omega t) \cdot (\gamma_0 \cdot \cos(\omega t))\right] dt \\ &+ \int_0^{\frac{2\pi}{\omega}} \left[E'' \varepsilon_0 \cos(\omega t) \cdot (\gamma_0 \cdot \cos(\omega t))\right] dt \\ &= 0 + \pi \cdot E'' \cdot \varepsilon_0^2 \end{aligned} \tag{Eq. 6.23}$$

The averaged dissipated power per cycle based on inter-molecular $\dot{Q}_{mc}$ friction follows the loss modulus term

$$\dot{Q}_{mc} = \frac{dW}{dt} = \frac{W_{mc}}{\frac{2\pi}{\omega}} = \frac{\omega \cdot \varepsilon_0^2 \cdot E''}{2} \tag{Eq. 6.24}$$

with the oscillation frequency ω, strain amplitude ε_0 and loss modulus E''.

Besides the linear influence of generator frequency f (ω), two points are from greater importance: firstly, the quadratic dependency of dissipated power on the strain amplitude representing the amplitude $a_{S,0}$, and secondly, the linear dependence only on the polymer loss modulus E''.

Thus, the amplitude is a sensitive instrument since a doubled amplitude creates four times higher intermolecular heat dissipation. In addition, polymers with higher loss moduli show better heating behaviours. Recalling the previous chapter, PPS matrices showed much better weldability than PEEK in the pre-testing campaign. Following (Eq. 6.24), PPS should exhibit a higher loss modulus. Indeed, the loss tangent of PPS was found to be up to one order of magnitude lower than the one of PEEK at room temperature (Ho and Jow 2009, 10) hence $E''_{PPS} \gg E''_{PEEK}$. Lower T_g and T_m are further indications for this circumstance.

Benatar and Gutowski (1989) proved a strong temperature dependency of PEEK's loss modulus especially around T_g (Figure 6.2). Thus, the aim is to quickly establish zones with polymer temperatures around T_g by frictional heat to enhance viscoelastic heating there inducing faster melt front progression.

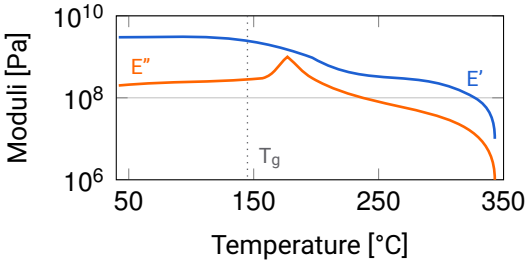

Figure 6.2 – Storage (E') and Loss (E") Moduli for PEEK at 20 kHz (Data: Benatar and Gutowski 1989)

6.5 Combined Heating Mechanisms

Ziegltrum (2001, 51-53) investigated the influence of static contact force for heating and melting of thermoplastics with two main conclusions: 1) below a certain applied contact force there is no effective coupling between sonotrode and part increasing heating time drastically, and 2) generally leads an increase of contact force to an remarkable decrease in process time. This outcome is confirmed by observations of Villegas (2015).

For further increase of contact force, Potente (2004, 177) determined two regions of heating according to Figure 6.3. Below a distinct break point (blue) marks the region of combined interfacial and intermolecular frictional heating whereas above (red), only intermolecular heating was observed. Based on that, he developed a constitutive model for the simplified adiabatic heating process under ultrasonic oscillations as

$$(\pi\eta + 2m\mu)\, E\hat{\varepsilon}^2 f = \rho c \frac{dT}{dt} \qquad \text{(Eq. 6.25)}$$

with

$$m = 0.25\left[1 - \left(\frac{p}{p_k}\right)^{0.7}\right] \qquad \text{(Eq. 6.26)}$$

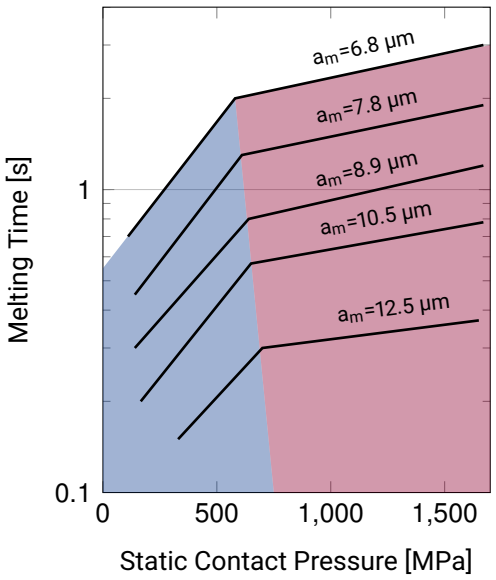

Figure 6.3 – Melting Time of PMMA over Contact Pressure for Different Amplitudes (Data: Potente 2004, 177)

using damping constant η, friction coefficient μ, Young's Modulus E, amplitude strain $\hat{\varepsilon}$, oscillation frequency f, polymer density ρ and specific thermal capacity c as well as static pressure p and pressure at break point p_k.

In case of solely intermolecular friction, the facial friction term $2m\mu$ disappears. Above T_g, the shear heating term $\tau\dot{\gamma}$ replaces it.

Thereout, one can conclude that interfacial friction gets redeemed since relative movement necessary for frictional heating is more limited with increased contact pressure and eventually no relative motion between adherends is possible. By this, contact pressure shall be chosen high enough to ensure good transmission of energy throughout vibration application, but low enough to avoid limited relative motion of the parts. This includes the fixture of parts.

6.6 Multi-Body Dynamics and Interfacial Friction

The oscillating system of ultrasonic welding set-up can be represented by a serial spring--damper system (Benatar and Gutowski 1989). Energy loss per cycle in a damper under harmonic oscillation follows (Stutts 2013)

$$W_d = \oint F_d dx = \oint D\dot{x}dx = \oint D\dot{x}^2 dt = D\omega^2 x_0^2 \int_0^{\frac{2\pi}{\omega}} cos\,(\omega t)\,dt = \pi D\omega x_0^2 \qquad \text{(Eq. 6.27)}$$

with the respective damping coefficient D. For an increasing number of masses with associated springs and dampers, energy losses must be summed up. Depending on the damping system, this dissipated energy is not implicitly involved in the heating mechanism.

In addition, (Eq. 6.14) shows an indirect proportionality of dissipated friction heat and applied surface. Either by inserting an additional loose layers and/or by deploying flat EDs, the surface is increased drastically by factor two or more, causing less generated friction heat important for initial heating due to less energy concentration and larger heat conduction effects. This assumption is confirmed by the study of Villegas et al. (2014). They investigated ultrasonic weldability of different ED shapes and conducted their study with triangular EDs directly moulded on the substrate, triangular EDs moulded on a loose resin stripe and a flat ED film (Figure 6.4). The characteristic power-displacement curves revealed fastest initial heating for EDs on the substrate, followed by moulded resin stripes and far behind the flat ED film. However, the final cycle time differs since an interaction of all heating mechanisms takes place after initial melting and during adhesion development.

(a) Triangular ED moulded on Substrate

(b) Triangular ED moulded on Loose Resin Stripe

(c) Flat ED Film

Figure 6.4 – Investigated ED Forms

BRANSON follows previous elaborations for ultrasonic welding of three separate parts: in a two-step process, input energy is concentrated on one interface after the other, firstly joining the upper and middle part, and secondly, the joined with lower part.

Lastly, each interface layer does not only provide an additional surface but affiliated transmission losses further decreasing the process efficiency.

6.7 Composite Heat Flow Behaviour

Since composites exhibit no isotropic material behaviour, basic law of heat conduction – FOURIER'S LAW – (Baehr and Stephan 2016, 4)

$$\dot{q} = -\lambda \cdot \nabla T \tag{Eq. 6.28}$$

must be rewritten as

$$\dot{q}_i = -\lambda_{ij} \cdot \frac{\partial T}{\partial x_i} \qquad \text{with} \qquad i,j = (1,2,3) \tag{Eq. 6.29}$$

with the heat conductivity λ_{ij} as 2nd order tensor. Assuming the unit cell method (Thomas et al. 2008), the tensor reads

$$\lambda_{ij} = \begin{pmatrix} \lambda_{11} & 0 & 0 \\ 0 & \lambda_{22} & 0 \\ 0 & 0 & \lambda_{33} \end{pmatrix}. \tag{Eq. 6.30}$$

For the given 0/90° fabric, λ_{11} and λ_{22} represent fibre directions ($\lambda_{\parallel}$), λ_{33} the thickness direction ($\lambda_{\perp}$). The latter can be determined by applying rules of mixture

$$\lambda_{\perp} = \varphi \cdot \lambda_f + (1-\varphi) \cdot \lambda_m \tag{Eq. 6.31}$$

with the fibre volume content φ and thermal conductivities of fibres and matrix $\lambda_f = 10.46\ {}^{W}/_{m \cdot K}$ and $\lambda_m = 0.29\ {}^{W}/_{m \cdot K}$, respectively. Values are taken from the data sheets of deployed materials (see Appendix A). Fibre volume content in aerospace applications typically ranges between 0.55 – 0.65. For the given laminate, φ is denoted as 0.5.

For a rough approximation, thickness direction can be modelled as a flat composite wall consisting of layers of fibres and matrix, alternately. Occurring stationary heat flow $\dot{Q}$ can be generally described expanding (Eq. 6.28) by an arbitrarily chosen area element dA to

$$d\dot{Q} = -\lambda \cdot \nabla T dA. \tag{Eq. 6.32}$$

Considering a one-dimensional heat flow in thickness direction z reads

$$d\dot{Q}_z = -\lambda_z \cdot \frac{\partial T}{\partial z} dx dy. \tag{Eq. 6.33}$$

Integration, rearranging and anew integration yields

$$\dot{q}_z = -\frac{\lambda_z}{t} \cdot \Delta T = -k \cdot \Delta T. \qquad \text{(Eq. 6.34)}$$

Heat conductivity in thickness direction can be computed according to a serial arrangement of layers (Figure 6.5). For simplification, heat transfer between layers is assumed as ideal hence $\alpha_i = \alpha_o \rightarrow \infty$. With the fibre volume content, relative thicknesses are used finally getting the thermal resistance

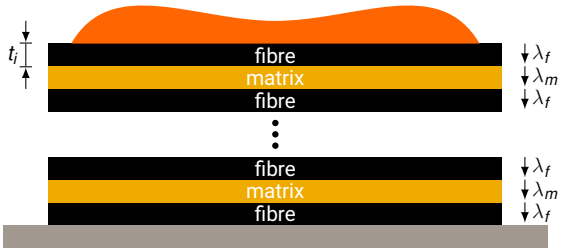

Figure 6.5 – Composite Wall Model

$$k_z = \frac{1}{\sum_{i=1}^{n} \frac{t_i}{\lambda_i}} = \frac{1}{\frac{\varphi}{\lambda_f} + \frac{1-\varphi}{\lambda_m}} = \frac{1}{\frac{0.5}{10.46} + \frac{1-0.5}{0.29}} \frac{W}{m^2 \cdot K} = 0.564 \frac{W}{m^2 \cdot K}, \qquad \text{(Eq. 6.35)}$$

and the ratio of heat conductivity in and transverse fibre direction

$$\frac{\lambda_\parallel}{\lambda_\perp} = \frac{\lambda_f}{\lambda_z} = \frac{\lambda_f}{k_z \cdot 1} = \frac{10.46}{0.564} = 18.53 \qquad \text{(Eq. 6.36)}$$

In reality, ratio of melt front propagation in and transverse fibre direction should exhibit a lower value since coupling of fibre and matrix hence heat transfer coefficient α_i and α_o will provide a non-neglectable influence. In addition, no stationary process will be observed and heat transport towards laminate edges away from the heat source, i.e. melt will be present.

Already at this stage, the anisotropic behaviour of composite materials marks several peculiarities for later continuous process. Since a UD tape laying process is envisaged, main heat flux will go away from the joint interface and will run ahead of the sonotrode movement. Yet, heating in direction of motion must not be neglected and leads to a pre-heated condition once the sonotrode will arrive at a later position on the joint line.

Due to this pre-heating, a reduced input energy is necessary for completion of the welding process. Appropriate countermeasures are described by Senders (2016, 61) as halved amplitude and contact pressure. The latter contributes as well to a lower lateral force during movement.

A FEM simulation of the given pre-heating scenario is worth considering.

6.8 Theory Conclusion

Respective dependencies of input, frictional and intermolecular power dissipation as well as enthalpy of fusion from the previous considerations are summarised in the following Table 6.1, giving an indication of the form of proportionality by the schematics.

Table 6.1 – Parameter Influence

	Frequency f	Amplitude $a_{S,0}$	Contact Force F_C	Surface Roughness R_a	Contact Area A	Loss Modulus E''
H_m						
$\dot{Q}_{in}$						
$\dot{Q}_{fric}$						
$\dot{Q}_{mc}$						
$\dot{Q}_{fric}/\dot{Q}_{mc}$						

6.9 Scientific Approach

During the parametric study (Chapter 8), the discussed and below elucidated parameters shall be adjusted in a way to maximise joint quality, weld strength and joint extension/melt front propagation.

The operating frequency is constant at 20 kHz; frequency fluctuations are recorded and determined distinctively under 1 % of the operating frequency.

The amplitude varies for each weld since the microprocessor determines the most efficient power-energy-ratio and adjusts the peak power (linear proportionality to amplitude) automatically.

The contact force shall be a direct input parameter changed in the generator's user interface.

The surface roughness is highly depending on the manufacturing process. For influence investigations, hot press and vacuum consolidated laminates are observed exhibiting different finish roughness due to the varying processes.

The projected contact area remains constant since only flat energy directors are deployed. However, the ED dimensions and thicknesses shall be varied.

The loss modulus is solely depending on the material used. In this case, all materials shall remain the same throughout the experiments.

Despite elaborated influences of amplitude and contact force, in accordance with typical parameters in comparative studies, the parameter set shall be complemented with the consideration of energy input (Senders 2016; Villegas and Palardy 2017) and the ED film thickness (Palardy and Villegas 2017; Senders 2016).

However, input energy represents a certain amount of energy for the given set-up. In view of later continuous application, input time – calculated out of the ratio of input energy and power – can be more easily transferred into a longitudinal motion since the feed velocity will be the crucial process parameter in that case – considering the effective duration of ultrasonic oscillation during movement.

7 Experimental Set-Up

7.1 Material

For more detailed data extracted from respective data sheets of used materials, please refer to Appendix A.

7.1.1 Laminate

Unlike later tape laying application with UD ply stack up, 0°/90° fabrics were acquired for this parametric study providing better comparability with respective studies.

The acquired product are Carbon Fibre (CF)/Polyetheretherketone (PEEK) plates by HAUFLER COMPOSITES. Wrought material is a 0°/90° fabric semi-prepreg (five harness satin) consisting of T300 HT-Carbon fibres (3K) and Victrex® 150G matrix. Seven plies of [0/90] fabrics are consolidated in a hot press process to plates of 1160 x 550 mm^2 with a final fibre volume content around 50 %.

During manufacturing, a release film was used in the hot press and removed afterwards. Furthermore, all specimen are cleaned with acetone immediately before welding to remove release agent or grease debris from handling.

A second batch of plates was produced with same materials mentioned above, but with a vacuum consolidation process at DLR Augsburg.

7.1.2 Energy Directors

Energy directors are either an APTIV® 1300 black neat resin film (soot-blackened) based on Victrex® PEEK with a thickness of 50 µm or a LITE® TK 100 µm PEEK films.

In case of weldings with 200 µm ED thickness, two LITE® TK films are placed loose above each other and positioned via a spot weld fixation (Figure 7.4) created with a handheld BRANSON 40 kHz LPe 40:0.50:4T unit and rectangular sonotrode of 0.1" x 0.15" (1.27 x 3.81 mm).

7.1.3 Test Specimen Design

To ensure comparability of test results, ASTM D 1002 is utilised as standard for test specimen design. Intensive studies on CF/PPS and CF/PEI ultrasonic welding were con-

ducted by Senders (2016), Villegas et al. (2013), Villegas and Palardy (2017) or Villegas (2014) using this standard type providing a good database for later evaluation and comparison.

Test specimen dimensions can be taken from Figure 7.1. It should be noted, that thickness is increased from 1.62 mm to 2.21 mm due to manufacturing reasons of test plates. Overlap is only a recommended length in the standard and harmonised with existing test set-ups. Further information extracted from ASTM D 1002 can be found in Appendix A.

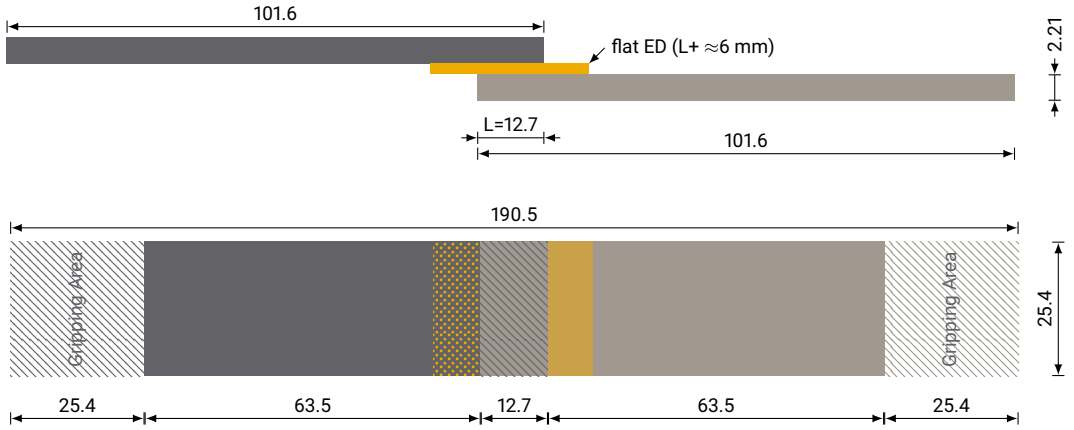

Figure 7.1 – Test Specimen Dimensions acc. to ASTM D 1002

Specimens were produced out of the delivered test panels via water jet cutting operation offering a high quality and least impact on the material, e.g. by overheating or mechanical damage.

The cutting method provided test specimen of hot press processed parts with a 0°/90° fibre orientation and vacuum consolidated specimen with a $\pm 45°$ fibre orientation, respectively.

7.2 Manufacturing Equipment

7.2.1 Ultrasonic Welding Machine

All tests are conducted with BRANSON System 2000Xd with a peak power of 4000 W. The generator works with an operating frequency of 20 kHz and provides a maximum number of 80 cycles per minute. The integrated feed drive 2000aec 2.5 with a 3" pneumatic cylinder offers a maximum weld force of 1.96 kN and a dynamic trigger range from

44 N upwards (Figure 7.3). The microprocessor controlled machine opens the field for time, energy and displacement controlled applications (BRANSON 2015).

7.2.2 Sonotrode

The deployed sonotrode is an OF-30886 rectangular steel sonotrode with a planar contact surface of 16 x 60 mm. It is combined with a gold booster for a 1:1.5 transmission and a final peak-to-peak amplitude of 80 µm, measured with a dial gauge. Planarity of the sonotrode on the specimen was verified with a sheet of white and carbon paper. When pushing the sonotrode manually against inserted sheets on the specimen, the carbon imprint indicates the necessary adjustments of the machine table in order to achieve a plain contact interface.

7.2.3 Fixture

Two fixture solutions are deployed: a machine modified item® profile 80x40 mm in heavy design with 8 mm groove width and 40 mm groove distance, respectively. The T-slots provide a variable clamp distance. Clamping jaws were designed individually for the application and manufactured out of steel. For variability and concerning the hole pattern of the testing machine environment, a second profile was introduced offering a 360° mountability of the fixture (Figure 7.2a) – at location, no use of second profile was necessary.

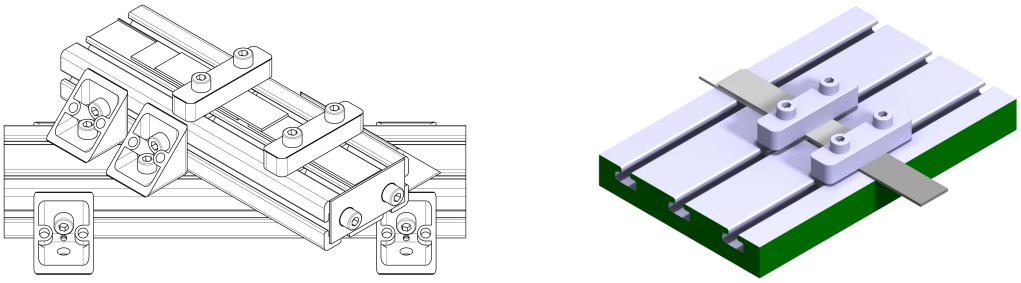

(a) Machined item® Profile (b) Steel Clamping Table

Figure 7.2 – Fixture/Anvil Variants

The second fixture reuses the clamping jaws in combination with a steel clamping table as anvil (Figure 7.2b), provided by BRANSON.

Additional steel plates and peek film patches are used to level the set-up for a planar contact surface between sonotrode and upper adherend as well as between upper and

lower adherend (Figure 7.5).

Screws of the clamping jaws are tightened with a torque wrench to maintain, on the one hand, a comparative fixation throughout experiments and, on the other hand, to avoid huge asymmetries in longitudinal or lateral direction hence introduced pre-stress.

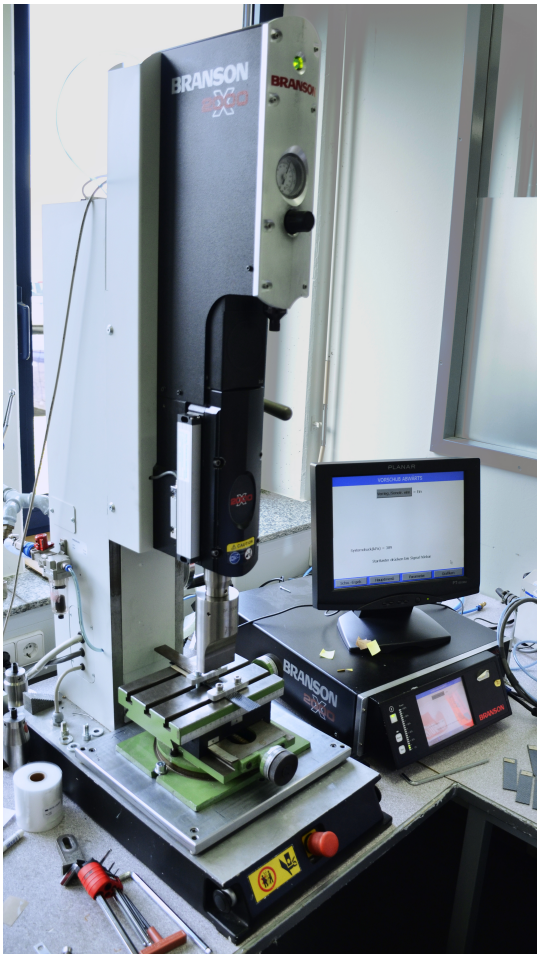

Figure 7.3 – Test Stand

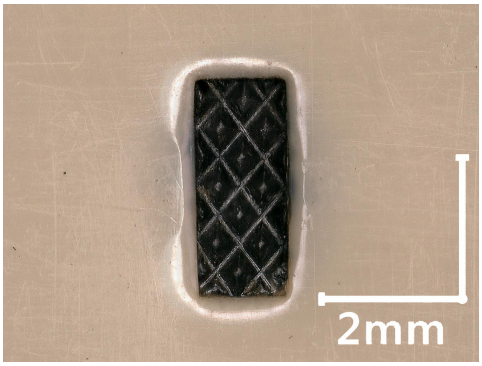

Figure 7.4 – Ultrasonic Prefixation of Two Loose PEEK films on Laminate with Handheld Unit

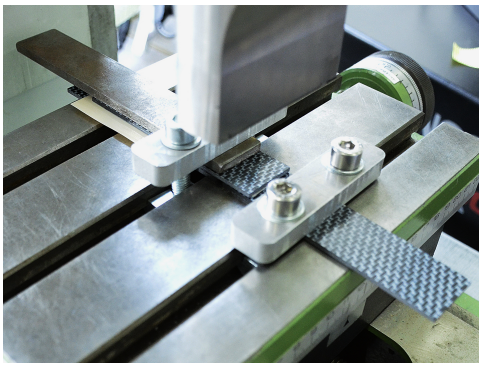

Figure 7.5 – Steel Table Anvil

7.3 Analysis Methods

The used methods for the evaluation and discussion of the test results are described in the following sections.

7.3.1 Manual Bending/Breaking

At the beginning of the experiments, test specimen are bended and broken manually (Figure 7.6) to investigate the degree of melt fronts at the fracture surface for adjusting the process parameters towards more effective parameter sets and configurations.

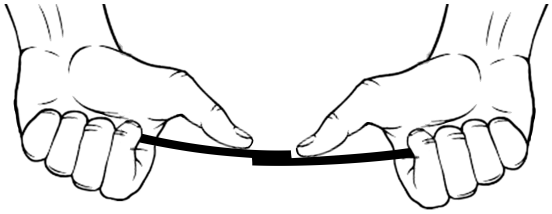

Figure 7.6 – Manual 3-Point-Bending Test

7.3.2 Lap Shear Tension Test

The specimen design is chosen in accordance with ASTM D 1002 to provide standardised lap shear tests with representative strength results. For this purpose, the ZWICK 1475 tension testing machine is used with a 100 kN load cell and a traverse path sensor, located at the DLR Institute of Structures and Design, Stuttgart.

7.3.3 Fracture Surface Analysis

For manually as well as automatically tested and destroyed specimen, fracture surfaces are carefully investigated offering valuable information about melt front propagation or unwelded areas. Visual inspection with naked eye shall be performed as well as by digital microscope using the KEYENCE VHX-5000.

8 Parametric Study, Results and Discussion

8.1 Anvil Stiffness

During first welding experiments with the aluminium item® profile, no or only very little joining was achieved. After changing to a steel machine table as anvil, joints are established much more easily. The hypothesis, the aluminium profile shape and material do not provide sufficient stiffness for ultrasonic oscillation introduction, arose.

This theory can be verified with an ANSYS harmonic response analysis of deployed fixtures (Figure 8.1). The operating frequency is varied between 19950 and 20150 Hz (corresponding to the actual measured frequency during testing), the introduction area is a box representing actual specimen thickness and joint position. Fixed supports are set at the bottom of item® brackets and machine table screw slotted holes, respectively. The bottom surfaces are restricted with a remote displacement in motion in vertical direction.

The simulation results show an over six times larger maximum total deformation for the aluminium item® profile (56.5µm) compared to the steel table (9.50µm). In addition, maximum deformation occurred near the introduction area hence in the direct range of influence for test specimen (Figure 8.1a). Contrary to that, lower deformation of the machine table occurred far away from sonotrode position and at a much smaller extent.

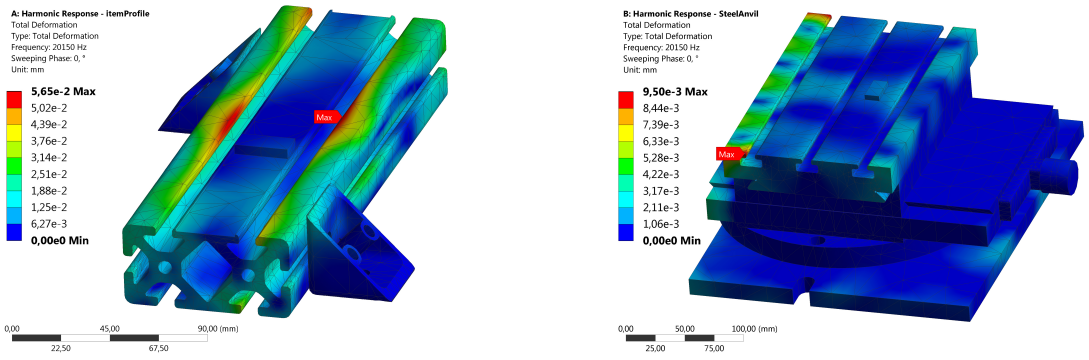

(a) Aluminium item® Profile

(b) Steel Machine Table

Figure 8.1 – ANSYS FEM Harmonic Response Simulation for Total Deformation of Deployed Anvil Variations at a Frequency Range of 19950 to 20150 Hz;
Point of Oscillation Introduction is chosen at the Actual Specimen Position with the used Sonotrode Area (Block)

Consequently, input energy by the ultrasonic unit is transferred at a higher degree into

deformation work for the aluminium profile. This energy is missing at the joint interface for heating and melting of adherends hence inferior ultrasonic welding performance. Another disadvantageous material property of aluminium is the by two orders of a magnitude lower damping factor (Beards 1995, 43) and an almost pure elastic behaviour of steel (Ehrenstein et al. 2012, 238).

Concluding, the anvil must exhibit sufficient stiffness determined by material and shape to enable ultrasonic welding. Villegas and Bersee (2009) followed the approach of a combined aluminium fixture with steel anvil from solid blocks (Figure 8.2).

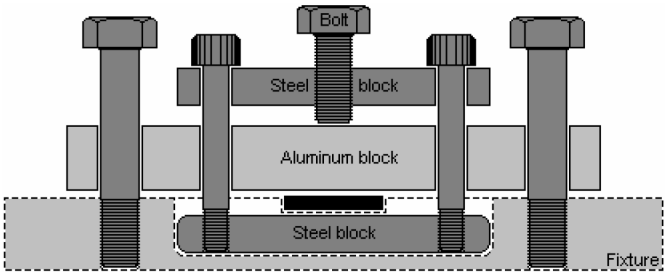

Figure 8.2 – Combined Aluminium-Steel Solid Fixture Design (Villegas and Bersee 2009)

8.2 Specimen Arching

After clamping and before welding, depending on the clamping screw torque, the specimen exhibited an arched position according to the schematic in Figure 8.3a. The lower adherend shows this as well but at a smaller extent.

The higher the torque chosen, the higher the induced compression stresses hence tilting. Since a firm clamping is required, reduction of the torque can only be achieved until a lower threshold.

As a containment action, a steel plate is inserted to compensate the arching at the outer specimen side and reduce the deflection at the joining interface (Figure 8.3b).

(a) Schematic Tilting (b) Steel Insert Plate

Figure 8.3 – Clamping-Tilting Issue

Despite aforementioned countermeasure, still some arching occurs which can influence the welding process dramatically. The ultrasonic welding machine works with a trigger force which compacts the stack before welding cycle. Once the trigger force is reached, the oscillation starts. Are the induced compression stresses little too high and trigger force in the sonotrode is reached before the deflection is compensated means adherends contact each other, the microprocessor could misinterpret recorded data and aborts the process. Is the pre-stress way too high, arching cannot be compensated and sonotrode oscillation sets off vibrating upper adherend only.

Therefore, it must be ensured that arching does not occur in an excessive manner via lower torques or closer clamping position. In addition, trigger force must be set high enough to start oscillation when adherends are in contact – preferably planar – otherwise leading to edge effects.

8.3 Edge Effects

Edge effects shall describe melt initiation at edges of the specimen. Edge effects at sidewards positions are solely a phenomenon on specimen size. For a continuous application, sideward edges “disappear” along the path of sonotrode motion due to large dimensions and must only be considered at the run in and run outs.

Edge effects shall be clustered into three groups of causes.

8.3.1 Unbalanced Clamping – Lateral

The preceding section described the case of unbalanced clamping around the lateral axis resulting in specimen arching. In case pre-stress is under a certain threshold, the welding process is executed, though.

However, no planar contact situation is present but an initial line contact at the inner edge of the lower adherend indicating a higher degree of curvature of the upper specimen at the beginning of the process. Frictional contact hence melt initiation at this side can be observed (Figure 8.4).

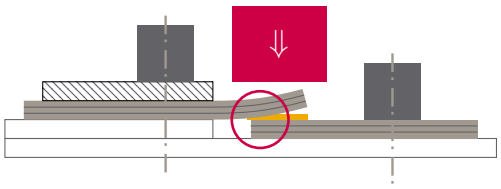

Figure 8.4 – Initial Line Contact

Over time with creation of melt, displacement of the sonotrode downwards sets in pushing the wedge-shaped melt front proceeds towards the other edge (Figure 8.5). The input energy limits the extent of molten resin.

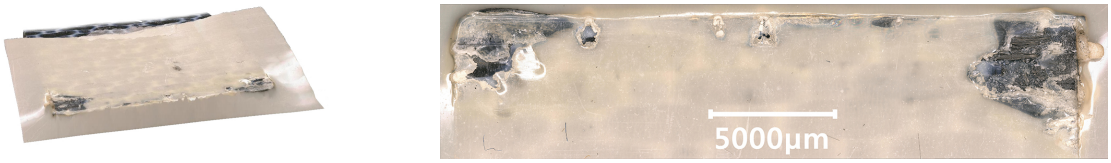

(a) 3D scan (b) 2D detail view

Figure 8.5 – Melt Flow from Inner Edge due to Initial Line Contact

8.3.2 Unbalanced Clamping – Longitudinal

Not only tilting around the lateral, but also around longitudinal axis occurs. If screws are not alternately tightened or with slightly different torques, higher contact pressures on different sides are achieved. Those lead to higher frictional energy dissipation than at areas with lower impact. The melt initiation will most likely start from this edge instead of evenly distributed over the welding area (Figure 8.6).

(a) higher clamping force on the right (b) higher clamping force on the left

Figure 8.6 – Sideward Edge Effect due to Longitudinal Unbalanced Clamping

A case of combined lateral and longitudinal unbalanced clamping can occur, too. Consequently, not only one edge shows an initial melting spot but an area expanding over the corner along two perpendicular edges on the side of higher areal loads (Figure 8.7).

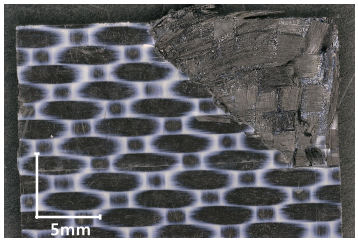

Figure 8.7 – Combined Lateral/Longitudinal Unbalanced Clamping Edge Effect

8.3.3 Edge Concentration Conditions

In general, edges inherit high potential for irregularities induced during manufacturing. Either the cutting of the specimen or insufficient deburring leads to little peaks acting as primary energy director at the initial stage. Frictional heat generation known as process starter focus on those points rather than an areal motion and melting.

The specimen in Figure 8.8 shows preferential melting on either sides speaking against unbalanced clamping towards one side. The 3D-scan reveals expected edge irregularities induced before welding stage.

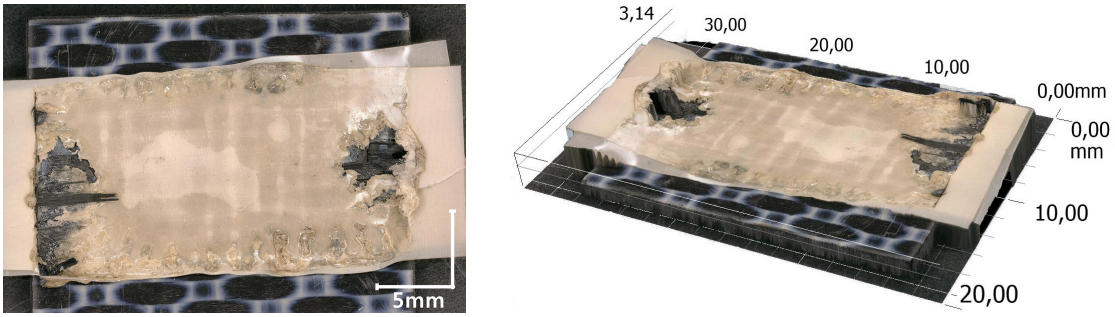

(a) top view (b) 3D scan

Figure 8.8 – Preferential Heating due to Edge Unregularities

8.4 Patch Approach

Since aforementioned edge effects had been discovered at an early stage, original experimental set-up was changed from areal deployment of flat ED (PEEK film) stepwise to strips omitting front and back edges and finally to patches placed centred on the lower adherend. Volkov et al. (1997a; 1997b) already proved the influence of surface micro irregularities on later welding quality.

The achieved effect is simple: by inserting material patches only in the central area, the outer edges are lifted by a small but sufficient amount to avoid friction concentrations at irregularities on the outer edges hence edge effects (Figure 8.9).

Figure 8.9 – Lifting Effect of ED Patches for Avoiding Edge Effects

Further was discovered a lack of matrix material at the interface with 50 and 100 µm PEEK films by reference to dry fibres on fracture faces and no matrix debris (Figure 8.10). This was compensated with insertion of two 100 µm loose films on top of each other with the need to ultrasonically pre-fix the flat EDs (acc. to Section 7.1.2) as experiments showed already shifting of strips during oscillation phase.

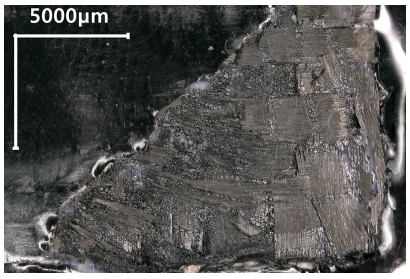

Figure 8.10 – Dry Fibres Indicate Lack of Matrix after Deployment of 50 µm PEEK film

The thickness of deployed flat ED films is strongly dependent on the thickness of unreinforced surface layer. For thinner matrix top layers, more additional resin must be inserted in form of thicker ED films and vice versa.

Those described adjustments let arose two phenomena elucidated hereafter.

8.4.1 Guided Melt Initiation

Several fracture surfaces indicate a preferential heating and initial melting near the ultrasonic pre-fixation joint. Figure 8.11a shows the initial stage of melting at and near by the pre-fixation. Figure 8.11b proves that even where the ED's lower right corner exhibited best circumstances for melting, the pre-joint started melting at a completely different position, too. Figure 8.11c represents a far molten state with a direction of propagation from the centre (point of pre-fixation) towards the outer edges.

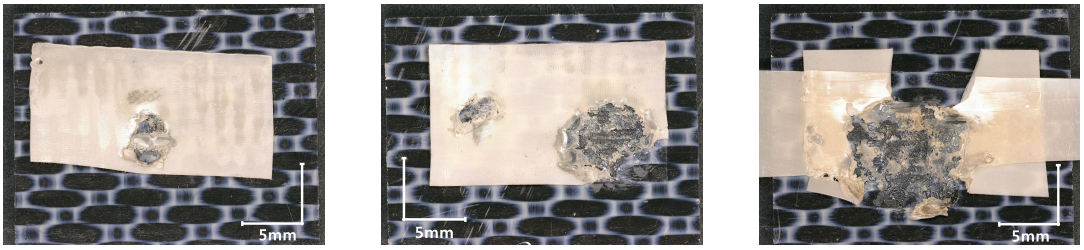

(a) (b) (c)

Figure 8.11 – Fracture Surfaces with Indication of Guided Melt Initiation

Although it is not possible to associate a certain amount of contribution to the pre-fixation joint, the experiments showed evidently that melting is more easily initiated when a pre-joint is present.

Reasons for this behaviour are various: the pre-created material bonding acts as starting point, the thinned ED film at the pre-joint requires less fusion enthalpy or the irregularity of the joint shape in the flat ED caused friction concentration.

Whether one or several of the listed factors influence the eased melting should be further investigated.

8.4.2 Interfacial Friction

The deployment of two loose ED films arises the issue of interfacial friction during oscillation phase. Although fixed at the pre-joint point, the outer areas are still able to execute relative motion between the two layers which creates an additional heat source. Indeed can such interlayer melting be observed (Figure 8.12). The line pattern of brighter and darker areas indicates unmolten and molten material shining through the film surface. As the top surface is still in an unmolten state, melting must be occurred between the layers. The small extent of melt fronts confirms the theory of reduced efficiency for multiple layered loose resin films (Section 6.6).

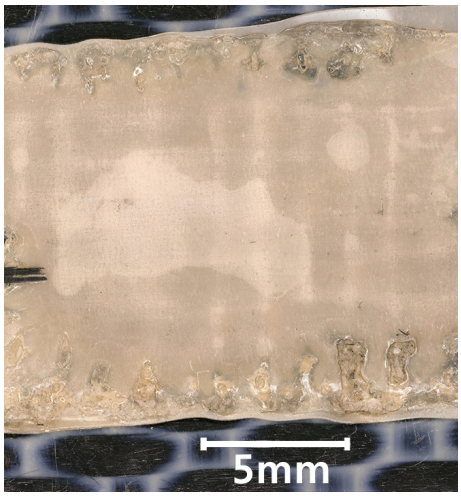

Figure 8.12 – Interlayer Melting Effect

8.5 Failure Modes

Failure modes for bonded composite joints are generally defined as 1) adhesive failure (interface adhesive/adherend), 2) cohesive failure (inside adhesive layer) and 3) substrate failure (Vassilopoulos 2014, 129). Strong et al. (1990) expanded them to four failure modes for ultrasonic welding: 1) weld interfacial failure in resin-rich areas, 2) combined interlaminar and interfacial failure, 3) interlaminar failure above and below energy susceptor layer and 4) coupon failure due to fibre damage (no weld failure).On that base, fracture surfaces are analysed.

Since all specimen were prepared with acetone to clean fusion surfaces and remove greasy debris, typical failure mode of bad surface preparation – adhesive failure – was

not expected and indeed not observed.

Generally, welding quality exhibits good to very good properties. Characteristic cohesive failure for given application with tore interlayer material (Figure 8.13a) is found as well as even some fibre pull-outs on specimen indicating Strong's failure modes 3 and 4, i.e. coupon failure hence stronger bond than substrate properties (Figure 8.13b). Some specimen show typical cohesive failure combined with fibre pull-outs created due to fibre re-orientation during intensive melting in thickness direction (Figure 8.13c). Then, upper plies get detached from substrate and "float" towards interface layers – such an effect is undesired since intended fibre orientation of top layers gets lost.

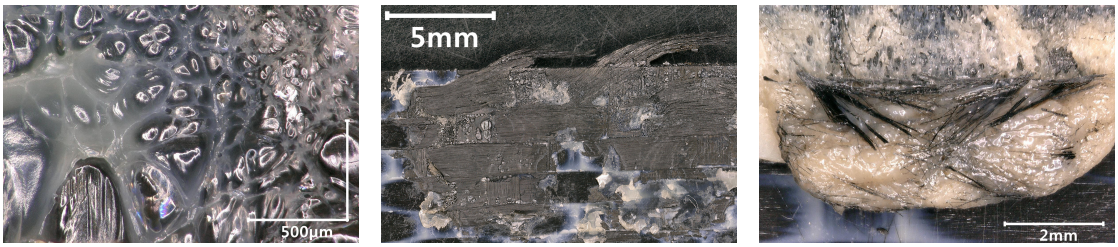

(a) Cohesive Failure with Tore Matrix

(b) Substrate Failure (Pulled-Out Fibres)

(c) Cohesive Failure and Fibre Pull-Outs at Weld Bead

Figure 8.13 – Observed Failure Modes on Fracture Surfaces

8.6 Heat Flow Behaviour

8.6.1 In-Plane Direction

The experiments show a clear dependency of top layer fibre direction on the melt front propagation. Section 6.7 already introduced the theoretical model based on that heat flow along fibres is at least one order of magnitude higher than transverse. Subsequently, fibre direction plays a major role in heat and thus melt propagation.

Figure 8.14a and 8.14b show evidently melt directions of laminates with $\pm 45°$ and 0°/90° top layers, respectively. Therefore, top layer fibre orientation can be a useful adjusting screw in combination with sonotrode geometry and motion as well as ED positioning to guide the meld flow. Since a UD tape laying process is envisaged, this tool might be even more powerful.

To note is the distinct higher edge heating compared to the surface temperature due to preferential fibre heat flow. Thus, squeezed out matrix contacting laminate edges is likely prone to overheating hence matrix decomposition and must be avoided.

(a) ±45° Top Layer with Corresponding Melt Direction

(b) 0/90° Top Layer with Corresponding Melt Direction

Figure 8.14 – Observed Failure Modes on Fracture Surfaces

8.6.2 Thickness Direction

The considerations in Section 6.7 do not only point out the role of fibres as major heat transfer medium, but does also give an estimation of heat propagation in and transverse fibre direction.

Experiments prove theoretical predictions and exhibit a typical triangular melt front shape (Figure 8.15). Further, the assumption of reduced ratio of heat conductivities compared to theoretical values is valid, too, via graphical determination of melt front propagation yielding

$$\frac{\lambda_{\parallel}}{\lambda_{\perp}} \sim \frac{d_{\parallel}}{d_{\perp}} = \frac{11.5}{1.25} = 9.2, \qquad \text{(Eq. 8.1)}$$

compared to the theoretical rough estimation (18.53) from (Eq. 6.36), the actual ratio is quite accurate half of the theoretical value.

Further evidently is no impact or even melting on possible outer aerodynamic surfaces opposite joining interfaces although vibration times were comparably long in the conducted study.

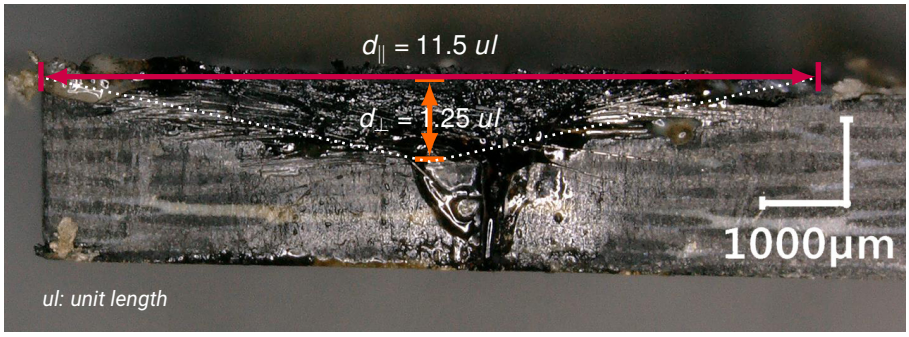

Figure 8.15 – Microscopical Analysis of Melt Front Propagation In/Transverse Fibre Direction

8.7 Parametric Study

Finally, after adjusting boundary conditions towards a better and repeatable welding quality, a test series of in total ten specimen had been conducted. Results and interpretations are elucidated in the following sections.

8.7.1 Obtained Experimental Data

The obtained experimental data (Table 8.2) consist of recorded US machine data (Amplitude, Energy Input, Weld Collapse/Force/Time, Frequency), tension testing machine data (F_{max}), microscopical determined fracture surface area (A) and computed values of mean power, energy density and lap shear strength (LSS).

One should note that determination of fracture surface area is crucial for LSS calculation. The definition of bonded area measured is ambiguous and shall be characterised as molten unreinforced top layer on the opposite adherend of the one with pre-fixed EDs. This guarantees measured areas being involved in the joint whereas molten ED/matrix only on the “pre-fixed” adherend does not explicitly have to form a joint but melt on one of the laminate.

Although technical aids of the digital microscope are used to ensure a systematic measurement, still considerable deviations among several measurements of the same specimen are observed. In addition, the set definition of bonded area still leaves room for interpretation, e.g. haze caused by matrix debris.

Statistical evaluation has been carried out according to the procedures presented in Appendix B.

8.7.2 Force-Elongation-Curves

The force-elongation curves cannot provide an overview of joint strength since reassessment to the respective area must be done. Nevertheless, they display the failure behaviour over time. A summary of all valid specimen curves is presented in Figure 8.16.

Most specimen exhibit characteristic curves with a distinct maximum (e.g. #29, #31, #38). By contrast #33 shows a stretched and #32 clinched shape. Regarding respective fracture surfaces, it is evident that #32 shows a rather random compartmentalised distribution of molten matrix (Figure 8.17a) contrary to the joint area of #33 with its main extent in direction of load (Figure 8.17b).

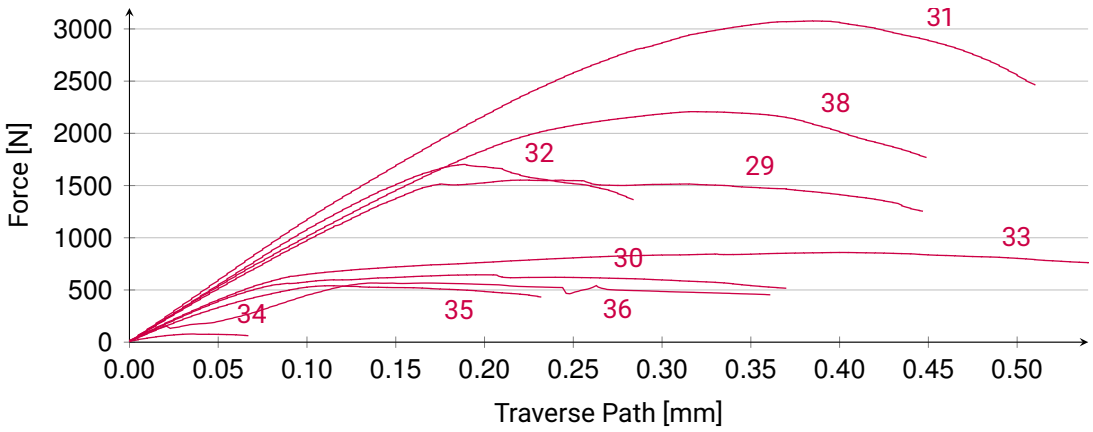

Figure 8.16 – Force over Traverse Path (with Specimen ID)

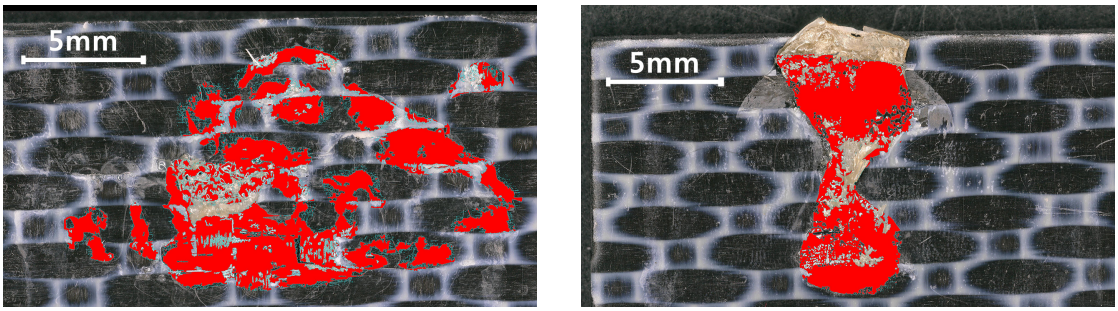

(a) #32 (b) #33

Figure 8.17 – Fracture Surfaces with Marked Joint Area

Stress analysis investigations detect maximum peel stresses at outer edges of single lap shear specimen with a parabolic distribution over the overlap length (Figure 8.18). Thus, one can conclude the shorter the actual overlap/joint length in load direction is, the higher is the peel stress gradient – in particular for compartmentalised formations. A decrease in overall shear strength leads in turn to an earlier failure and plasticity effects hence higher elongation does not appear.

This theory is further confirmed since experimental data show a similar trend (Figure 8.19). Smaller weld areas lead to lower LSS whereas infinitely large joint areas approximate asymptotically substrate strength hence ideal bond. Two outliers mark the highest and lowest measured values accounting for systematic errors in area determination.

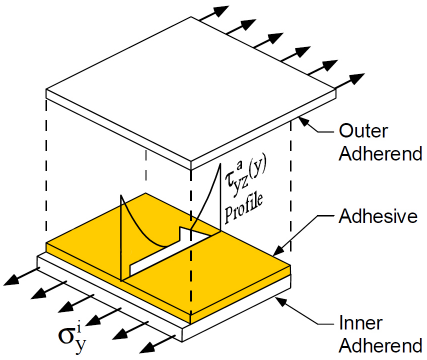

Figure 8.18 – Peel Stress Distribution (FAA 2001, 8)

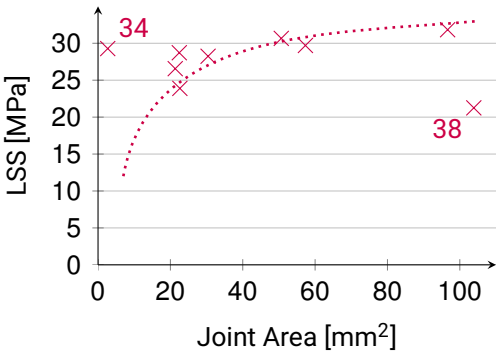

Figure 8.19 – LSS over Welded Area

Microscopical pictures of all specimen's fracture surfaces with marked joint areas are provided in Appendix C.

8.7.3 Vibration Time-Force-Correlation

Plotting vibration time over applied weld force exhibit – whilst with considerable deviations – a linear growth (Figure 8.20) and thus resembles the theoretical model by Potente (2004, 177) presented in Section 6.5. Albeit, from the obtained data, one cannot ascertain beyond doubt in which of the two regions (combined/solely intermolecular heating) the experimental data lies.

One should note, that different weld forces occurred for pneumatic cylinder pressure held constant. The need for a more precise electro-mechanical positioning unit becomes evident.

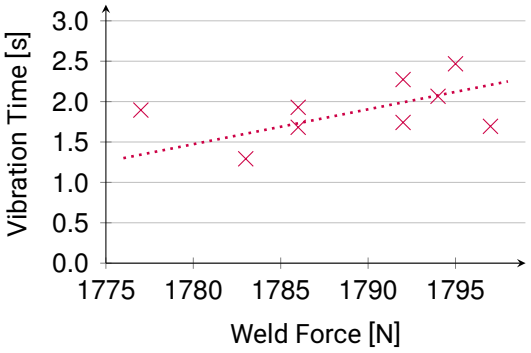

Figure 8.20 – Vibration Time over Weld Force

8.7.4 Vibration Time-Amplitude-Correlation

The graph of vibration time over applied amplitude provides the expected hyperbolic shape (Figure 8.21) validating the derivation of (Eq. 6.24) from Section 6.4 with its quadratic dependency on amplitude. Remarkable are two asymptotes: vertically marking the minimum amplitude required for welding. Horizontally, the minimum vibration time with a decreasing gradient for larger amplitudes. This state of equilibrium results due to multiplication of increasing amplitude but dropping loss modulus above T_g (refer to Figure 6.2) avoiding a further reduction in vibration time.

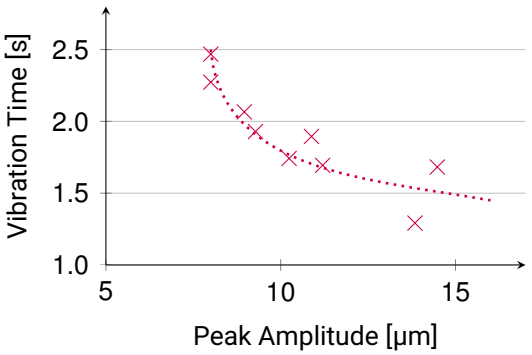

Figure 8.21 – Vibration Time over Weld Force

Note: variation in amplitude due to US welder amplitude automatic for optimum power.

8.7.5 Weld Area-Collapse-Correlation

The linear increase of weld area with greater weld collapse (Figure 8.22) can be explained as more weld collapse represents more molten material hence increased melt front propagation, i.e. larger welded area. Effects of squeeze-outs after melting of entire overlap area would form a knee in the graph since collapse rises but welded area remains constant. Specimen revealed melt propagation only within the overlap due to patch approach hence no such indications.

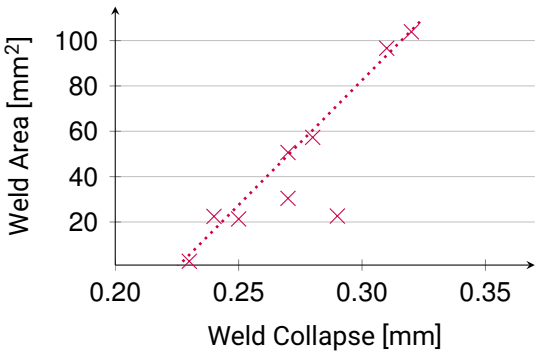

Figure 8.22 – Vibration Time over Weld Force

8.7.6 LSS-Energy Density-Correlation

The energy density is computed as quotient of input energy and welded area and is thus comparative to enthalpy of fusion. In Figure 8.23 an optimum processing window (15–25 J/mm^2)can be determined. A lower threshold similar to the fusion enthalpy marks a certain energy density that must be reached to enable melting. For higher energy densities, LSS decreases due to higher thermal burden for the matrix material and reduction of its properties. Above an upper threshold, matrix decomposition would set off. For some specimen and configuration enhanced smoke emission was observed indicating matrix decomposition.

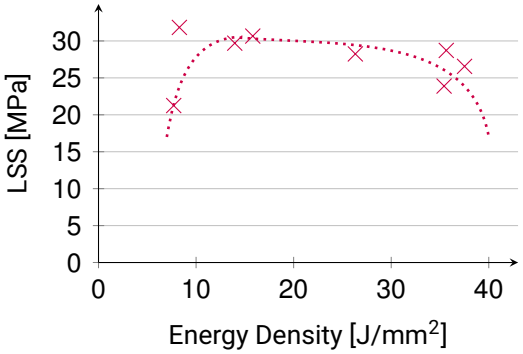

Figure 8.23 – LSS over Energy Density

8.7.7 LSS-Mean Power-Correlation

Mean power is the ratio of input energy and vibration time. The curve in Figure 8.24 exhibits again a distinct region for maximum LSS. Akin to the preceding curve for energy density, a lower threshold marks the minimum power required for melting, an upper threshold setting in matrix degradation with dropping LSS. The in-between window (350–550 W) provides best boundary conditions for good welding quality.

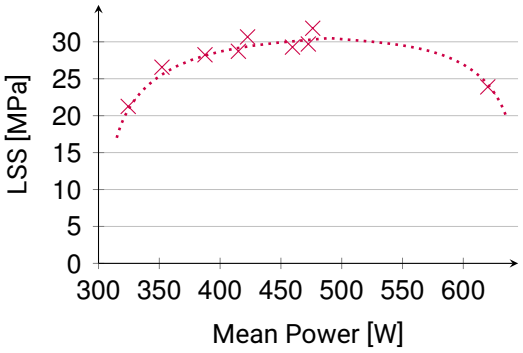

Figure 8.24 – LSS over Mean Power

8.7.8 LSS-Vibration Time-Correlation

Corresponding to mean power from previous consideration and since $P = {}^{E_{in}}/_{t}$ for constant input energy, a similar process window opens for LSS over vibration time according to Figure 8.25 between 1.6 and 2.0 s. Villegas and Palardy(2017) observed the same curve for CF/PPS specimen as well as Strong et al. (1990) for APC-2 materials. In addition, suitability to control the process by power, input energy or vibration time is proven.

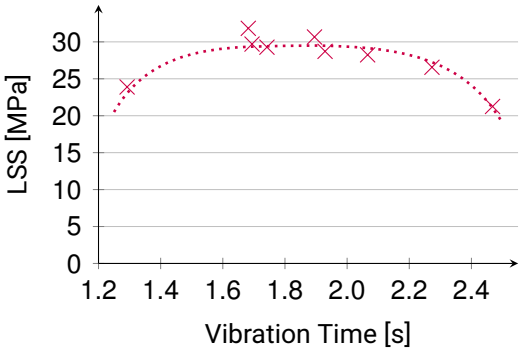

Figure 8.25 – LSS over Vibration Time

8.7.9 Comparative Lap Shear Strength / Weld Factor

For determination of a comparative lap shear strength, a base line is necessary from which the weld factor can be computed. The latter is referred to as "... ratio of weld strength to strength outside the welded zone, typically determined by tensile stress tests." (PDL 2008, 547) Hereby, interlaminar shear strength according to DIN /65148 can be used as well as the shear strength of the parent material – in composites the weaker matrix.

Tests were conducted following DIN 65148. Yet, only three out of nine specimen exhibited a shear failure mode (Figure 8.26) and computed results exhibited disproportionate and deviating results. Main disturbing factor was localised as notches cut by hand and missing guiding devices due to too little specimen.

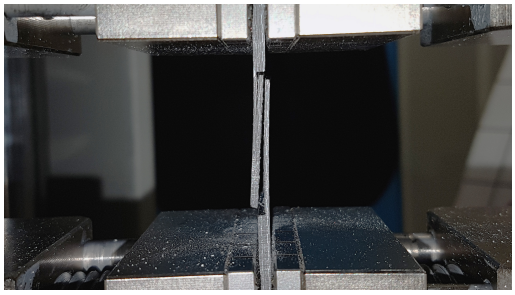

Figure 8.26 – Torn Interlaminar Lap Shear Specimen

As a consequence, weld factor is determined with the parent material properties. Laminate data sheet provide a shear strength of 53 MPa. Recalling the weld factor definition with given values reads

$$w_{US} = \frac{\sigma_w}{\sigma_p} = \frac{27.8}{53} = 0.52. \qquad \text{(Eq. 8.2)}$$

Table 8.1 gives an overview of achieved experimental results and a comparison with quantities of former publications and material combinations. According to this selection, the achieved welding quality shows the best weld factor and is among the best absolute weld strength values.

Table 8.1 – Weld Strengths and Factors for Material Combinations

		Villegas 2013	Villegas and Bersee 2009	Villegas et al. 2013	Senders 2016	Silverman and Griese 1989	Taylor and Jones 1990	Experiments
		CF/PEI		CF/PPS		APC-2 (CF/PEEK laminate)		
σ_p	[MPa]	103	103	82.0	82.0	93	55	**53**
σ_w	[MPa]	37.1	23.9-36.0	27.3	20.9-36.5	15	5	**27.8**
Weld Factor		0.36	0.23-0.35	0.33	0.25-0.45	0.16	0.09	**0.52**

Nevertheless, most recent publications investigated CF/PEI and CF/PPS, respectively. The database for ultrasonically welded CF/PEEK composites contains rather little and rather old state of work. Hereby, this work is another step to get an insight in an ultrasonic welding process with CF/PEEK laminates.

8.8 Conclusion

This conclusion shall lay the foundation for subsequent considerations on a continuous ultrasonic welding process and provide the necessary background for design and dimensioning.

For successful implementation, anvil shape and stiffness turned out to be of great importance. Even more severe appeared adherends planarity. Induced (lateral/longitudinal) arching or edge irregularities concentrate ultrasonic vibrations on single spots rather than the entire overlap area causing uncontrollable melt initiation and propagation. Countermeasures like steel insert plates and ED patch approach were deployed successfully and emphasise the importance of planarity once more. Adjustments in sonotrode geometry are considerable, too. Main challenge is assigned to achieving an areal weld hitting the process window between “no welding” and “local overheating/decomposition” for an equal melt propagation.

Preferential heating near ultrasonic pre-fixations was observed as well as interfacial melting between two loose ED film. The latter is a consequence of a lack of matrix at the

joint interface and doubling of inserted ED films. In combination with the unreinforced top layer of the laminates, this is an important adjusting screw for enough matrix at the interface. Only then, failure modes appear to be cohesive or even substrate failures like in the present case.

Further confirmed is the preferential heat flow in fibre direction which will arise an issue for the continuous approach over large lengths with its pre-heating phenomenon. Fibre orientation in the top layers sets another adjusting screw together with sonotrode geometry and motion as well as ED positioning.

Parametric study revealed good to very good welding qualities with comparable high LSS, weld factors and satisfying parameter correlations. Yet, vibration times and weld force turned out to be higher as usual or desired, respectively. Moreover, melt propagation i.e. welded area showed great deviations implying the need for further improvements towards a more stable process. Energy density, mean power and vibration time turned out to be crucial providing only certain process windows for maximum LSS and dropping flanges.

Finally, conducted experiments provide promising results, proves the feasibility of the envisaged process and justifies further investigations towards a continuous ultrasonic joining process in this direction.

Table 8.2 – Obtained Experimental Data

ID	Amplitude µm	Energy Input J	Weld Collapse* mm	Weld Force N	Freq Hz	Vibration Time s	Mean Power W	F_{max} N	A mm^2	Energy Density J/mm^2	LSS MPa
029	10.9	800.8	0.27	1777	20102	1.895	422.6	1552.951	50.650	15.810	30.660
030	9.3	800.6	0.24	1786	20124	1.929	415.0	645.029	22.461	35.644	28.718
031	14.5	800.9	0.31	1786	20124	1.682	476.2	3075.987	96.629	8.288	31.833
032	11.2	800.5	0.28	1797	20102	1.694	472.6	1702.580	57.323	13.965	29.702
033	9.0	800.7	0.27	1794	20090	2.066	387.6	859.033	30.417	26.324	28.242
034	10.2	800.5	0.23	1792	20110	1.742	459.5	78.473	2.680	298.694	29.281
035	13.8	801.2	0.29	1783	20106	1.292	620.1	540.418	22.620	35.420	23.891
036	8.0	800.5	0.25	1792	20097	2.273	352.2	566.730	21.337	37.517	26.561
037†	17.1	800.5	0.57	1776	20060	1.403	570.6	-	-	-	-
038	8.0	800.7	0.32	1795	20096	2.468	324.4	2207.673	103.867	7.709	21.255
Mean		800.7	0.30	1787	20101	1.775	450.1				27.794
dev.		±0.2	±0.08	±6	±14	±0.231	±68.9				±2.529

**setting path/displacement*

†specimen broke immediately after welding whilst handling

9 Continuous Welding Concept Development

9.1 Scope

The continuous welding process to be developed shall be derived from the application case of longitudinal joining for two aircraft shells (Figure 9.1). Therefore, the scope comprises

- establishing a continuous ultrasonic fusion bonding process for
- CF/PEEK composite shells
- in overlap configuration (20-50 mm overlap) with
- total joint length $\geq$500 mm,
- preferably flat energy directors,
- fully-integrated endeffector for a robotic device
- applied in semi-automatic/ automatic mode.

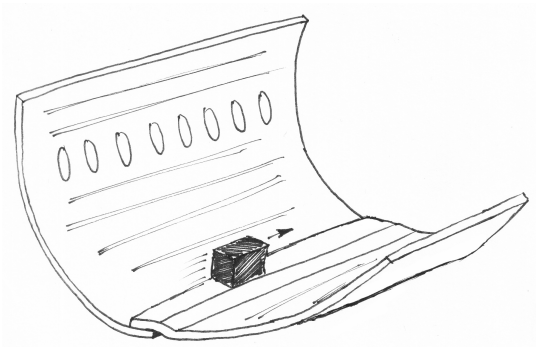

Figure 9.1 – Aircraft Shell Joining with Ultrasonic "Black Box" Endeffector

Combining these goals with the obtained experimental results from the previous chapter shall be done in the following sections.

9.2 Anvil

This point should regard the importance of a sufficient anvil stiffness as crucial prerequisite for ultrasonic welding. Today, thermoset prepreg tapes are laid-up in female steel tools (Figure 2.7); similar to that, thermoplastic UD tapes would be stacked. For joining and with compatible toolings, two shells can be positioned while remaining in the lay-up tool using the latter as anvil. Advantages are absence of further toolings or transfer stations hence time and cost saving plus suitable anvil usage. Disadvantage are possible higher burden and wear of tooling surfaces necessary for outer aerodynamic aircraft surface. Nevertheless, steel toolings for ultrasonic welding are widely spread and combine good wear resistance with required hardness (Irshad 2015, 19-20).

9.3 Robot

One of the main goals is an automated joining process noted in the scope for a robotic endeffector operating in semi-automatic and full-automatic mode. According to that, the robotic system – in particular robot and endeffector – must be dimensioned regarding collected experimental data. Contrary to stationary table machines which inherit natural stiffness, in the given case, the robot arm must provide required stiffness between sontorde and anvil – supported by its endeffector and the tooling.

The KR 300-2 PA is an existing robot at DLR Augsburg and chosen to be utilised for the continuous joining test stand. The most crucial limiting parameters are both, the operating range and the load capacity. “Both values (payload and mass moment of inertia) must be checked in all cases. Exceeding this capacity will reduce the service life of the robot and overload the motors and the gears [...]” (KUKA 2016, 17) The robot specification states a rated payload of 300 kg and a permissible moment of inertia of 150 kgm^2. The corresponding payload diagram for different endeffector weights is shown in Figure 9.2. Given distances are related to the distance of the load centre of gravity with respect to the mounting flange on robot axis 6.

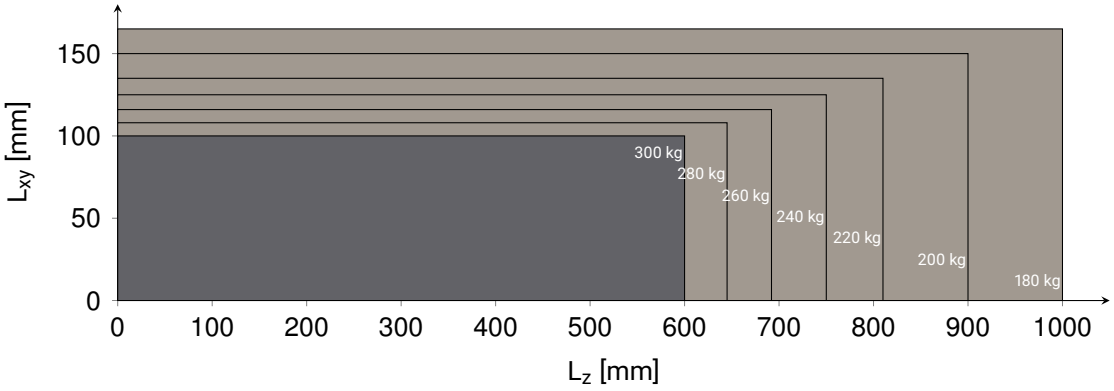

Figure 9.2 – Payload Diagram for KR 300-2 PA (Data: KUKA 2016, 17)

In case the required payload is not sufficient, an other robot must be chosen with a higher payload capacity.

The load required is decisively influenced on the one hand by the endeffector components and its weight and on the other hand by the applied process loads, i.e. weld and consolidation forces. Both are subject of the next section.

9.4 Endeffector

The endeffector is the central unit for execution of an ultrasonic fusion process. Several approaches have already led to patents for ultrasonic welding devices shown in Figure 9.3.

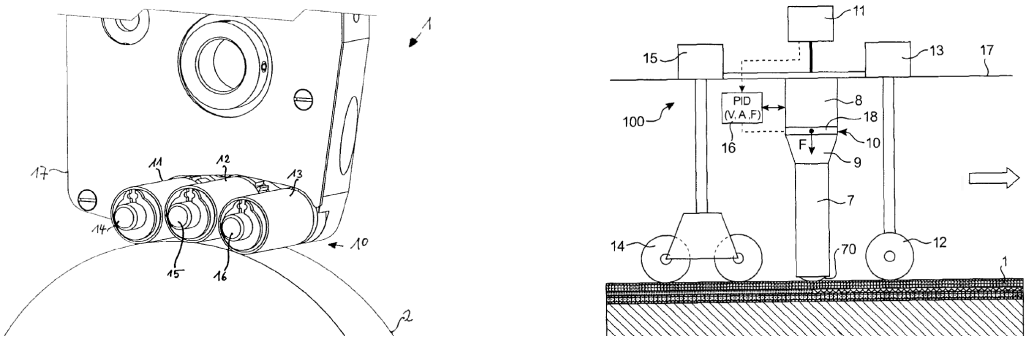

(a) (Gachnang 2008) (b) (Soccard 2011)

Figure 9.3 – Existing Patents on Endeffector Concepts

Derived from those approaches and from observations during experimental study, the endeffector must fulfil the capability of

- clamp/fix the specimen in planar position,
- incorporate US welding unit and
- provide a consolidation device.

The necessity of an appropriate clamping/fixation without any arching was intensively discussed in the previous chapter. Installation of the ultrasonic welding unit in the endeffector a fundamental prerequisite.

Senders emphasised the importance of a consolidation device during his investigations on continuous ultrasonic welding of CF/PPS: "... broken fibres are shown, but also large matrix flakes and voids are present. [...] Therefore it is concluded that a consolidation device is necessary in order to produce the same quality of welding as the static welding process." (2016, 67)

Following the principle of a positioning device in front and a consolidation device after the ultrasonic unit, the endeffector concept in Figure 9.4 is developed. Fixation and consolidation rollers frame the sonotrode mounted independently. Thus, different process forces can be applied and varied. Major disadvantage is adding up the process forces of each unit which shall not exceed the robot's payload capacity.

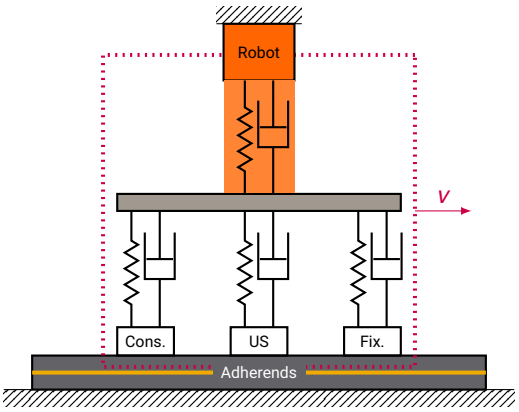

Figure 9.4 – Endeffector Concept

9.4.1 Process Forces

Total process forces are approximated as sum of used experimental forces.

Fixation was established with a torque of 20 Nm on the fixture screws in correspondence with former investigations (Senders et al. 2016). Thereof, after analysing the application case (Appendix D) with an chosen overlap width of 50 mm, the *HERTZIAN pressure* yields a reasonable magnitude of clamping force in the range of 500 to 1000 N. For a conservative approach, the latter shall be used for calculation.

According to observations in experimental study, ultrasonic welding set in at welding forces of not less than 850 N, later parametric study was conducted with 1800 N. Comparable studies with CF/PPS used 500 and 1000 N for static and continuous welding, respectively (Senders 2016), also in order to lower lateral forces when transferring the static into continuous approach. Thus, 1000 N shall be the baseline for subsequent calculation.

Consolidation is usually done with maintaining the welding force for a certain period of time after end of heating stage hence $F_{weld} = F_{cons}$.

Thus, minimum required force capability for solely process forces reads

$$\begin{aligned} F_{proc} &= F_{fix} + F_{weld} + F_{cons} = F_{fix} + 2F_{weld} \\ &= 200\ N + 2 \cdot 1000\ N = 2200\ N \qquad m_{proc} \approx 220\ kg \end{aligned} \tag{Eq. 9.1}$$

KR 300-2 PA payload capability of 300 kg has not been exceeded in this estimation. Still, there is additional weight impact due to deployed components.

9.4.2 Equipment Weight Impact

Apart from process forces, actual equipment brings in additional weight with every component mounted. Components for a *minimum working example* (MWE) are given in Table 9.1. First three positions are pneumatic and electro-mechanical actuators responsible for applying process forces controlled by three load cells. The ultrasonic unit comprises the converter, booster, sonotrode and clamping device. Custom-made rollers, coupling device and a framework round off the listing. If provided, weights are taken from parts data sheets or are estimated according to comparable components. To cover extra weight by additional devices and/or changes in purchased parts, a weight allowance of 20 % percent is added to the subtotal.

Table 9.1 – Equipment Weight Impact

Component	Supplier	Name	F_{max} N	l_S mm	Qty	m_i g	m_{total} g
Fixation Act.	FESTO	ADN-50-50-A-P-A	1178	50	1	795	795
US Actuator	FESTO	ELGA-BS-KF-150-400-0H-40P-ML	4000	400	1	33500	33500
Consolid. Act.	FESTO	ADN-50-50-A-P-A	1178	50	1	795	795
Load Cell	HBM	U9C	5000	-	3	100	300
US Converter	BRANSON	20 kHz CR-20S	-	-	1	300	300
US Booster	BRANSON	gold	-	-	1	350	350
US Sonotrode	BRANSON	2" x 1"	-	-	1	600	600
US Clamp	BRANSON	-	-	-	1	350	350
Rollers	-	-	-	-	2	215	430
Coupling Dev.	-	-	-	-	1	4500	4500
Framework	item	Profile 8 40x40 light	-	-	5	1.75 kg/m	8750
Subtotal							50670
Weight Allowance						20 %	10134
Total Weight							60804

By this estimation, total equipment weight impact is quantified to about 70 kg. Adding to process forces from previous estimation reads

$$\begin{aligned} m_{total} &= \frac{F_{proc}}{g} + m_{Equip} = \frac{2200\ N}{9.8065\ {}^{N}/_{kg}} + 70.644\ kg \\ &= 224.34\ kg + 60.804\ kg = \underline{285.14\ kg} \end{aligned} \tag{Eq. 9.2}$$

Thereby, robot's payload capacity is not exceed, if only just. Nevertheless, once specific

planning is completed, executed estimation must be adjusted/completed and payload capacity checked again.

9.4.3 Mass Moment of Inertia

Second load criteria is the mass moment of inertia. In correspondence to aforementioned robot specification (KUKA 2016), it must not exceed 150 kgm^2 in any case and shall remain within given constraints of the payload diagram (Figure 9.2) with distances to the load centre of gravity with respect to the mounting flange on robot axis 6. Thus, it is necessary to determine the centre of gravity (CG) and subsequently the mass moment of inertia (I) following the general formulae

$$CG_\xi = \frac{\sum_{i=1}^{n} m_i \cdot r_{\xi,i}}{\sum_{i=1}^{n} m_i} \qquad CG_\zeta = \frac{\sum_{i=1}^{n} m_i \cdot r_{\zeta,i}}{\sum_{i=1}^{n} m_i} \tag{Eq. 9.3}$$

$$I_{zz} = \sum_{i=1}^{n} m_i \cdot r_{z,i}^2 \qquad I = m \cdot \left(x^2 + y^2 + z^2\right) \tag{Eq. 9.4}$$

considering the MWE endeffector draft in Figure 9.5. CG calculation yields

$$CG_x = -40.27\ ul^1 \qquad CG_z = -121.33\ ul \tag{Eq. 9.5}$$

in an arbitrarily chosen axis system ξ, ζ marked in Figure 9.5. Translation into robot axis system x, z by simple zero point offset into mounting flange on robot axis 6 gives actual values (assuming no CG translation in y-direction)

$$CG_x = -40.27\ mm \qquad CG_z = 786.33\ mm \qquad I = 106.71\ kg\ m^2 \tag{Eq. 9.6}$$

1. ul: unit length

Due to much higher process forces created on adherend surface compared to endeffector equipment weight, the resulting centre of gravity shifts far below working plane. Total mass moment of inertia does not exceed maximum 150 kg m^2, but CG_z-position lies outside the given permitted envelope according to Figure 9.2. This calculation shall be repeated after detailed planning is completed and in agreement with the robot manufacturer which prescribes "[t]he mass inertia must be verified using KUKA.Load. It is imperative for the load data to be entered in the robot controller." (KUKA 2016, 18)

Thus, the use of envisaged and scheduled KR 300-2 PA is still regarded as feasible.

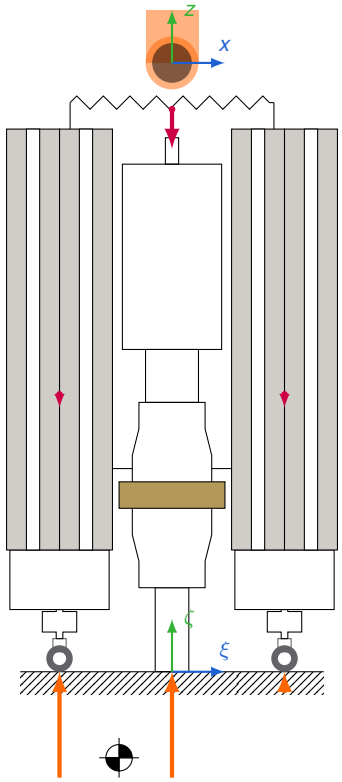

Figure 9.5 – Minimum Working Example Draft

9.5 Ultrasonic Welding Equipment

9.5.1 Generator

Contrary to static welding, power requirements on the ultrasonic generators are much higher for continuous applications.

Besides the experimentally used BRANSON 20:4.0 system (20 kHz/4000 W), the use case for already existing 40 kHz systems (40:0.8) at DLR Augsburg is questioned. During parametric study, mean power ranged between 324 and 620 W (Table 8.2), which sets the baseline for generator dimensioning. Regarding technical data of both systems (Table 9.2), it stands evidently to reason that no 40 kHz-system can provide a sufficient high continuous power; even lower 20 kHz-systems are discarded. The already at the laboratory utilised BRANSON 20:4.0 system (20 kHz/4000 W) is the most suitable one for further planning. The use of 20 kHz-systems in comparable studies (Villegas et al. 2013; Villegas 2015; Senders 2016) is further justified.

Table 9.2 – Technical Data of Available Ultrasonic Generators

DCX A/F Model		20:1.25	20:2.5	20:4.0	40:0.4	40:0.8
Frequency	kHz	20	20	20	40	40
Peak Output Power	W	1250	2500	4000	400	800
Max. Continuous Power	W	625	1250	2000	200	400

Data: BRANSON 2013

9.5.2 Sonotrode

Due to abrasive carbon reinforcement of thermoplastic composites and prevailing sonotrode motion under load, a steel sonotrode is recommended unlike aluminium or titanium sonotrodes show lower wear resistance.

Main challenge is detected as planarity of the sonotrode. Reducing sonotrode dimensions to at least overlap size as well as potential use of a rounded sonotrode are reasonable countermeasures. For spot welding, Rozenberg found an invariant specific contact pressure for flat unlike a continuous growth of weld areas for spherical sonotrode tips (2013, 113-16) which might be transferable for a more uniform oscillation introduction.

The use of circular sonotrodes might comes along with other melt flow initiation and guiding over the overlap profile. Yet, such a sonotrode shape was not subject of the preceding investigations and thus no profound knowledge on such an alternative can be provided. Variations in sonotrode shape need further investigation.

9.6 Energy Directors

The conducted study proved feasibility of flat energy directors which are seen as best suited for a continuous process. Deployment of a neat resin film can be easily automated – even in actual welding endeffector. Due to the planarity issue, the question of different ED shapes arose again.

As a matter of fact, shaped EDs provide better focal points particularly for initial melting and are in turn starting point for melt front propagation (Figure 9.6a). The most challenging point is to mould shaped EDs on composite laminates since fibres must not be distorted or destroyed. For hot press manufacturing, Villegas and Palardy (2017) introduced a pre-moulding process with triangular ED strips (Figure 9.6b). With their height of 0.5 to 0.7 mm, they mitigate inaccuracies in planarity remarkably better. However, for a tape laying process, such a technique is rather complicated to implement. Profiled

heated rollers could apply a shaped resin film as final step. Still, thickness must be large enough so fixation force does not squeeze pre-moulded EDs back to a flat resin layer without preferential melting properties.

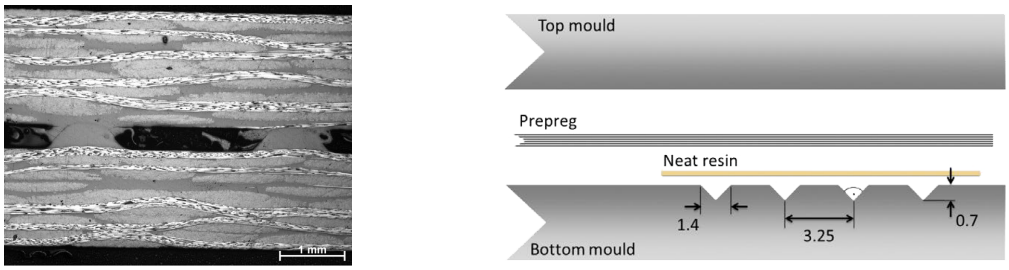

(a) Initial Stage of Molten EDs (b) Schematic for Triangular ED Moulding

Figure 9.6 – Triangular Energy Director Investigation (Villegas and Palardy 2017)

Another technique which is at the forefront of technological revolution is again additive manufacturing. Besides the opportunity to “print” EDs on the top layer of the laminate, it provides a high degree of freedom for the chosen shape, pattern and thickness.

So far, flat energy directors seem to be best choice for an automated process, but if planarity issue shows unbearable influence, there are existing techniques taking their place.

10 Conclusion

10.1 Summary

At the beginning, main drivers for recent increase in composite aircraft structure were shown since there is still high (lightweight) potential compared to the state of the art "black metal" approach. A detailed overview presented already existing fibre-fair fusion bonding techniques waiting to be implemented. Despite, ultrasonic, resistance and induction welding approaches are the most promising ones for aviation applications. Evaluation revealed partly severe disadvantages of one or another fusion bonding process. Thereby, ultrasonic welding possessed best behaviour and was chosen for further investigation. Manual pre-testing showed encouraging results for subsequent theoretical elaborations. Important process parameters were identified and quantified during following parametric study. Moreover, experiments gave a unique insight in the process and revealed once more its peculiarities and effects. Still, expected parameter correlations were proven in the results discussion. Eventually, this collected knowledge laid the foundation for continuous process development.

Evidently, ultrasonic welding was chosen due to its persuasive advantages compared to the other two approaches – not due to absence of disadvantages. The rather simple, quick and clean set-up convinces as well as easy accessibility, ideal continuous properties and good automation without critical and costly foreign materials. There are certain drawbacks – mainly in form of required planarity and deployment of flat energy directors – which need to be solved in order to implement this process successfully in aircraft series production. Achieved results in front of the background of limited time show impressively the potential of this technique. Material combinations like CF/PPS or CF/PEI are investigated intensively these days whereas CF/PEEK still exhibits a lack of knowledge and experience. Based on this work, there is the chance to change this.

Main challenge for the future will be to establish a stable process incorporating constant joint quality, i.e. particularly areal welds of equal size, controlled melt front propagation and quality monitoring. The transfer from static to continuous will be a challenging task but worth going onward in this direction. The future in continuous joining will be ultrasonic.

10.2 Outlook

So far, the main scope contained joining of longitudinal geometries. Nevertheless, this process can be tailor for circumferential joining of aircraft shell, too (Figure **??**). The small curvature as well as the rather small sonotrode dimensions are fulfilled conditions for an three dimensional application. Self-evidently, process control must be stable and sensor technology must be deployed in a way to enable curved robot paths and maintain required process boundaries. Thereby, ultrasonic welding exhibits once more its versatile and flexible nature.

Many approaches go in the direction of not just establishing a stable ultrasonic process but develop an in-situ monitoring of key process parameters to track and adjust them for optimum weld quality. This work showed strongly the various variable influencing and/or disturbing the process. Online measurement and immediate reaction towards a closed-loop process are the next steps in the direction of automation and industrialisation of ultrasonic welding – particularly in highly regulated aviation industry.

Often referred is "[...] power and displacement data provided for microprocessor controlled ultrasonic welders [that] can be utilised for in situ monitoring of the welding process and ultimately of the quality of the welds." (Villegas 2015) Other observations even suggest "... that if the output power is be constant, the weld are also will be homogeneous." (Senders 2016, 61) Whether this hypothesis is proven valid, this will be an outstanding leverage point for future process controlling.

This approach eventually lays the ground for a sophisticated quality management collecting data in real time, assessing and recording it for each and every part providing full traceability as a major requirement for certification in aircraft manufacturing. Steps are – chronologically – development and deployment of suitable measurement technologies for collecting data, analysing for achieving an insight in the process mechanisms finally leading to a bundle of parameters setting an envelope for quality control. Important is the screening of the entire process and extracting of valuable information (Figure 10.1). A consequent and holistic strategy will provide all tools for a successful implementation in series production in the future.

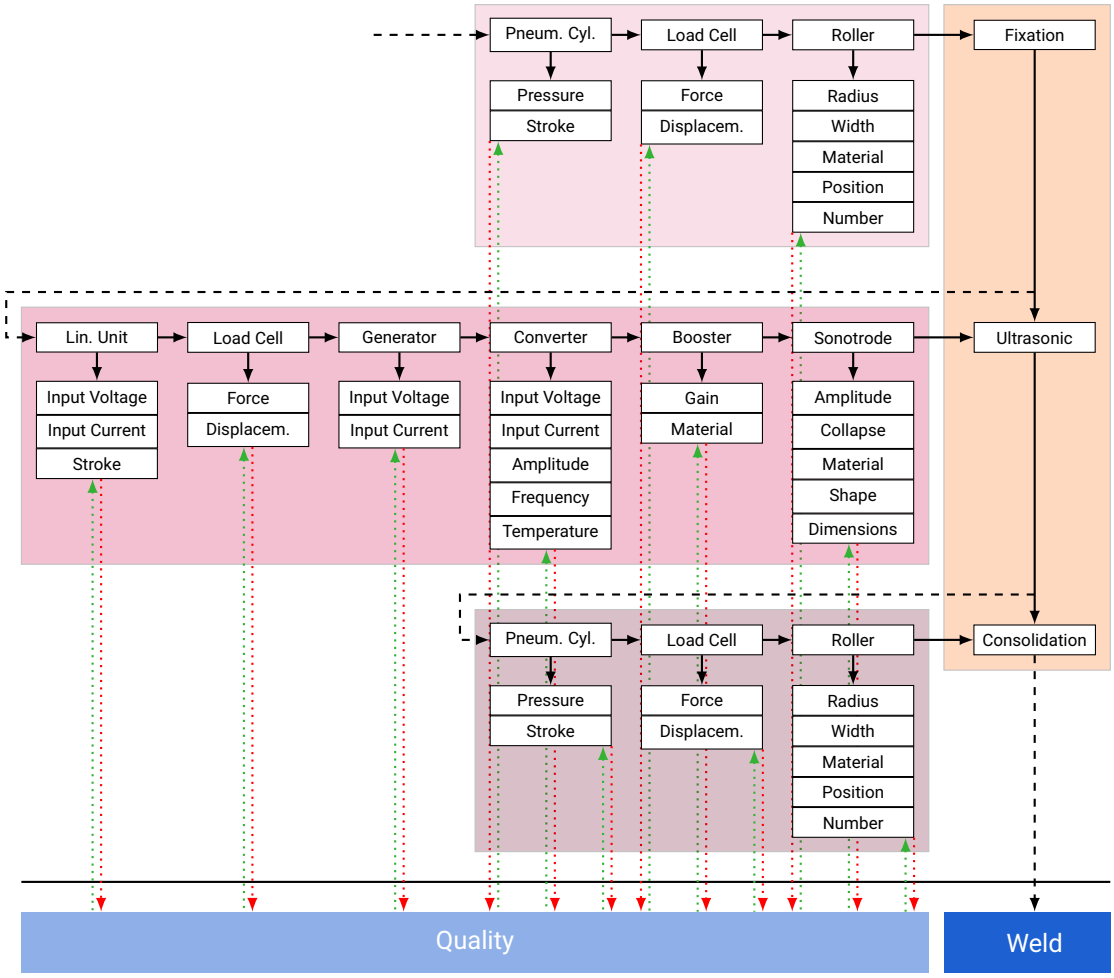

Figure 10.1 – Quality Management Schematic

Acknowledgements

Many thanks to the DLR Augsburg for opening my eyes to the world of scientific research, giving me the opportunity to dream, explore, discover and create solely with the power of mind. Namely my supervisor, Dr. Stefan Jarka who gave me both, a free hand in developing the idea and concept of the work as well as his expertly competence, knowledge and advice whenever I needed it. The same applies to my academic supervisor Prof. André Baeten. The way how he supports and demands is inspiring, encouraging and awakens one's ambitions to think out of the box and break new ground.

Further thanks to Manuel Endraß and Simon Bauer at DLR Augsburg/Stuttgart for their words of advice and active support throughout these six months at their institutes.

Big thanks to BRANSON Ultrasonics, namely Daniel Lorenz and Serdar Genc, for their quick, competent and straightforward activities in preparation and execution of our experimental study. Their spontaneity and openness to our requests and wishes as well as their hospitality was commendable, providing a pleasant atmosphere necessary for professional laboratory work and achieving results of scientific value.

Finally, the greatest and most important thanks go particularly to my parents and further my whole family. This work marks the end of my five year lasting study during which they supported me extraordinarily, unconditionally and tolerated many hours, days and weeks of academic work uncomplainingly. Without their love, consolation and encouragement I could not evolve into the one I am today. Important achievements and milestones of my life would not be possible. All merits and appreciations belong to them as well. *Unendlichen Dank!*

A Experimental Set-Up Addendum

A.1 Computed Maximum Overlap Length

ASTM D 1002 requires a maximum permissible overlap length as

$$L_{max} = \frac{\sigma_y \cdot t}{\tau_{max}} \qquad \text{(Eq. A.1)}$$

with σ_y as yield strength (for composites: tensile strength), t as thickness of the material, τ_{max} as 150 % of the estimated average shear strength in joint. For utilised CF/PEEK plates, data sheets gives a shear strength of 53 MPa yielding

$$L_{max} = \frac{600\ MPa \cdot 2.21\ mm}{1.5 \cdot 53\ MPa} = 16.68\ mm > 12.7\ mm \quad \checkmark \qquad \text{(Eq. A.2)}$$

fulfilling the standard requirement.

A.2 Laminate/Film Properties

Table A.1 – Haufler CF/PEEK Plate Properties

Fibre		Torayca T300 HT-Carbon, 3K
Fibre orientation		0°/90°
Weave		5HS (Harness Satin)
Matrix		Victrex 150G (PEEK)
Fibre Volume Content	%	ca. 50
Density	g/cm^3	ca. 1.5
Tensile Strength	MPa	600
Shear Strength	MPa	53
Young's Modulus ($E_{\parallel}$)	GPa	56.1
Young's Modulus ($E_{\perp}$)	GPa	55.6
Poisson Ratio	-	0.29
Compressive Strength	MPa	500
CTE 0°/90°	1/K	5 x 10E-6
Max. Service Temperature	°C	260

Data: Haufler 2017

Table A.2 – TORAYCA® T300 Carbon Fibre Properties

Property	Test Method	Units	T300
Tensile Modulus	TY-030B-01	GPa	230
Tensile Strength	TY-030B-01	MPa	3530
Tensile Elongation	TY-030B-01	%	1.5
Density	TY-030B-02	g/cm^3	1.76
Filament Diameter		µm	7
Thermal Conductivity		W / m · K	10.46
CTE		10^{-6} / K	-0.41
Volume Resistivity		Ω· cm	0.0017

Data: TORAY 2017

Table A.3 – Aptiv® 1300 black PEEK Film Properties

Property	Test Method	Test Condition	Units	1300-050G
Glass Transition Temperature	ISO 11357		°C	143
Melting Point	ISO 11357		°C	343
Tensile Modulus	ISO 527	23°C	GPa	2.5
Tensile Strength	ISO 527 (at break)	23°C	MPa	120
Tensile Elongation	ISO 527 (at break)	23°C	%	>150
Shrinkage	TM-VX-84	200°C	%	$\leq$2
Density	ISO 1183	23°C	g/cm^3	1.30
Thermal Conductivity	ISO 22007-4	Average, 23°C	W / m · K	0.29
CTE	ISO 11359	Average below T_g	10^{-6} / K	50
Dielectric Strength	ASTM D149	23°C	kV/mm	190
Volume Resistivity	ASTM D257	23°C, 100V	Ω· cm	4.00E+16

Data: Victrex 2017

Table A.4 – LITE® TK PEEK Film Properties

Property	Test Method	Test Condition	Units	TK
Glass Transition Temperature	ISO 11357		°C	143
Melting Point	ISO 11357		°C	343
Tensile Modulus	ISO 527	23°C	GPa	3.2
Tensile Strength	ISO 527 (at break)	23°C	MPa	130
Tensile Elongation	ISO 527 (at break)	23°C	%	170
Density	ISO 1183	23°C	g/cm^3	1.30
Thermal Conductivity	DIN 52612		W / m · K	0.25
CTE	E831		10^{-6} / K	46
Dielectric Strength	IEC 243	23°C	kV/mm	180
Volume Resistivity	IEC 93		Ω· cm	1.00E+18

Data: LITE 2017

B Statistical Evaluation

A test result of an arbitrarily chosen measurement series p with the main parameter x and a limited number of measures must be provided in the form of

$$p\colon\ (\bar{x} \pm \Delta x)\ \mathit{unit} \qquad \mathit{with} \qquad \Delta x = \frac{t \cdot s_x}{\sqrt{n}} \tag{Eq. B.1}$$

with standard deviation s_x of the arithmetic mean value according to

$$s_x = \sqrt{\frac{1}{n-1} \sum_{i=1}^{n} (x_i - \bar{x})^2} \tag{Eq. B.2}$$

The value for t – also known as STUDENT's t-distribution – can be taken out of table works referring to respective probability levels P and considering the number of measured values n just as given in Table B.1. A classification of precision is made, too. Despite the level of reliability, often times values are referred to the level of failure α, i.e. $P = (1 - \alpha) \cdot 100\ \%$.

In this work, nine out of ten specimen provided valid test results after welding and tension test. Selecting a level of reliability of 95 %, the related Student's factor can be read as 2.262, inserted in (Eq. B.1) yields

$$\Delta x = \frac{2.262 \cdot s_x}{\sqrt{9}} = 0.754 \cdot s_x \tag{Eq. B.3}$$

Table B.1 – Student's t-Distribution Values

Number of Measured Values		Level of Reliability/Failure			
		orientation	operational	precision	
	I	1σ	1.96 σ	2.58 σ	4 σ
	P	68.27 %	95 %	99 %	99.99 %
	α	0.3173	0.05	0.01	0.0001
1		1.84	12.706	63.657	636.6
2		1.32	4.303	9.925	31.60
3		1.20	3.182	5.841	12.92
4		1.15	2.776	4.604	8.610
5		1.11	2.571	4.032	6.869
6			2.447	3.707	5.959
7		1.08	2.365	3.499	5.408
8			2.306	3.355	5.041
9			2.262	3.250	4.781
10		1.06	2.228	3.169	4.587
15		1.04	2.132	2.949	4.229
20		1.03	2.086	2.845	3.849
∞		1.00	1.96	2.576	3.291

Source: Kuchling 2011, 609; Zeidler et al. 2012, 92; Parthier 2016, 91

C Fracture Surface Microscopic Analysis

Lower	Adherend	Upper
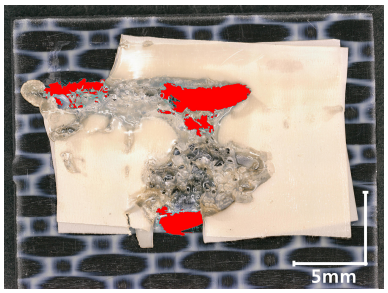	#29	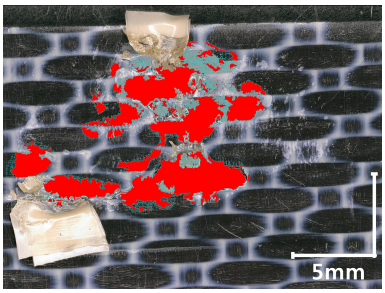
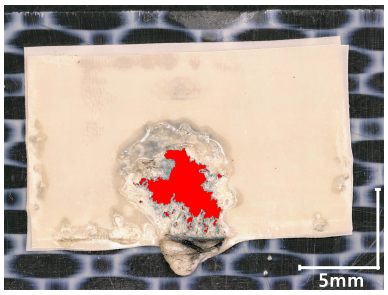	#30	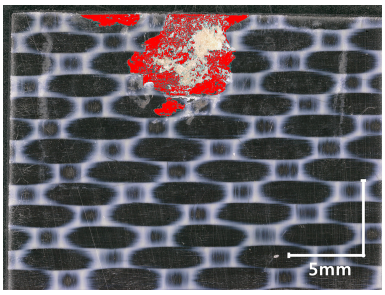
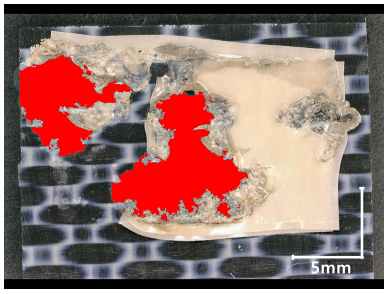	#31	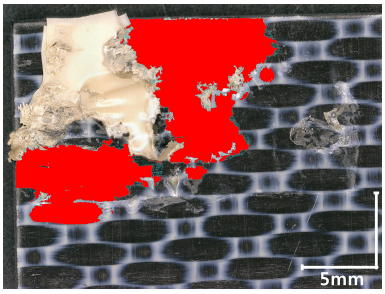
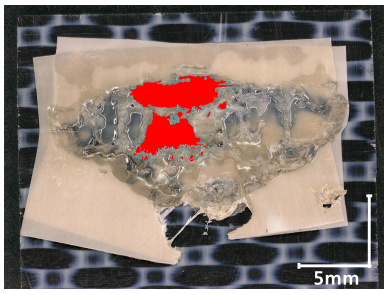	#32	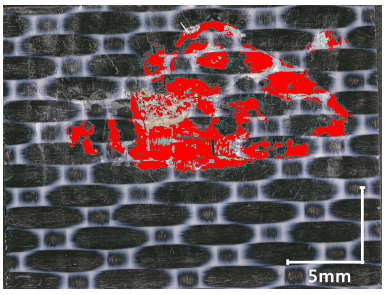

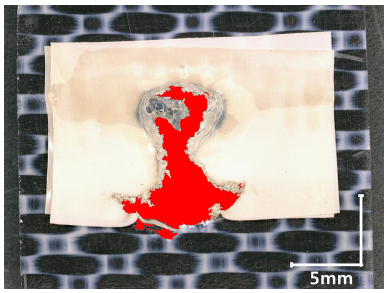

#33

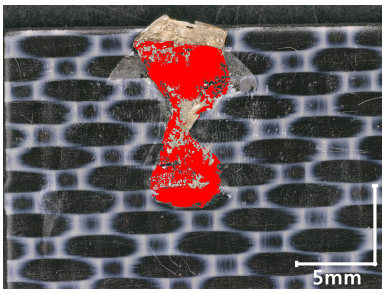

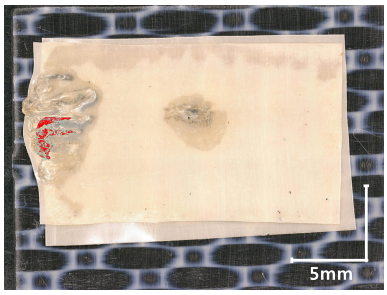

#34

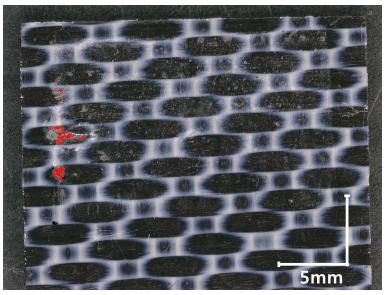

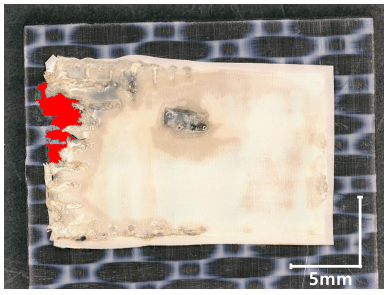

#35

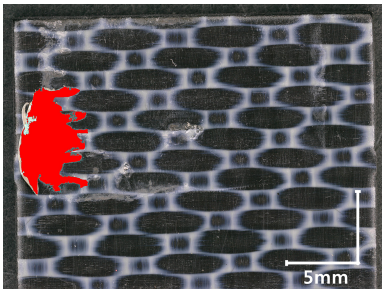

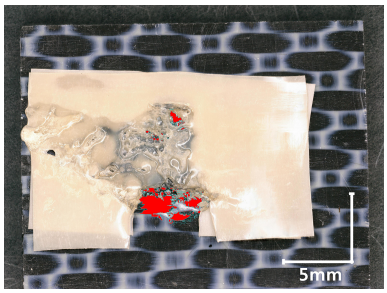

#36

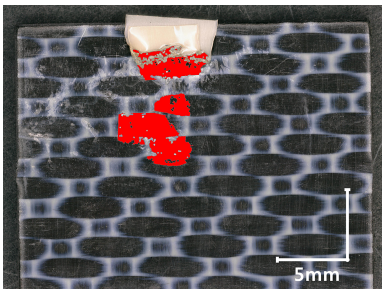

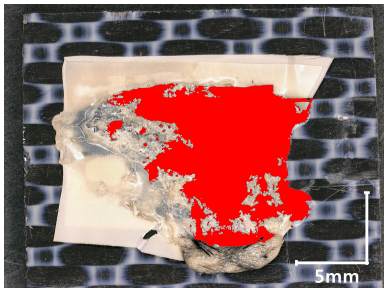

#38

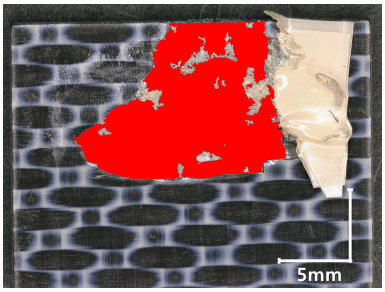

D Clamping Force Estimation

Clamping screws during experiments are tightened with a torque of 20 Nm. The rule of thumb for fastening screws (Wittel et al. 2011, Eq. 8.28) yields

$$F_{fix} = \frac{M_A}{0.17 \cdot d} = \frac{20\ Nm}{0.17 \cdot 8 \cdot 10^{-3} m} = 14705.88\ N. \tag{Eq. D.1}$$

This clamping force acts on each screw left and right, thus the resulting reaction force of specimen is double the fixation force. This force is applied by the clamping jaws with a width of 20 mm covering the whole specimen width of 25.4 mm, i.e. an effective contact pressure of

$$p_{fix} = \frac{F_{fix}}{w_{clamp} \cdot w_{specimen}} = \frac{29411.76\ N}{20\ mm \cdot 25.4\ mm} = 57.90\ MPa \tag{Eq. D.2}$$

For consolidation and fixation, utilisation of rollers is envisaged. In this case, contact pressure is computed as *Hertzian pressure* according to (Eq. 4.4)

$$p_H = \sqrt{\frac{F_N \cdot E}{2\pi\rho \cdot l}} \tag{Eq. D.3}$$

whereof

$$\rho = \frac{\rho_1 \cdot \rho_2}{\rho_1 + \rho_2} \qquad \text{and} \qquad E = \frac{2 \cdot E_1 \cdot E_2}{(1-\nu_1^2) \cdot E_2 + (1-\nu_2^2) \cdot E_1} \tag{Eq. D.4}$$

with curvature radii ρ_1, ρ_2, Young's moduli E_1, E_2, Poisson's ratii ν_1, ν_2 and contact length l here representing the roller width, i.e. overlap width. For a cylinder-plane contact, $\rho = r_{roll}$ and with composite properties (Appendix A) as well as a steel roller, parameters are determined as

$$\begin{aligned} E &= \frac{2 \cdot E_{roll} \cdot E_\perp}{(1-\nu_{roll}^2) \cdot E_\perp + (1-\nu_\perp^2) \cdot E_{roll}} \\ &= \frac{2 \cdot 210\ GPa \cdot 55.6\ GPa}{(1-0.3^2) \cdot 55.6\ GPa + (1-0.29^2) \cdot 210\ GPa} \\ &= 96.12\ GPa \end{aligned} \tag{Eq. D.5}$$

After simplifying, rearranging and inserting, (Eq. D.3) reads

$$F_N = \frac{p_H^2 \cdot 2\pi r_{roll} \cdot l}{E} = \frac{(57.90\ MPa)^2 \cdot 2\pi r_{roll} \cdot l}{96.12 \cdot 10^3\ MPa} = 0.219 \cdot r \cdot l. \qquad \text{(Eq. D.6)}$$

Figure D.1 shows the plot of the function for required force depending on different roller radii and overlap (roller) width. For a desired overlap of 50 mm, roller radius must not exceed about 92 mm to keep the resulting force below 1000 N.

In order to minimise the distance between the sonotrode and consolidation roller to apply force as soon as possible to the heated section, rollers should not get too large. In previous works, rollers exhibited radii of maximum 20 mm. Corresponding force is about 200 N and shall be used for further calculations.

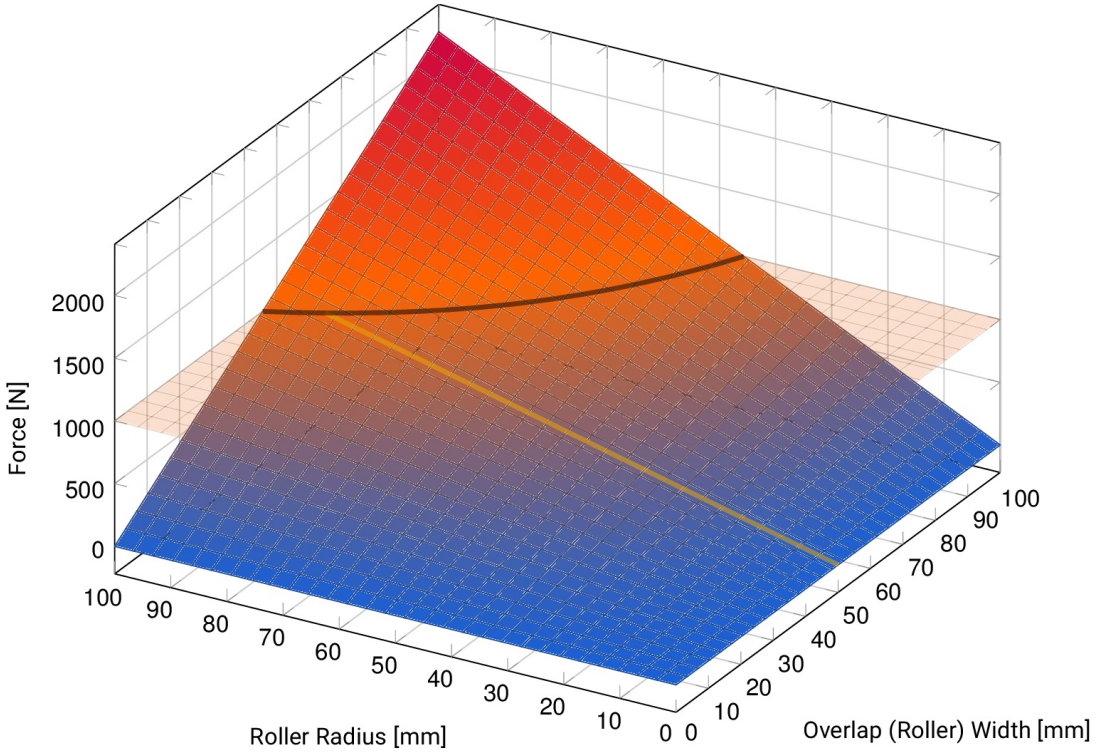

Figure D.1 – Required Force Dependency on Roller Radius and Width with Virtual 1000 N Limit

About the Author

ALEXANDER SÄNGER is master student for Lightweight Construction and Composite Technology at the University of Applied Sciences Augsburg. Priorly, he graduated at the same institution as Bachelor of Engineering in Mechanical resp. Aerospace Engineering. Within this time, he studied one semester abroad at the University of Limerick, Ireland, at the Faculty of Aerospace Engineering. Due to his dual study at Premium AEROTEC GmbH, Augsburg, he already gained working experience as a manufacturing engineer introduced by his bachelor thesis on *NC Runtime Optimisation of a Clip-Frame-Riveting Robot in the A350 Production via Nominal-Actual Feed Analysis* (2016). Besides several company-internal projects, he was in the lead of the university-approved "ALARIS" project *Design, Dimensioning and Production Planning of a Body Wing Aircraft of Composite Materials* (2015) and the master projects *Concept Development of an Integrated Air Extraction for CFRP Milling Applications* (2016) and *Biocomposites in the Field of Mechanical Engineering* (2017). He lives in Munich.

Bibliography

Ageorges, Christophe, and Lin Ye. 2001a. "Resistance welding of thermosetting composite/thermoplastic composite joints." *Composites Part A: Applied Science and Manufacturing* 32 (11): 1603–1612. ISSN: 1359-835X. doi:http://doi.org/10.1016/S1359-835X(00)00183-4.

———. 2001b. "Simulation of impulse resistance welding for thermoplastic matrix composites," 8:133–147. 2.

———. 2012. *Fusion Bonding of Polymer Composites.* Engineering Materials and Processes. London: Springer. ISBN: 9781447101710.

Ageorges, Christophe, Lin Ye, and Meng Hou. 2000a. "Experimental investigation of the resistance welding for thermoplastic-matrix composites: Part I: heating element and heat transfer." *Composites Science and Technology* 60 (7): 1027–39. ISSN: 0266-3538. doi:http://doi.org/10.1016/S0266-3538(00)00005-1.

———. 2000b. "Experimental investigation of the resistance welding of thermoplastic-matrix composites: Part II: optimum processing window and mechanical performance." *Composites Science and Technology* 60 (8): 1191–1202. ISSN: 0266-3538. doi:http://doi.org/10.1016/S0266-3538(00)00025-7.

———. 2001. "Advances in fusion bonding techniques for joining thermoplastic matrix composites: a review." *Composites Part A: Applied Science and Manufacturing* 32 (6): 839–857. ISSN: 1359-835X. doi:http://dx.doi.org/10.1016/S1359-835X(00)00166-4.

AH, (Airbus Helicopters). 2016. Internal Meeting/Unpublished.

Ahmed, N. 2005. *New Developments in Advanced Welding.* Woodhead Publishing Series in Welding and Other Joining Technologies. Elsevier Science. ISBN: 9781845690892.

Ahmed, T.J., D. Stavrov, H.E.N. Bersee, and A. Beukers. 2006. "Induction welding of thermoplastic composites—an overview." *Composites Part A: Applied Science and Manufacturing* 37 (10): 1638–1651. ISSN: 1359-835X. doi:http://doi.org/10.1016/j.compositesa.2005.10.009.

Airbus. 2006. "Taking the lead: the A350 XWB." Accessed April 17, 2017. https://www.airbusgroup.com/dam/assets/airbusgroup/int/en/investor-relations/documents/2006/untitled/further_pre_a350_xwb_launch_2006.pdf.

AM. 2013. "More Control for Ultrasonic Welding." *Assembly Magazine* (June).

Arias, M., and G. Ziegmann. 1996. "Impulse resistance welding: a new technique for joining advanced thermoplastic composite parts." In *Proceedings of the 41st International SAMPE Symposium and Exhibition.* Anaheim.

ASTM D 1002, (Deutsches Institut für Normung). 2001. *Standard Test Method for Apparent Shear Strength of Single-Lap-Joint Adhesively Bonded Metal Specimens by Tension Loading (Met-*

al-to-Metal). Deutsche Industrienorm. ASTM International (American Society for Testing and Materials), West Conshohocken. doi:10.1520/D1002-10.

Baehr, Hans Dieter, and Karl Stephan. 2016. *Wärme- und Stoffübertragung.* Berlin Heidelberg: Springer. ISBN: 9783662496770.

Bargel, Hans-Jürgen, and Günter Schulze. 2013. *Werkstoffkunde.* Springer-Lehrbuch. Berlin and Heidelberg: Springer. ISBN: 9783642177170.

Bayerl, Thomas, Miro Duhovic, Peter Mitschang, and Debes Bhattacharyya. 2014. "The heating of polymer composites by electromagnetic induction – A review." *Composites Part A: Applied Science and Manufacturing* 57:27–40. ISSN: 1359-835X. doi:http://doi.org/10.1016/j.compositesa.2013.10.024.

Beards, C. 1995. *Engineering Vibration Analysis with Application to Control Systems.* Elsevier Science. ISBN: 9780080523651.

Beevers, A. 1991. "Welding: the way ahead for thermoplastics?" ACE11-2, *Engineering:* 231.

Beland, Sylvie. 2012. *High Performance Thermoplastic Resins and Their Composites.* Elsevier Science. ISBN: 9780815517900.

Benatar, A., J.W. Gillespie Jr., and K. Kedward. 1997. "Joining of polymer composites." Chap. 14 in *Advanced Composites Manufacturing,* by T.G. Gutowski. New York: John Wiley / Sons. ISBN: 9780471153016.

Benatar, Avraham, and Zuhang Cheng. 1989. "Ultrasonic welding of thermoplastics in the far--field." *Polymer Engineering & Science* 29 (23): 1699–1704. ISSN: 1548-2634. doi:10.1002/pen.760292312.

Benatar, Avraham, Raman V. Eswaran, and Satinder K. Nayar. 1989. "Ultrasonic welding of thermoplastics in the near-field." *Polymer Engineering & Science* 29 (23): 1689–1698. ISSN: 1548-2634. doi:10.1002/pen.760292311.

Benatar, Avraham, and Timothy G. Gutowski. 1986. "Methods for fusion bonding thermoplastic composites." *SAMPE Quaterly* 18 (1): 35–42.

———. 1988. "Ultrasonic Welding of Advanced Thermoplastic Composites." In *33rd International SAMPE Symposium,* 1787–1797.

———. 1989. "Ultrasonic welding of PEEK graphite APC-2 composites." *Polymer Engineering & Science* 29 (23): 1705–1721. ISSN: 1548-2634. doi:10.1002/pen.760292313.

Benkowsky, G. 1990. *Induktionserwärmung: Härten, Glühen, Schmelzen, Löten, Schweissen.* Grundlagen und praktische Anleitungen für Induktionserwärmungsverfahren, insbesondere auf dem Gebiet der Hochfrequenzerwärmung. Verlag Technik. ISBN: 9783341008133.

BMW Group. 2017. "How a BMW i is created: The LifeDrive concept in four steps." Accessed April 15, 2017. http://www.bmwgroup-plants.com/en/leipzig/production/bmw-i-composition.html.

Boeing. 2016. "Jährliche Wachstumsraten für den Passagierbereich im Luftverkehr von 2016 bis 2035 nach Regionen (gemessen an Revenue-Passagier-Kilometern)." Statista. Accessed April 12, 2017. https://de.statista.com/statistik/daten/studie/165532/umfrage/wachstumsraten-fuer-den-passagier--und-cargobereich-im-luftverkehr/.

Border, J., and R. Salas. 1989. In *Proceedings of the 34th International SAMPE Symposium,* 2569–78.

Boyard, Nicolas. 2016. *Heat Transfer in Polymer Composite Materials: Forming Processes.* Mechanical engineering and solid mechanics series. Wiley. ISBN: 9781848217614.

BRANSON. 2011. *Ultrasonic Welding Characteristics of Textiles and Films.* PW-7, Danbury.

———. 2013. *DCX A and F Power Supplies.* PJ-0003-13.

———. 2015. *2000Xc: Ultraschall-Fertigungssysteme für Kunststoffschweißen.* PJ-0018-15.

Campbell, Flake C. 2003. *Manufacturing Processes for Advanced Composites.* Elsevier Science. ISBN: 9780080510989.

Chursin, Alexander, and Yury Makarov. 2015. *Management of Competitiveness: Theory and Practice.* Springer International Publishing. ISBN: 9783319162447.

Clean Sky JU. 2016. *Clean Sky at a Glance.* Brussels, March.

Cole, K.C. 1992. "A review of Recent Developments in Joining High-Performance Thermoplastic Composites." In *Proceedings of Canadian International Composites Conference and Exhibition,* edited by S.V. Hoa and R. Gauvin, 341–348.

Costa, Anahi Pereira da, Edson Cocchieri Botelho, Michelle Leali Costa, Nilson Eiji Narita, and José Ricardo Tarpani. 2012. "A Review of Welding Technologies for Thermoplastic Composites in Aerospace Applications." *Journal of Aerospace Technology and Management* 4 (3): 255–265. ISSN: 04033912. doi:10.5028/jatm.2012.04033912.

CUP, (Cambridge University Press). 2008. *Cambridge Advanced Learner's Dictionary.* Cambridge University Press. ISBN: 9780521674683.

Davies, P., W.J. Cantwell, P.-Y. Jar, P.-E. Bourban, V. Zysman, and H.H. Kausch. 1991. "Joining and repair of a carbon fibre-reinforced thermoplastic." *Composites* 22 (6): 425–431. ISSN: 0010-4361. doi:http://dx.doi.org/10.1016/0010-4361(91)90199-Q.

Delgado Labrandero, Sofía. 2009. "Characterization of metallic meshes used for resistance welding of thermoplastic composites." Ingeniería Industrial Thesis, Universidad Carlos III de Madrid.

DIN 1910-100, (Deutsches Institut für Normung). 2005. *Schweißen und verwandte Prozesse - Begriffe: Teil 100: Metallschweißprozesse mit Ergänzungen zu DIN EN 14610:2005.* Deutsche Industrienorm. Deutsches Institut für Normung.

DLR, (Deutsches Zentrum für Luft- und Raumfahrt). 2015. *DLR-Luftfahrtforschung.* Cologne, December.

———. 2017a. Internal Meeting/Unpublished.

DLR, (Deutsches Zentrum für Luft- und Raumfahrt). 2017b. "DLR at JEC World 2017 in Paris." March 13. Accessed May 13, 2017. http://www.dlr.de/dlr/en/desktopdefault.aspx/tabid-10081/151_read-21690/#/gallery/26534.

Domininghaus, Hans. 2013. *Kunststoffe: Eigenschaften und Anwendungen.* Edited by Peter Elsner, Peter Eyerer, and Thomas Hirth. VDI-Buch. Berlin-Heidelberg: Springer. ISBN: 9783642161735.

Don, R.C., L. Bastien, T.B. Jakobsen, and J.W. Gillepsie Jr. 1990. "Fusion bonding of thermoplastic composites by reistance heating." *SAMPE Journal* 26:59–60.

Dorsch, Jessica Katrin. 2013. "Experimentelle Ermittlung der Prozessparameter zum automatisierten Ultraschall-Heften von Carbonfaser-verstärkten Thermoplast-Lagen." Master Thesis, University of Applied Sciences Augsburg.

Dubé, Martine. 2007. "Static and Fatigue Behaviour of Thermoplastic Composite Laminates Joined by Resistance Welding." 18695. PhD Thesis, McGill University Montréal.

Dubé, Martine, P. Hubert, A. Yousefpour, and J. Denault. 2008a. "Current leakage prevention in resistance welding of carbon fibre reinforced thermoplastics." *Composites Science and Technology* 68:1579–1587. ISSN: 0266-353. doi:10.1016/j.compscitech.2007.09.008.

Dubé, Martine, Pascal Hubert, Jan N.A.H. Gallet, Darko Stavrov, Harald E.N. Bersee, and Ali Yousefpour. 2008b. "Fatigue performance characterisation of resistance-welded thermoplastic composites." *Composites Science and Technology* 68 (7–8): 1759–1765. ISSN: 0266-3538. doi:http://doi.org/10.1016/j.compscitech.2008.02.012.

Dubé, Martine, Pascal Hubert, Ali Yousefpour, and J. Denault. 2009. "Fatigue failure characterisation of resistance-welded thermoplastic composites skin/stringer joints." *International Journal of Fatigue* 31 (4): 719–725. ISSN: 0142-1123. doi:http://doi.org/10.1016/j.ijfatigue.2008.03.012.

Dubé, Martine, Pascal Hubert, Ali Yousefpour, Johanne Denault, and Matthew Wadham-Gagnon. 2007. "Resistance welding of Thermoplastic Composite Skin/Stringer Specimens." *Composites Part A Applied Science and Manufacturing* 38, no. 12 (December). doi:10.1016/j.compositesa.2007.07.014.

Duhovic, Miro, Joachim Hausmann, Pierre L'Eplattenier, and Inaki Caldichoury. 2015. "A Finite element Investigation into the Continuous Induction Welding of Dissimilar Material Joints." In *Proceedings of the 10th European LS-DYNA Conference 2015.*

Dukane. 2011. *Guide to Ultrasonic Plastics Assembly.* 403-536-02. St. Charles: Dukane Intelligent Assembly Solutions, August.

EC, (European Commission). 2011. "End-of-life aircraft recycling offers high grade materials." June 24. Accessed May 27, 2017. http://ec.europa.eu/environment/ecoap/about-eco-innovation/good-practices/eu/719_en.

Ehrenstein, Gottfried W., Gabriela Riedel, and Pia Trawiel. 2012. *Thermal Analysis of Plastics: Theory and Practice.* München: Carl Hanser Verlag GmbH & Company KG. ISBN: 9783446434141.

EU, (European Union). 1999. *Directive on Landfill of Waste.* 99/31/EC, April 26.

EU, (European Union). 2000. *Directive on End-of Life Vehicle.* 2000/53/EC, September 18.

Eveno, C.E., and J.W. Gillespie Jr. 1989. "Experimental Investiagtion of Ultrasonic Welding of Graphite Reinforced Polyetheretherketone Composites." *21st International SAMPE Technical Conference,* no. 21: 923–934.

Eveno, E.C., and J.W. Gillespie Jr. 1988. "Resistance welding of graphite polyetheretherketone composites: an experimental investigation." *Journal of Thermoplastic Composite Materials* 1:322–38.

FAA, (Federal Aviaton Administration). 2001. *Stress Analysis of In-Plane, Shear-Loaded, Adhesively Bonded Composite Joints and Assemblies.* Final Report DOT/FAA/AR-01/7. U.S. Department of Transportation, April.

———. 2012. *Aviation Maintenance Technician Handbook: Airframe.* Vol. 1. Newcaslte: Aviation Supplies & Academics Inc. ISBN: 9781560279501.

Fernie, J.A., P.L. Threadgill, and M.N. Watson. 1991. "Progress in Joining Advanced Materials." *Welding and Metal Fabrication* (June): 179–84.

Fischer, Frederic, Yannick Mezakeu Tongnan, Matthias Beyrle, Tobias Gerngross, and Michael Kupke. 2015. "Characterization of Production-Induced Defects in Carbon Fiber Reinforced Thermoplastic Technology." Edited by Randolf Hanke, Christian Boller, and Matthias Purschke. Bremen, November.

Fish, J.C., M.L. Vitlip, and S.P. Chen. 1992. "Interlaminar Fracture Characteristics of Bonding Concepts for Thermoplastic Primary Structures." *AIAA Journal* 30:1602–1608.

Fokker. 2013. *New evolution: Progress in thermoplastic composites.* Brochure. Papendrecht: Fokker Aerostructures.

Frantz, J. 1997. "Joining Plastics the Sound Way." *Machine Design,* no. 2: 61–65.

Freist, Carsten. 2013. "Experimentelle und numerische Untersuchungen zum Widerstandsschweißen endlosfaser- und kurzfaserverstärkter thermoplastischer Hochleistungsstrukturen." Dissertation, Universität Stuttgart.

Gachnang, Hans Rudolf. 2008. *Ultrasonic welding device.* EP Patent App. EP20,060,024,020, May.

Gallego-Juárez, J.A., and K.F. Graff. 2014. *Power Ultrasonics: Applications of High-Intensity Ultrasound.* Woodhead Publishing Series in Electronic and Optical Materials. Elsevier Science. ISBN: 9781782420361.

Gardiner, Ginger. 2011. "Thermoplastic composites: Primary structure?" February 5. Accessed May 11, 2017. `http://www.compositesworld.com/articles/thermoplastic-composites-primary-structure`.

Gerdeen, James C., James C. Gerdeen, Harold W. Lord, and Ronald A.L. Rorrer. 2005. *Engineering Design with Polymers and Composites.* Engineering Design with Polymers and Composites, Vol. 1. Boca Raton: Taylor & Francis. ISBN: 9780824723798.

Gleich, D.M., M.J.L van Tooren, and A. Beukers. 2001. "Analysis and evaluation of bondline thickness effects on failure load in adherends bonded structures." *Journal of Adhesion Science and Technology* 15 (9): 1901–1101.

Grewell, D.A., A. Benatar, and J.B. Park. 2003. "Ultrasonic welding." Chap. 8 in *Plastics and Composites Welding Handbook.* Munich: Hanser. ISBN: 3446195343.

Grimm, R.A. 1990. "Fusion Welding Techniques." *Welding Journal* 69:23–28.

Guess, T.R., and R.E. Allred. 1977. "Comparison of Lap Shear Specimens." *Journal of Testing and Evaluation,* no. 5: 84–93.

Haimbaugh, R.E. 2001. *Practical Induction Heat Treating.* ASM International. ISBN: 9781615031528.

Harras, B., K. C. Cole, and T. Vu-Khanh. 1996. "Optimization of the Ultrasonic Welding of PEEK--Carbon Composites." *Journal of Reinforced Plastics and Composites* 15 (2): 174–182. doi:10.1177/073168449601500203. eprint: http://dx.doi.org/10.1177/073168449601500203.

Haufler, (Haufler Composites GmbH & Co. KG). 2017. *Carbon PEEK Platten.* Datasheet. Blaubeuren.

Heimerdinger, M.W. 1995. "Repair Technology for Thermoplastic Aircraft Structures." *Composite Repair of Military Aircraft Structures: 79th Meeting of the AGARD Structures and Materials Panel, Seville* (Qudbec), no. AGARD-CP-550 (January): 1–12.

Ho, Janet, and Richard Jow. 2009. *Characterization of High Temperature Polymer Thin Films for Power Conditioning Capacitors.* Report. ARL-TR-4880. Adelphi: Army Research Laboratory, July.

Holmes, S.T., R.C. Don, J.W. Gillespie Jr., I. Howie, and A. Ortona. 1991. "Sequential resistance welding of large-scale IM7/PEEK double lap joints." In *CCM Report 91-55.* Centre for Composite Materials, University of Delaware.

Hopmann, Christian, and Walter Michaeli. 2015. *Einführung in die Kunststoffverarbeitung.* München: Carl Hanser Verlag GmbH & Company KG. ISBN: 9783446446281.

Hou, M., and K. Friedrich. 1992. "Resistance welding of continuous carbon fibre/polypropylene composites." *Plastic, Rubber and Composites Processing and Applications* 18 (4): 205–13.

Hou, Meng, and K. Friedrich. 1992. "Resistance welding of continuous glass fibre-reinforced polypropylene composites." *Composites Manufacturing* 3 (3): 153–163. ISSN: 0956-7143. doi:http://dx.doi.org/10.1016/0956-7143(92)90078-9.

Hou, Meng, Mingbo Yang, Andrew Beehag, Yiu-Wing Mai, and Lin Ye. 1999a. "Resistance welding of carbon fibre reinforced thermoplastic composite using alternative heating element." Tenth International Conference on Composite Structures, *Composite Structures* 47 (1–4): 667–672. ISSN: 0263-8223. doi:http://dx.doi.org/10.1016/S0263-8223(00)00047-7.

Hou, Meng, L. Ye, and Y.-W. Mai. 1999b. "An Experimental Study of Resistance Welding of Carbon Fibre Fabric Reinforced Polyetherimide (CF Fabric/PEI) Composite Material." *Applied Composite Materials* 6 (1): 35–49. ISSN: 1573-4897. doi:10.1023/A:1008879402267.

Hussey, Robert John, and Josephine Wilson. 2012. *Advanced Technical Ceramics Directory and Databook*. Springer US. ISBN: 9781441986627.

Irshad, K.T. 2015. "Anvil Design & Experimental Investigation for Ultrasonic Welding of Thin Dissimilar Metals." Master Thesis, National Institute of Technology Rourkela.

Irving, E.P., and C. Soutis. 2014. *Polymer Composites in the Aerospace Industry.* Woodhead Publishing series in composites science and engineering. Cambridge: Elsevier Science. ISBN: 9780857099181.

Jakobsen, Tom B., Roderic C. Don, and John W. Gillespie. 1989. "Two-Dimensional thermal analysis of resistance welded thermoplastic composites." *Polymer Engineering & Science* 29 (23): 1722–1729. ISSN: 1548-2634. doi:10.1002/pen.760292314.

Jen, Ming-Hwa R., Yu-Chung Tseng, Huang-Kuang Kung, and J.C. Huang. 2008. "Fatigue response of APC-2 composite laminates at elevated temperatures." *Composites Part B: Engineering* 39 (7–8): 1142–1146. ISSN: 1359-8368. doi:http://doi.org/10.1016/j.compositesb.2008.03.005.

Jiang, Han, Robert Browning, Jason Fincher, Anthony Gasbarro, Scooter Jones, and Hung-Jue Sue. 2008. "Influence of surface roughness and contact load on friction coefficient and scratch behavior of thermoplastic olefins." *Applied Surface Science* 254 (15): 4494–99. ISSN: 0169-4332. doi:http://dx.doi.org/10.1016/j.apsusc.2008.01.067.

Jouin, P., T. Lee, and R. Vitlip. 1991. "Manufacture of a Primary Flight Structure using Thermoplastics." *Proceedings of the 36th International SAMPE Symposium:* 1014–1027.

Kaczmar, J.W., K. Pietrzak, and W. Włosiński. 2000. "The production and application of metal matrix composite materials." *Journal of Materials Processing Technology* 106 (1–3): 58–67. ISSN: 0924-0136. doi:http://dx.doi.org/10.1016/S0924-0136(00)00639-7.

Kagan, Val A., and Russell J. Nichols. 2005. "Benefits of Induction Welding of Reinforced Thermoplastics in High Performance Applications." *Journal of Reinforced Plastics and Composites* 24 (13): 1345–1352. doi:10.1177/0731684405048846. eprint: http://dx.doi.org/10.1177/0731684405048846.

Kaiser, Wolfgang. 2015. *Kunststoffchemie für Ingenieure: Von der Synthese bis zur Anwendung.* München: Carl Hanser Verlag GmbH & Company KG. ISBN: 9783446447745.

Khmelev, V.N., A.N. Slivin, and A.D. Abramov. 2007. "Model of process and calculation of energy for a heat generation of a welded joint at ultrasonic welding polymeric thermoplastic materials." In *Electron Devices and Materials, 2007. EDM'07. 8th Siberian Russian Workshop and Tutorial on,* 316–22. IEEE.

Khmelev, V.N., A.N. Slivin, A.V. Lehr, and A.D. Abramov. 2010. "Theoretical investigations of continuous ultrasonic seam welding of thermoplastic polymers and fabrics." In *2010 11th International Conference and Seminar on Micro/Nanotechnologies and Electron Devices,* 341–344. June. doi:10.1109/EDM.2010.5568791.

Krüger, S., G. Wagner, and D. Eifler. 2004. "Ultrasonic Welding of Metal/Composite Joints." *Advanced Engineering Materials* 6 (3): 157–159. ISSN: 1527-2648. doi:10.1002/adem.200300539.

Ku, H.S. 2003. "Joining of Thirty Three Percent by Weight Random Carbon Fibre Reinforced Low Density Polyethylene using Variable Frequency Microwave," University of Southern Queensland.

Kuchling, Horst. 2011. *Taschenbuch der Physik.* Leipzig: Hanser Fachbuchverlag. ISBN: 9783446424579.

KUKA, (KUKA Roboter GmbH). 2016. *Robots KR 300-2 PA, KR 470-2 PA.* Spez KR 300 470-2 PA. Specification. Augsburg, March 16.

Labeas, G.N., G.A. Moraitis, and Ch.V. Katsiropoulos. 2010. "Optimization of Laser Transmission Welding Process for Thermoplastic Composite Parts using Thermo-Mechanical Simulation." *Journal of Composite Materials* 44 (1): 113–130. ISSN: 0021-9983. doi:10.1177/0021998309345325.

Lambing, C.L.T., S.M. Andersen, S. Holmes, R. Don, S. Leach, and J. Gillespie. 1993. *Apparatus and method for resistance welding.* US Patent 5,225,025, July.

Lambing, C.L.T., R.C. Don, S.M. Andersen, S.T. Holmes, B.S. Leach, and J.W. Gillespie Jr. 1991. "Design and Manufacture of an Automated Resistance Welder for Thermoplastic Composites." In *Proceedings of the 49th Annual Technical Conference,* 2527–2531.

Leatherman, A.F. 1977. *Composite plastic-metallic bonding means and method.* US Patent App. 13/323,790, June.

Levy, Arthur, Steven Le Corre, and Irene Fernandez Villegas. 2014a. "Modeling of the heating phenomena in ultrasonic welding of thermoplastic composites with flat energy directors." *Journal of Materials Processing Technology* 214 (7): 1361–71. ISSN: 0924-0136. doi:http://dx.doi.org/10.1016/j.jmatprotec.2014.02.009.

Levy, Arthur, Steven Le Corre, and Arnaud Poitou. 2014b. "Ultrasonic welding of thermoplastic composites: a numerical analysis at the mesoscopic scale relating processing parameters, flow of polymer and quality of adhesion." *International Journal of Material Forming* 7 (1): 39–51. ISSN: 1960-6214. doi:10.1007/s12289-012-1107-6.

Lewis, C.F. 1990. *Materials Science and Engineering* 107, no. 6 (June): 41–44.

Li, Hui, and Karl Englund. 2017. "Recycling of carbon fiber-reinforced thermoplastic composite wastes from the aerospace industry." *Journal of Composite Materials* 51 (9): 1265–1273. doi:10.1177/0021998316671796. eprint: http://dx.doi.org/10.1177/0021998316671796.

Lin, W., O. Buneman, and A.K. Miller. 1991. "Induction heating model for graphite fiber/thermoplastic matrix composites." *Sampe Journal* 27:45–51.

LITE, (LITE GmbH). 2017. *LITE TK (PEEK).* Datasheet. Gaflenz.

Liu, G., and A.N. Gent. 1991. *A triangular double cantilever beam test for measuring adhesive or cohesive fracture energy.* Technical Report 29. AD-A243 151/N00014-85-K-0222/91-17317. Akron: Institute of Polymer Engineering, University of Akron.

Löwer, Chris. 2017. "Ultraleicht und extrem stabil." *weiter.vorn,* no. 1: 36. ISSN: 1868-3428.

Lu, H.M., A. Benatar, and F.G. He. 1991. "Sequential ultrasonic welding of peek/Graphite composite plates." In *Society of Plastics Engineers Annual Technical Conference,* 2523–2526.

Luratec. 2015. "CFK Next Generation: Luftfahrttechnik." Accessed April 17, 2017. `http://www.luratec.com/11fo/01lt/cf01.jpg`.

Maguire, D.M. 1989. "Joining Thermoplastic Composites." *SAMPE Journal* 25 (1): 11–14.

Mahon, J., C. Rutkowski, and W. Oelcher. 1991. "Induction bonding procedures for graphite reinforced thermoplastic assemblies." In *Proceedings of the 23rd International SAMPE Technical Conference,* 724–738. A92-51501 21-23. Covina: Society for the Advancement of Material / Process Engineering.

Markatos, D.N., K.I. Tserpes, E. Rau, S. Markus, B. Ehrhart, and Sp. Pantelakis. 2013. "The effects of manufacturing-induced and in-service related bonding quality reduction on the mode-I fracture toughness of composite bonded joints for aeronautical use." *Composites Part B: Engineering* 45 (1): 556–564. ISSN: 1359-8368. doi:`https://doi.org/10.1016/j.compositesb.2012.05.052`.

Martienssen, Werner, and Hans Warlimont. 2006. *Springer Handbook of Condensed Matter and Materials Data.* Springer Handbook of Condensed Matter and Materials Data. Berlin and Heidelberg: Springer. ISBN: 9783540304371.

Matsen, M.R. 1995. *Combined inductive heating cycle for sequential forming the brazing.* US Patent 5,420,400, May.

———. 1997. *Superplastically formed part.* US Patent 5,700,995, December.

Matsen, M.R., and A.R. Hodges. 1998. *Internal tooling for induction heating.* US Patent 5,710,414, February.

Matsen, M.R., and D.A. McCarville. 1998. *Bonding using induction heating.* US Patent 5,793,024, August.

Matsen, M.R., R.J. Poel, W.B. Crow, and D.S. Nansen. 1996. *Joining large structures using localized induction heating.* WO Patent App. PCT/US1996/009,634, December.

Mattia, F.B. 2003. *Elsevier's Dictionary of Acronyms, Initialisms, Abbreviations and Symbols.* Elsevier Science. ISBN: 9780080544137.

McCarville, Douglas A., and Henry A. Schaefer. 2001. *Processing and Joining of Thermoplastic Composites.* ASM Handbook. ASM International. ISBN: 0871707039.

McKnight, Steven H., Scott T. Holmes, John W. Gillespie, Cynthia L. T. Lambing, and James M. Marinelli. 1997. "Scaling issues in resistance-welded thermoplastic composite joints." *Advances in Polymer Technology* 16 (4): 279–295. ISSN: 1098-2329. doi:`10.1002/(SICI)1098-2329(199711)16:4<279::AID-ADV3>3.0.CO;2-S`.

Menges, Georg, Edmund Haberstroh, Walter Michaeli, and Ernst Schmachtenberg. 2014. *Menges Werkstoffkunde Kunststoffe.* München: Carl Hanser Verlag GmbH & Company KG. ISBN: 9783446443532.

Metaxas, A.C., and Roger J. Meredith. 1983. *Industrial Microwave Heating.* Chap. 2. Energy Engineering Series, Bd. 1. P. Peregrinus. ISBN: 9780906048894.

Mitchell, M.R., and R.W. Landgraf. 1996. *Advances in Fatigue Lifetime Predictive Techniques.* ASTM special technical publication, Bd. 3. ASTM. ISBN: 9780803120297.

Mitschang, P., R. Rudolf, and M. Neitzel. 2002. "Continuous Induction Welding Process, Modelling and Realisation." *Journal of Thermoplastic Composite Materials* 15 (2): 127–153. doi:10.1177/0892705702015002451. eprint: http://dx.doi.org/10.1177/0892705702015002451.

Moser, Lars, Peter Mitschang, and Alois K. Schlarb. 2008. "Induction welding: an automated joining process for composites." *JEC Magazine* 45 (November): 50–51. ISSN: 1639-965X.

MTorres. 2012. "R & D Laboratory for Composite Materials." Accessed November 21, 2015. http://www.mtorres.es/en/aeronautics/laboratory.

Neitzel, Manfred, Peter Mitschang, and Ulf Breuer. 2014. *Handbuch Verbundwerkstoffe: Werkstoffe, Verarbeitung, Anwendung.* 2nd ed. München: Carl Hanser Verlag GmbH & Company KG. ISBN: 9783446436978.

Niu, C., and M.C.Y. Niu. 1999. *Airframe Structural Design: Practical Design Information and Data on Aircraft Structures.* Airframe book series. Adaso Adastra Engineering Center. ISBN: 9789627128090.

Noor, Ahmed Khairy. 2000. *Structures Technology for Future Aerospace Systems.* Progress in astronautics and aeronautics. American Institute of Aeronautics & Astronautics. ISBN: 9781600864407.

NRC, (National Research Council). 1996. *Accelerated Aging of Materials and Structures: The Effects of Long-Term Elevated-Temperature Exposure.* Edited by Committee on Evaluation of Long-Term Aging of Materials, Commission on Engineering Structures Using Accelerated Test Methods, and National Research Council Technical Systems. Washington D.C.: National Academies Press. ISBN: 0309586607.

NRCC, (National Research Council Canada). 2012. "Resistance welding of thermoplastic composites." Government of Canada. September 26. http://www.nrc-cnrc.gc.ca/eng/solutions/facilities/amtc/thermoplastic_composites.html.

Offringa, Arnt. 2010. "New thermoplastic composite design concepts and their automated manufacture." *JEC Composites Magazine,* no. 57 (June): 45–49.

O'Shaughnessey, Patrice Gouin, Martine Dubé, and Irene Fernandez Villegas. 2016. "Modeling and experimental investigation of induction welding of thermoplastic composites and comparison with other welding processes." *Journal of Composite Materials* 50 (21): 2895–2910. doi:10.1177/0021998315614991. eprint: http://dx.doi.org/10.1177/0021998315614991.

Palardy, G., F.M. Agricola dn C. Dransfeld, and I.F. Villegas. 2015. *Up-Scaling of the Ultrasonic Welding Process for Joining Thermoplastic Composites.* Presentation, May.

Palardy, Genevieve, and Irene Fernandez Villegas. 2016. "Smart Ultrasonic Welding of Thermoplastic Composites." In *Proceedings of the American Society for Composites: Thirty-First Technical Conference,* edited by B.D. Davidson, M.W. Czabaj, and J.G. Ratcliffe.

———. 2017. "On the effect of flat energy directors thickness on heat generation during ultrasonic welding of thermoplastic composites." *Composite Interfaces* 24 (2): 203–14. doi:10.1080/09276440.2016.1199149. eprint: http://dx.doi.org/10.1080/09276440.2016.1199149.

Pappadà, Silvio, Andrea Salomi, Jeanette Montanaro, Alessandra Passaro, Antonio Caruso, and Alfonso Maffezzoli. 2015. "Fabrication of a thermoplastic matrix composite stiffened panel by induction welding." *Aerospace Science and Technology* 43:314–320. ISSN: 1270-9638. doi:https://doi.org/10.1016/j.ast.2015.03.013.

Parthier, Rainer. 2016. *Messtechnik: Grundlagen und Anwendungen der elektrischen Messtechnik.* Wiesbaden: Springer Fachmedien. ISBN: 9783658135980.

PDL, (Plastics Design Library). 2008. *Handbook of Plastics Joining: A Practical Guide.* Edited by Michael J. Troughton. Plastics Design Library. Elsevier Science. ISBN: 9780080950402.

Pickering, S.J. 2006. "Recycling technologies for thermoset composite materials—current status." The 2nd International Conference: Advanced Polymer Composites for Structural Applications in Construction, *Composites Part A: Applied Science and Manufacturing* 37 (8): 1206–1215. ISSN: 1359-835X. doi:https://doi.org/10.1016/j.compositesa.2005.05.030.

Pimenta, Soraia, and Silvestre T. Pinho. 2011. "Recycling carbon fibre reinforced polymers for structural applications: Technology review and market outlook." Environmental Implications of Alternative Materials in Construction and Treatment of Waste, *Waste Management* 31 (2): 378–392. ISSN: 0956-053X. doi:https://doi.org/10.1016/j.wasman.2010.09.019.

Potente, Helmut. 2004. *Fügen von Kunststoffen: Grundlagen, Verfahren, Anwendung.* München: Hanser. ISBN: 9783446227552.

Puyal, D., C. Bernal, J. M. Burdio, J. Acero, and I. Millan. 2007. "Methods and procedures for accurate induction heating load measurement and characterization." In *2007 IEEE International Symposium on Industrial Electronics,* 805–810. June. doi:10.1109/ISIE.2007.4374700.

Qin, Tianliang, Libin Zhao, and Jianyu Zhang. 2013. "Fastener effects on mechanical behaviors of double-lap composite joints." *Composite Structures* 100:413–423. ISSN: 0263-8223. doi:http://dx.doi.org/10.1016/j.compstruct.2013.01.008.

Rao, N. Shama, T.G.A. Simha, K.P. Rao, and G.V.V. Ravi Kumar. 2015. *Carbon Composites Are Becoming Competitive And Cost Effective.* Whitepaper. Infosys.

Rapoport, E., and Y. Pleshivtseva. 2006. *Optimal Control of Induction Heating Processes.* Mechanical Engineering. CRC Press. ISBN: 9781420019490.

Rodgers, B.A., and P.J. Mallon. 1993. In *Proceedings of the 14th SAMPE International European Chapter Conference,* 259–70.

Rose, J.L., F. Yan, Y. Liang, and C. Borigo. 2012. "Ultrasonic Vibration Method for Damage Detection in Composite Aircraft Components." In *Topics in Modal Analysis II, Volume 6: Proceedings of the 30th IMAC, A Conference on Structural Dynamics, 2012,* edited by R. Allemang, J. De Clerck, C. Niezrecki, and J.R. Blough, 359–367. New York: Springer. ISBN: 9781461424192. doi:10.1007/978-1-4614-2419-2_36.

Rotheiser, Jordan. 2004. *Joining of Plastics: Handbook for Designers and Engineers.* Hanser Publishers. ISBN: 9781569903544.

Rozenberg, L. 2013. *Physical Principles of Ultrasonic Technology.* Ultrasonic Technology. Springer US. ISBN: 9781468482171.

Rudolf, R., P. Mitschang, and M. Neitzel. 2000. "Induction heating of continuous carbon-fibre-reinforced thermoplastics." *Composites Part A: Applied Science and Manufacturing* 31 (11): 1191–1202. ISSN: 1359-835X. doi:http://doi.org/10.1016/S1359-835X(00)00094-4.

Rudolf, R., P. Mitschang, M. Neitzel, and C. Rueckert. 1999. "Welding of High-Performance Thermoplastic Composites." 286997113, *Polymers & Polymer Composites* 7, no. 5 (January): 309–315.

Sakamoto, Shigeyasu. 2010. *Beyond World-Class Productivity: Industrial Engineering Practice and Theory.* Chap. 6. London: Springer. ISBN: 9781849962698.

Sanders, Peter. 1987. "Electromagnetic welding: an advance in thermoplastics assembly." *Materials & Design* 8 (1): 41–45. ISSN: 0261-3069. doi:http://dx.doi.org/10.1016/0261-3069(87)90059-8.

Schinner, G., J. Brandt, and H. Richter. 1996. "Recycling Carbon-Fiber-Reinforced Thermoplastic Composites." *Journal of Thermoplastic Composite Materials* 9 (3): 239–245. doi:10.1177/089270579600900302. eprint: http://dx.doi.org/10.1177/089270579600900302.

Schulshenko, M.N. 2007. *Konstruktion von Flugzeugen.* Leipzig: Elbe-Dnjepr-Verlag. ISBN: 9783933395993.

Schulze, M. 2013. "Produktion des BMW i3 setzt neue Maßstäbe." *VDI Nachrichten,* no. 40 (October 4).

Schürmann, Helmut. 2007. *Konstruieren mit Faser-Kunststoff-Verbunden.* 2nd ed. VDI-Buch. Berlin and Heidelberg: Springer-Verlag. ISBN: 9783540721901.

Schwartz, M.M. 1994. *Joining of Composite Materials.*

Senders, F.J.M. 2016. "Continuous Ultrasonic Welding of Thermoplastic Composites." Master Thesis, Delft University of Technology.

Senders, Frank, Martijn van Beurden, Genevieve Palardy, and Irene F. Villegas. 2016. "Zero-flow: a novel approach to continuous ultrasonic welding of CF/PPS thermoplastic composite plates." *Advanced Manufacturing: Polymer & Composites Science* 2 (3-4): 83–92. doi:10.1080/20550340.2016.1253968. eprint: http://dx.doi.org/10.1080/20550340.2016.1253968.

Shehab, Essam, Weitao Ma, and Ahmad Wasim. 2013. "Manufacturing Cost Modelling for Aerospace Composite Applications." In *Concurrent Engineering Approaches for Sustainable Product Development in a Multi-Disciplinary Environment: Proceedings of the 19th ISPE International Conference on Concurrent Engineering,* edited by Josip Stjepandić, Georg Rock, and Cees Bil, 425–433. London: Springer. ISBN: 9781447144267. doi:10.1007/978-1-4471-4426-7_37.

Shi, H. 2014. "Resistance Welding of Thermoplastic Composites: Process and Performance." PhD Thesis, Delft University of Technology. doi:10.4233/uuid:58f16f99-afc1-4713-842e-562412583340.

Shi, Huajie, Irene Fernandez Villegas, Marc-André Octeau, Harald E.N. Bersee, and Ali Yousefpour. 2015. "Continuous resistance welding of thermoplastic composites: Modelling of heat generation and heat transfer." *Composites Part A: Applied Science and Manufacturing* 70:16–26. ISSN: 1359-835X. doi:http://doi.org/10.1016/j.compositesa.2014.12.007.

Siddiq, A., and E. Ghassemieh. 2008. "Thermomechanical analyses of ultrasonic welding process using thermal and acoustic softening effects." *Mechanics of Materials* 40 (12): 982–1000. ISSN: 0167-6636. doi:http://doi.org/10.1016/j.mechmat.2008.06.004.

Silverman, E.M., and B.A. Griese. 1989. "Joining methods for graphite/PEEK thermoplastic composites." *SAMPE Journal* 25 (5): 34–38.

Siores, E., and D.D. Rego. 1994. "Joining Materials with Microwave Energy." *Australasian Welding Journal:* 18–21.

Smiley, A. J., A. Halbritter, F. N. Cogswell, and P. J. Meakin. 1991. "Dual polymer bonding of thermoplastic composite structures." *Polymer Engineering & Science* 31 (7): 526–532. ISSN: 1548-2634. doi:10.1002/pen.760310709.

Smith, Christopher B. 2000. "Robotic friction stir welding using a standard industrial robot." In *2nd International Friction Stir Welding Symposium.* Gothenburg: TWI Ltd.

Smith, R. A. 2001. *Composite Defects and their detection: Materials Science and Engineering.* Physical Sciences, Engineering and Technology Resources. Encyclopedia of Life Support Systems (EOLSS). Developed under the Auspices of the UNESCO. Paris: UNESO, Eolss Publishers.

Soccard, Eric. 2011. *Ultrasonic assembly method.* US Patent 7,896,994, March.

Stavrov, D., and H.E.N. Bersee. 2003. "Thermal aspects in resistance welding of thermoplastic composites." In *Proceedings of ASME Summer Heat Transfer Conference.* 47222. Las Vegas, July.

———. 2005. "Resistance welding of thermoplastic composites-an overview." *Composites Part A: Applied Science and Manufacturing* 36 (1): 39–54. ISSN: 1359-835X. doi:http://doi.org/10.1016/j.compositesa.2004.06.030.

Stavrov, D., H.E.N. Bersee, and A. Beukers. 2003. "The influence of the heating element on resistance welding of thermoplastic composite materials." In *Proceedings of ICCM-14 Conference.* ID-1552. San Diego: International Committee on Composite Materials (ICCM), July.

Stokes, Vijay K. 1989. "Joining methods for plastics and plastic composites: An overview." *Polymer Engineering & Science* 29 (19): 1310–1324. ISSN: 1548-2634. doi:10.1002/pen.760291903.

Strong, A. Brent. 1993. *High performance and engineering thermoplastic composites.* Technomic Pub. Co.

———. 2008. *Fundamentals of Composites Manufacturing, Second Edition: Materials, Methods and Applications.* Society of Manufacturing Engineers. ISBN: 9780872638549.

Strong, Brent A., D.P. Johnson, and B.A. Johnson. 1990. "Variables Interactions in Ultrasonic Welding of Thermoplastic Composites." *SAMPE Quaterly* 21 (2): 36–41.

Sturma, Claus. 2016. *Aircraft Structures: General Design Principles and Corrosion Protection.* Lecture Notes. University of Applied Sciences Augsburg, Augsburg.

Stutts, Daniel S. 2013. "Equivalent Viscous Damping," Missouri University of Science and Technology.

Suresh, K.S., M. Roopa Rani, K. Prakasan, and R. Rudramoorthy. 2007. "Modeling of temperature distribution in ultrasonic welding of thermoplastics for various joint designs." *Journal of Materials Processing Technology* 186 (1–3): 138–146. ISSN: 0924-0136. doi:http://doi.org/10.1016/j.jmatprotec.2006.12.028.

Swartz, H.D., and J.L. Swartz. 1989. "Focused infrared melt fusion: another option for welding thermoplastic composites." *Joining Composites:* 1–16.

Tackitt, K.D., and J.W. Gillespie Jr. 1996. "Through transmission ultrasonics for process monitoring of thermoplastic fusion bonding." In *Proceedings of the 11th Technical Conference of the American Society for Composites,* 812–21.

Tateishi, N., T.B. Zach, R.T. Woodhams, and T.H. North. 1989. "Ultrasonic bonding of roll-drawn polypropylene using tie-layers." In *Proceedings of the 47th Annual Technical Conference,* 496–498.

Taylor, N.S., and R. Davenport. 1991. "The resistive implant welding of thermoplastic composite materials." In *Proceedings of the 49th Annual Technical Conference,* 2038–41.

Taylor, N.S., and S.B. Jones. 1990. "The Feasibility of Welding Thermoplastic Composite Materials." In *Proceedings of the International Conference on Advances in Joining and Cutting Processes,* 424–435.

Teßmer, Jan. 2006. *Strukturmechanik des CFK-Rumpfes.* Wissenschaftstag 2006. DLR, Braunschweig, September 28.

Thomas, M, N Boyard, Y Jarny, and D Delaunay. 2008. "Estimation of effective thermal conductivity tensor from composite microstructure images." *Journal of Physics: Conference Series* 135 (1): 012097.

Todd, S.M. 1990. "Joining thermoplastic composites." In *22nd International SAMPE Technical Conference*, 383–92. 22 vols.

Tooley, Mike. 2009. *Design Engineering Manual*. Elsevier Science. ISBN: 9781856178648.

TORAY, Inc.), (TORAY Carbon Fibers America. 2017. *TORAYCA® T300*. Datasheet. Santa Ana.

Troughton, Michael J. 2008. *Handbook of Plastics Joining: A Practical Guide*. Plastics Design Library. Elsevier Science. ISBN: 9780815519768.

UN DESA and Boeing. 2014. "Durchschnittliche Flugkilometer pro Kopf im weltweiten Luftverkehr von 2007 bis 2014 (in RPK pro Kopf)." Statista. Accessed April 12, 2017. https://de.statista.com/statistik/daten/studie/159843/umfrage/flugkilometer-pro-kopf-im-luftverkehr/.

USDoD, (U.S. DEPARTMENT OF DEFENSE). 1999. *COMPOSITE MATERIALS HANDBOOK: POLYMER MATRIX COMPOSITES*. MIL-HDBK-17-2F. Handbook.

USITC, (US International Trade Commission. 1993. *Global Competitiveness of U.S. Advanced Technology Manufacturing Industries: Large Civil Aircraft, Inv. 332-332*. 2667. 332-332. DIANE Publishing, August. ISBN: 9781457826092.

Varadan, V.K., and V.V. Varadan. 1991. "Microwave Joining and Repair of Composite Materials." *Polymer Engineering and Science* 31 (7): 470–86.

Vassilopoulos, Anastasios. 2014. *Fatigue and Fracture of Adhesively-Bonded Composite Joints*. Woodhead Publishing series in composites science and engineering. Elsevier Science. ISBN: 9780857098122.

Vervlied, J., and C. Heward. 1991. "Susceptor-less Induction Welding Using Filmix Co-spun Thermoplastic Blends." In *Proceedings of the Conference: COmposites in manufacturing*, 1–10. Society of Manufacturing Engineers.

Victrex, (Victrex Polymer Solutions). 2017. *APTIV® 1300 Series Films*. Datasheet. Lancashire.

Villegas, Irene Fernandez. 2013. "Optimum Processing Conditions for Ultrasonic Welding of Thermoplastic Composites." In *Proceedings of the 19th ICCM*. Montreal: International Committee on Composite Materials (ICCM).

———. 2014. "Strength development versus process data in ultrasonic welding of thermoplastic composites with flat energy directors and its application to the definition of optimum processing parameters." *Composites Part A: Applied Science and Manufacturing* 65:27–37. ISSN: 1359-835X. doi:http://dx.doi.org/10.1016/j.compositesa.2014.05.019.

———. 2015. "In situ monitoring of ultrasonic welding of thermoplastic composites through power and displacement data." *Journal of Thermoplastic Composite Materials* 28 (1): 66–85. doi:10.1177/0892705712475015. eprint: http://dx.doi.org/10.1177/0892705712475015.

Villegas, Irene Fernandez, Harald E.N. Bersee, and Ali Yousefpour. 2010. "Performance analysis of resistance welded and co-consolidated joints in continuous fibre reinforced thermoplastic composites." *Proceedings of International SAMPE Symposium and Exhibition* (Seattle).

Villegas, Irene Fernandez, and H.E.N. Bersee. 2009. "Ultrasonic Welding of Advanced Thermoplastic Composites: An Investiagtion on Energy Directing Surfaces." In *Proceedings of the 17th ICCM.* Edinburgh: International Committee on Composite Materials (ICCM).

Villegas, Irene Fernandez, B. Valle Grandea, H.E.N. Bersee, and R. Benedictus. 2014. "A Comparative Evaluation between Flat and Traditional Energy Directors for Ultrasonic Welding of Thermoplastic Composites." In *Proceedings of the 16th ECCM.* Seville: European Committee on Composite Materials (ECCM).

Villegas, Irene Fernandez, Lars Moser, Ali Yousefpour, Peter Mitschang, and Harald E.N. Bersee. 2013. *Process and Performance Evaluation of Ultrasonic, Induction and Resistance Welding of Advanced Thermoplastic Composites.* Delft University of Technology.

Villegas, Irene Fernandez, and Genevieve Palardy. 2017. "Ultrasonic welding of CF/PPS composites with integrated triangular energy directors: melting, flow and weld strength development." *Composite Interfaces* 24 (5): 515–528. doi:10.1080/09276440.2017.1236626. eprint: http://dx.doi.org/10.1080/09276440.2017.1236626.

Visakh, P. M., and Sigrid Lüftl. 2016. *Polyethylene-Based Biocomposites and Bionanocomposites.* Thermoplastic Bionanocomposites Series. Wiley. ISBN: 9781119038443.

Vodicka, Roger. 1996. *Thermoplastics for Airframe Applications: A Review of the Properties and Repair Methods for Thermoplastic Composites.* DSTO-TR-0424. DSTO Aeronautical / Maritime Research Laboratory, October.

Volkov, S.S., I.N. Garanin, and Y.V. Kohlopov. 1997a. "Ultrasound welding of different types of plastics using a thermoplastic liner and the effect of the surface roughness on the weldability." *Russian Ultrasonics* 27:71–77.

———. 1997b. "Ultrasound welding of dissimilar plastics using a thermoplastic interlayer and the effect of surface roughness on weldability." *Welding International* 11 (5): 393–395. doi:10.1080/09507119709451984. eprint: http://dx.doi.org/10.1080/09507119709451984.

Volkov, S.S., and Y.V. Kholopov. 1998a. "Technology and equipment for ultrasonic welding of polymer based composite structures." *Welding International* 12 (5): 400–403.

———. 1998b. "Technology and equipment for ultrasonic welding of polymer based composite structures." *Russian Ultrasonics* 28:145–155.

Völlner, Georg. 2009. "Rührreibschweißen mit Schwerlast-Industrierobotern." PhD Thesis, Technical University Munich.

Volpe, V. 1980. "Estimation of Electrical Conductivity and Electromagnetic Shielding Characteristics of Graphite/Epoxy Laminates." *Journal of Composites Materials,* no. 14: 189–98.

Wedgewood, R., and P.E. Hardy. 1996. "Induction Welding of Thermoset Composite Adherends using Thermoplastic Interlayers and Susceptors." In *Proceedings of the 28th International Sampe Technical Conference,* 850–61.

Wijngaarden, M.J. van. 2005. "Robotic induction welding of carbon fiber reinforced thermoplastics." In *SAMPE fall technical conference.* 68836. Seattle.

Wise, I. D., R. J. and Froment. 2001. "Microwave welding of thermoplastics." *Journal of Materials Science* 36 (24): 5935–5954. ISSN: 1573-4803. doi:10.1023/A:1012993113748.

Withworth, H.A. 1998. "Fatigue evaluation of composite bolted and bonded joints." *Journal of Advanced Materials* 30 (2): 25–31.

Wittel, Herbert, Dieter Muhs, Dieter Jannasch, and Joachim Voßiek. 2011. *Roloff/Matek Maschinenelemente: Normung, Berechnung, Gestaltung - Lehrbuch und Tabellenbuch.* SpringerLink : Bücher. Vieweg+Teubner Verlag. ISBN: 9783834882790.

Wolcott, J. 1989. "Recent Advances in Ultrasonic Welding Technology." In *Porceedings of the 47th Annual Technical Conference,* 502–505.

Worrall, Chris, and Roger Wise. 2014. "Novel Induction Heating Technique for Joining of Carbon Fibre Composites." In *Proceedings of the 16th European Conference on Composite Materials.*

Wu, S.-I.Y. 1991. "Dual Resin Bonding of Thermoplastic Composites." *36th International SAMPE Symposium,* no. 36: 2174–2183.

Xiao, X.R., Hoa S.V., and K.N. Street. 1992. "Processing and modelling of resistance welding of APC-2 composites." *Journal of Composite Materials* 26 (7): 1031–49.

Yarlagadda, Prasad K.D.V, and Tan Chuan Chai. 1998. "An investigation into welding of engineering thermoplastics using focused microwave energy." *Journal of Materials Processing Technology* 74 (1–3): 199–212. ISSN: 0924-0136. doi:http://dx.doi.org/10.1016/S0924-0136(97)00269-0.

Yarlagadda, S., B. K. Fink, and Jr. J. W. Gillespie. 1998. "Resistive Susceptor Design for Uniform Heating during Induction Bonding of Composites." *Journal of Thermoplastic Composite Materials* 11 (4): 321–337. doi:10.1177/089270579801100403. eprint: http://dx.doi.org/10.1177/089270579801100403.

Yarlagadda, Shridhar, Hee June Kim, John W. Gillespie Jr., Nicholas B. Shevchenko, and Bruce K. Fink. 2002. "A Study on the Induction heating of conductive Fiber Reinforced Composites." *Journal of Composite Materials* 36 (4): 401–21. ISSN: 0021-9983. doi:10.1106/002199802023171.

Yousefpour, Ali. 2006. "Resistance Welding of Thermoplastic Composites using Metal Mesh Heating Elements." In *Joining Plastics 2006,* edited by Rapra Technology Limited, 99–106. Conference Proceedings Series 11. London: Rapra Technology. ISBN: 9781859575703.

Yousefpour, Ali, and M. Hojjati. 2007. "Static and fatigue behaviour of fusion bonded APC-2/AS4 thermoplastic composites joints." In *Proceedings of the SAMPE Europe International conference,* 559–564. Paris.

Yousefpour, Ali, Mehdi Hojjati, and Jean-Pierre Immarigeon. 2004. "Fusion Bonding/Welding of Thermoplastic Composites." *Journal of Thermoplastic Composite Materials* 17 (4): 303–341. doi:10.1177/0892705704045187. eprint: http://dx.doi.org/10.1177/0892705704045187.

Yousefpour, Ali, and Marc-Andre Octeau. 2009. *Resistance Welding of Thermoplastics.* US Patent App. 11/887,847, February.

Yousefpour, Ali, M. Simard, M.-A. Octeau, and M. Hojjati. 2005. "Process Optimization of Resistance-Welded Thermoplastic Composites Using Metal Mesh Heating Elements." (Long Beach).

Zach, T., J. Lew, T.H. North, and R.T. Woodhams. 1989. "Joining of high strength oriented polypropylene using electromagnetic induction bonding and ultrasonic welding." *Materials Science and Technology:* 281–87.

Zaeh, Michael F., and Georg Voellner. 2010. "Three-dimensional friction stir welding using a high payload industrial robot." *Production Engineering* 4 (2): 127–133. ISSN: 1863-7353. doi:10.1007/s11740-009-0184-y.

Zeidler, Eberhard, Wolfgang Hackbusch, Ilja N. Bronstein, Juraj Hromkovic, Bernd Luderer, Hans-Rudolf Schwarz, Jochen Blath, et al. 2012. *Taschenbuch der Mathematik.* 3rd ed. Wiesbaden: Springer Fachmedien. ISBN: 9783835101234.

Zhang, Ming Qiu, and Min Zhi Rong. 2011. *Self-Healing Polymers and Polymer Composites.* Wiley. ISBN: 9781118082584.

Ziegltrum, Michael. 2001. *Untersuchungen von Ultraschallschweißverbindungen in der Kombination unterschiedlicher Thermoplaste mit einer und mehreren Fügeebenen: Examination of ultrasonic welding in combination of different thermoplastics with one and more joining planes.* Herbert Utz Verlag. ISBN: 9783896758903.

Declaration of Authorship

I hereby declare that I have authored this thesis independently, that I have not used other than the declared sources/resources, and that I have explicitly marked all material which has been quoted either literally or by content from the used sources. The master thesis was not used in the same or in a similar version to achieve an academic grading or is being published else-where.

I read and took note of the code of conduct in the case of plagiarism at the University of Applied Sciences Augsburg. I assure that the handed thesis is no plagiarism and does not content any text or pictures made by third persons.

City Date Signature of the Author